NOTE TO USERS

A Study of Design Improvements for a Multi-Tethered Aerostat System

François Deschênes

Department of Mechanical Engineering
McGill University
Montréal, Québec, Canada

March 2005

A thesis submitted to the Faculty of Graduate Studies and Research in partial fulfillment of the requirements of the degree of
Masters of Engineering

Your file Votre référence
ISBN: 0-494-12594-2
Our file Notre référence
ISBN: 0-494-12594-2

Abstract

The Large Adaptive Reflector is a Canadian design for a new radio telescope. The receiver is held at the focus of the reflector by an aerostat tethered to the ground by multiple tethers. One of the main goals in the design of this system is the minimization of the motion of the receiver. Most perturbations are produced by the action of the wind on the aerostat and transmitted to the confluence point via the leash that connects the aerostat to the receiver. For that reason, this work focused on leash-related stabilization techniques. Computer simulations were used to evaluate the benefits of different passive and active methods. Among the passive approaches studied were the use of a constant force spring and of a passive heave compensator. The active methods evaluated included aerostat pitch control and active heave compensation. One of the more promising approaches, a leash made of bungee cable, was evaluated experimentally on a prototype of the system in Penticton, BC. Finally, a pitch control mechanism was designed. This mechanism displaces the leash attachment point on the harness to pitch the aerostat nose up or down.

Résumé

Le LAR est un radiotélescope novateur conçu par un consortium canadien. Une des principales composantes du LAR est un système de positionnement du récepteur comprenant un ballon d'hélium retenu au sol à l'aide de câbles. Le but de ce système est de positionner le récepteur au foyer du réflecteur et d'en minimiser le mouvement. Comme la majeure partie des perturbations du système provient de l'action du vent sur l'aérostat et que celles-ci sont transmises au récepteur à travers la laisse qui le relie à l'aérostat, les techniques de stabilisation du récepteur étudiées dans la présente thèse sont en lien avec la laisse. Afin d'évaluer les avantages des différentes techniques (passives et actives) étudiées, une simulation numérique du système de positionnement fut utilisée. L'utilisation d'un ressort à force constante ainsi que d'un compensateur passif de la laisse font partie des méthodes passives étudiées tandis que le contrôle du lancement de l'aérostat ainsi la compensation active de la laisse font partie des méthodes actives étudiées. Une des méthodes les plus prometteuses, le remplacement de la laisse par un câble élastique, fut évaluée expérimentalement sur un prototype situé à Penticton, Colombie-Britannique. Finalement, un mécanisme permettant le déplacement du point d'attache de la laisse sur le harnais dans le but de contrôler le lancement de l'aérostat fut conçu.

Table of Contents

List of Figures

List of Tables

Acknowledgments

First and foremost, I would like to express my sincere gratitude to my advisor, Professor Meyer Nahon. Although he probably does not suspect it, his determination has given me the courage and motivation to persevere and to see my thesis to the end. I thank him for his constant guidance, his dedication and his perspective, which has helped look at old problems in new ways.

I would also like to acknowledge a number of McGill students with whom I worked on the LAR project. I thank Casey Lambert for his advice and his help regarding the analysis of the Penticton facility data, and I thank Gabriele Gilardi for helping me code the half-bungee/half-Spectra leash in the LAR simulation. I thank Philippe Coulombe-Pontbriand and Jennifer Pereira for their work on the integration of the wireless backup communication system, and, Philippe, thank you for these incredible escapades at MacDonald campus. My gratitude also goes out to Alexandre Boyer for waking me up at the airport an hour before takeoff. Without his call, I would have missed a really nice week in British Columbia.

Thanks to all the people at the Dominion Radio Astrophysical Observatory in Penticton, especially Peter Dewdney, Donna Morgan and the aerostat "flight crew": Dean Chalmers, Richard Hellyer, Andrew Gray and Dave "Toffee" Del Rizzo. Dean, thank you for introducing me to one of British Columbia's greatest singers; and Richard, thanks for shouting "RUN!" at the right moment. Quite possibly, you saved my life. I also cannot forget Jean Bastien who installed the battery backup on the aerostat ballonet platform and Angel Garcia who lodged me and drove me back and forth to the observatory every day for a month.

Before working on the LAR, I had the chance to start a masters project in the Ambulatory Robotics Laboratory, where I stayed even after my switch to the LAR project. I consider this a chance since I met, in this lab, individuals who had a huge impact on my life and radically changed my way of thinking. I thank James Andrew Smith, one of the finest Francophiles I know, for all the conversations that allowed me to see my province from a brand new perspective. I also thank Neil Neville for being my first McGill teammate. This may seem insignificant today, but back then it meant a lot to me since I hardly spoke English and I was a little scared. I also want to thank Christina Georgiades for accompanying me through my thesis writing and job searching processes. Her moral support was a lot more meaningful knowing that she was going through the same obstacles. I thank Christopher Prahacs, the best opponent at Quake, for helping me design the variable leash attachment point mechanism. I also express my sincere appreciation to all the other great ARL people I had the chance to know: Don Campbell, Evgeni Kiriy, Julien Marcil, Jacqui McCallum, Dave McMordie, Ioannis Poulakakis, Enrico Sabelli, Akihiro Sato, Aaron Saunders, John "No Love" Sheldon, Matthew Smith, Charles Steeves, Mike Tolley and Geneviève Vinois.

Outside the laboratory, I thank Philippe Cardou for his friendship and also for introducing me to a lot of amazing people during these two years. I thank Geneviève Houde for all her get-togethers, especially knowing that she would have preferred not to be the only one who planned them. I thank them both, as well as Katia Bilodeau, Gabriel Meunier and Guy Rouleau for the wonderful lunch times we shared at McGill.

Finally, thanks to Professor Clément Gosselin for arousing and feeding my interest in robotics and to Professor Martin Buehler for giving me my first chance at McGill University. Without your generosity and effort, none of this would be possible.

Funding for this research was provided by the Natural Sciences and Engineering Research Council of Canada (NSERC). My personal funding was from le Fonds Québécois de la Recherche sur la Nature et les Technologies (FQRNT).

À mes parents et
ma soeur Andrée-Anne.
Je vous adore!

Chapter 1

Introduction

1.1 Square Kilometre Array

Astronomers use radio telescopes (also named radio interferometers) to detect the relatively long wavelength electromagnetic radiations emitted by outer space matter. Since the first observations in 1932, radio astronomy has led, amongst others, to the discovery of radio galaxies, quasars, pulsars and the cosmic microwave background. According to the international radio astronomy community, the next step is the observation of the formation of the early universe, including the emergence of the first stars and galaxies. To achieve this, a revolutionary instrument, with an increase in sensitivity of two orders of magnitude relative to existing interferometers, is needed [1][2]. Since increasing a telescope's sensitivity implies increasing its collecting area, this instrument would need one square kilometre of collecting area – thirty times more than the largest radio telescope ever built. This revolutionary instrument would be composed of many antennas and is commonly known as the Square Kilometre Array (SKA) [3][4].

The project of designing the Square Kilometre Array has been undertaken by an international consortium of radio astronomers and engineers representing more than fifteen countries including Canada, USA, Europe, Australia, China, India and South Africa. To keep the cost of such a large project reasonable, several international research centres are presently developing completely new technologies. These include large arrays of low-cost parabolic antennas, adaptive array technology and novel concepts for very large, single-aperture antennas such as the LAR, which is the Canadian solution. The timeline of the SKA project includes selection of the site in 2006 and of the final design

in 2008 for construction between 2012 and 2020. The expected cost of the SKA is one billion US dollars.

1.2 Large Adaptive Reflector

Researchers at the National Research Council of Canada's Herzberg Institute of Astrophysics have suggested a novel design concept for the SKA known as the Large Adaptive Reflector (LAR) [5][6], which is illustrated in Figure 1.1. Approximately 60 LAR antennas would be required to make up a square kilometre of collecting area.

Fig. 1.1. An artist's conception of the LAR installation.

The LAR telescope would be composed of two main components: (a) a very large reflector and (b) a multi-tethered aerostat system. The LAR's reflector is composed of several flat panels actuated to form a steerable parabolic dish with diameter and focal length of respectively 200 and 500 meters. Figure 1.2 shows a prototype of an actuated panel located at the NRC's Dominion Radio Astrophysical Observatory in Penticton, British Columbia. Approximately 185 such panels would compose a single 200-metre diameter reflector. The actuator sizes are impressive since this panel is designed to be one of the outermost panels of the reflector and thus must achieve very large motion.

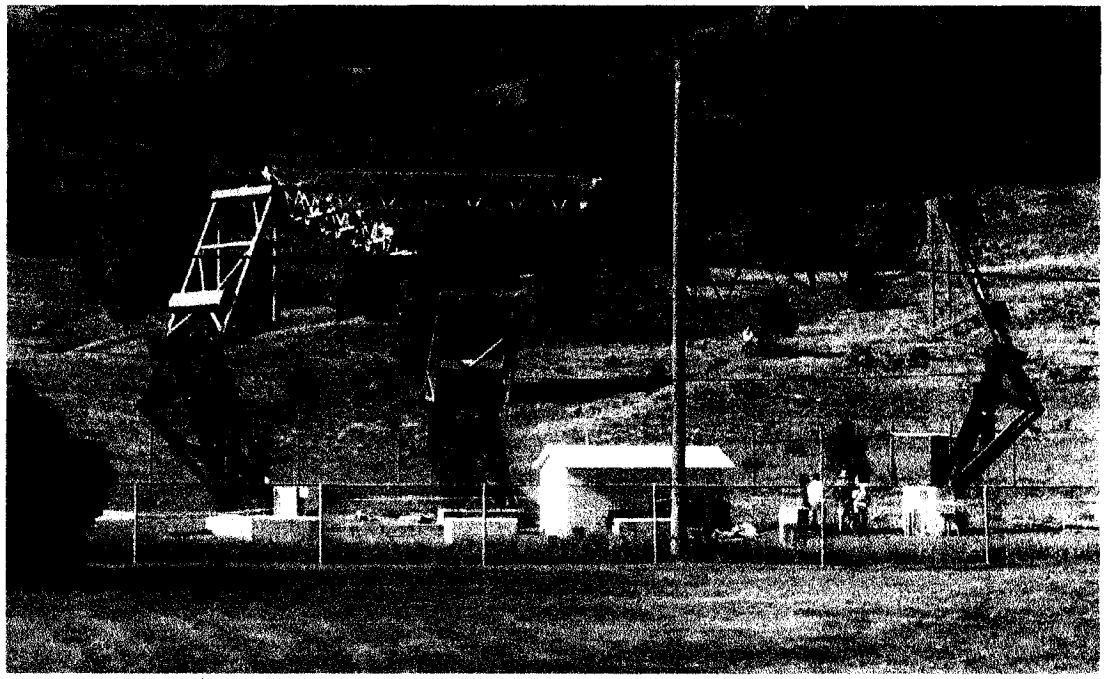

Fig. 1.2. An actuated panel prototype in Penticton, BC.

A multi-tethered aerostat system is used to hold the receiver package at the focal point of the reflector, 500 metres aloft. This system is composed of a helium-filled aerostat attached to the receiver package by a single tether commonly called the leash. The receiver, also called focal package or payload, is fixed to the ground by three or more tethers (see Figure 1.1). The LAR telescope is steered by modifying the reflector's shape and simultaneously varying the lengths of these tethers with winches located at the base of each tether to position the receiver at the new focal point. For sufficient coverage of the sky, the multi-tethered aerostat system must be able to position the focal package for a range of zenith angles from 0 to 60° for all azimuths.

The Large Adaptive Reflector concept is a very promising approach for radio telescope design. First, it permits the construction of larger fully steerable parabolic reflectors with field-of-views comparable to those of much smaller antennas. Secondly, since it uses a reflector with a large focal ratio (focal length divided by diameter), its off-axis performance is exceptional. Finally, the relatively flat reflecting surface can be supported on the ground in a distributed manner instead of being supported by a single mechanical part as in the traditional designs, decreasing the cost per square metre of collecting area by roughly an order of magnitude relative to conventional designs [5].

1.3 Thesis Objective and Motivations

The Large Adaptive Reflector concept looks very promising; however, its practical feasibility raises some questions. One of the main uncertainties is whether or not the multi-tethered aerostat system has the capacity to position the focal package to centimetre accuracy, which is the precision required for good signal reception. The multi-tethered tension structure is stiff enough to successfully resist wind forces and large enough to filter out the highest frequency turbulence, but the present design is not good enough to stabilize the receiver to centimetre accuracy.

In order to address the remaining payload disturbances, two active controllers will be implemented in the LAR multi-tethered aerostat system. The first controller uses the ground winches to vary the tether lengths and respond to the low frequency disturbances. The second controller uses a parallel mechanism, mounted at the confluence point of the tethers, to precisely stabilize the receiver at higher frequencies. It is estimated that this five degrees of freedom parallel mechanism, which is called the Confluence Point Mechanism (CPM), would be capable of correcting errors in a sphere of one metre and to provide rotations of 0.5 rad about two axes.

However, the capacity of these two controllers to stabilize the receiver to centimetre accuracy for all the configurations of the LAR multi-tethered aerostat system is far from certain at this point as their design is not completed yet. In the eventuality that the winch controller and the CPM are not sufficient, other stabilization techniques for the focal package must be investigated. This is the focus of the present work, which is intended to be preliminary. If they prove to be worthwhile, the stabilization techniques analysed here will be further investigated and may be implemented in the LAR multi-tethered aerostat system.

1.4 Literature Survey

This literature survey reviews the research performed on single-tethered and multi-tethered aerostats. Additionally, work on heave compensation, which is a technique commonly used in marine tethered systems, is presented. It is included since it is

envisioned that such a technique could be used in the LAR multi-tethered aerostat system to decouple the aerostat and payload motions.

1.4.1 Single-Tethered Aerostats

Nearly all the literature on aerostats deals with streamlined aerostats. These consist of a teardrop-shape ("streamlined") hull with 3 or 4 tailfins at the rear for stability, as shown in Figure 1.3. The principal advantage of this shape relative to a spherical shape is that they have lower drag and tend to have better survivability in high wind speeds. Single-tethered aerostats have been the subject of many investigations, which can be separated into linear and non-linear studies. DeLaurier performed the first study on the non-linear dynamics of a single-tethered aerostat in 1972 [7]. His work consisted of a stability analysis on a 2-D model for steady state wind conditions. DeLaurier added turbulence to his analysis in 1977 [8]. Five years later, Jones and Krausman developed the first 3-D non-linear dynamics model of a tethered aerostat, which included a lumped mass discretized tether [9]. In 1983, Jones and DeLaurier enhanced this model by developing a discretized aerostat modeling technique that took into account turbulence variation along the length of the hull [10]. This work also estimated the aerodynamic properties of an aerostat based on semi-empirical data. By linearizing the equations of motion developed by Jones and DeLaurier, Badesha and Jones conducted a stability analysis of a large commercial aerostat in 1993 [11]. Lambert and Nahon used another 3-D non-linear dynamics model to perform a stability analysis of a single-tethered streamlined aerostat in 2003 [12]. In this work, the aerostat model was based on a component breakdown method and the tether was discretized into lumped-mass nodes connected by lumped stiffness and damping elements. It was found that the system remained stable for wind speeds up to 20 m/s and that the tether length had an effect on the stability.

Other works on single-tethered aerostats deal with experimental validation. In 1973, Redd *et al.* presented a linear model of a tethered aerostat in a steady wind and validated it using experimental data [13]. Even if this linear model neglected the coupling between the tether and the aerostat, it highlighted that certain physical parameters of the system had an important effect on its stability. Humphreys also used experimental data in 1997 to validate his 3-D non-linear model of a towed, scaled aerostat [14]. Finally, in 2001, the

linearized dynamics model developed by Badesha and Jones [11] was validated by Jones and Shroeder using real flight data provided by the US Army [15].

1.4.2 Multi-Tethered Aerostats

Little work has been done on multi-tethered aerostats other than on the LAR aerostat system. The first researchers to demonstrate an interest in multi-tethered aerostats were Leclaire and Rice in 1973 and Leclaire and Schumacher in 1974 [16][17]. These U.S. Air Force researchers conducted an experimental study of tri-tethered aerostat systems. Their experiments indicated that: (a) the payload of a tri-tethered system was much more stable than the payload of an equivalent single-tethered system, and (b) separating the payload and the aerostat by a leash reduced the payload motion further. In an attempt to capture snapshot images of star surfaces, Le Coroller *et al.* designed and prototyped a hypertelescope with focal optics suspended by a multi-tethered helium balloon in 2004 [18]. The multi-tethered system consisted of two interconnected tether tripods, one restraining the payload at an altitude of 35.6 metres and one restraining the leash movement a few metres below the aerostat, which flew at an altitude of 140 metres. With this system, they measured payload displacements of few millimetres for wind speeds up to 3 m/s.

Research on the LAR multi-tethered aerostat system started in 1997. In 2000, Fitzsimmons *et al.*, of the National Research Council of Canada, presented a steady state study of a tri-tethered aerostat system [19]. At the same time, Nahon assembled a preliminary dynamics 3-D simulation of a multi-tethered spherical aerostat system including a lumped mass tether model as well as winch control [20]. The encouraging results of these studies regarding the precision of the multi-tethered aerostat as a positioning system for the LAR led to a more detailed stage of analysis, which consisted of simulation investigations together with experimental validations. In 2002, Nahon *et al.* implemented a streamlined aerostat model in the computer simulation and performed a comprehensive performance evaluation for different system configurations [21]. It was found from that study that: (a) the system was mainly sensitive to the low frequency turbulent gusts, (b) the spherical aerostat performed relatively better than the streamlined aerostat in terms of receiver stabilization, and (c) for the worst-case receiver

configuration, which is 60° in zenith and azimuth, the receiver position error could be kept under one metre if 50 kW were available at each winch.

Later, Lambert *et al.* used dimensional analysis to design a one-third-scale prototype of the LAR positioning system [22][23]. The purpose of this prototype was to validate the dynamics model used in the simulation and to evaluate the operational issues inherent to multi-tethered aerostat systems. A streamlined aerostat was selected since it was thought at that time that its relative low drag would be an important advantage for the positioning system. However, this advantage came at the price of a fluctuating lift generated by wind gusts on the aerostat hull [21]. The prototype was constructed on a National Research Council site in Penticton, British Columbia, and is operational since the fall of 2002. Figure 1.3 shows a picture of this tri-tethered streamlined aerostat prototype. In this picture, we see the aerostat attached to the payload by the leash. The payload is attached to the ground by four tethers: three of them resist the aerostat lift while the fourth one, called the central tether (the darkest one in Figure 1.3), is slack and is used to power the system. In 2005, Nahon *et al.* used experimental data provided by this prototype to validate the simulation dynamics models, which proved to be remarkably accurate [24].

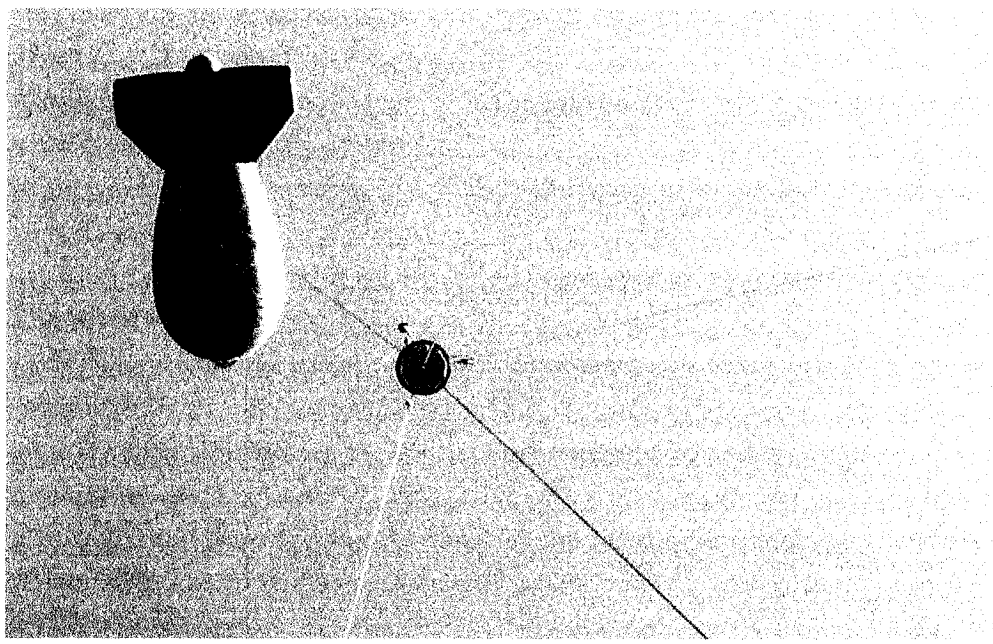

Fig. 1.3. LAR's receiver positioning system prototype in Penticton, BC.

1.4.3 Heave Compensation

Heave compensation has been mainly investigated for use with remotely operated vehicle (ROV) systems, which consist of a caged vehicle, a cable housing electrical and optical conductors, and a support vessel. These unmanned systems are used for undersea operations such as inspection and repair of marine structures and scientific exploration in depths greater than two kilometres. In order to maximize the operating life of ROV systems in rough seas, scientists have developed passive and active heave compensation systems to decouple the motion of the cage from its support vessel. In 1988, Niedzwecki and Thampi presented a study of a ship-mounted passive heave compensator [25]. Another analysis of a ship-mounted system was presented by Hover *et al.* in 1994 [26]. Both of these works highlighted that the cage motion could be exacerbated if the compensator stiffness was poorly chosen. The first study of a cage-mounted passive heave compensator was performed by Driscoll *et al.* in 2000 [27]. By including a lumped-parameter heave compensation element into a ROV system computer simulation using a lumped-mass tether model, it was found that the performance of ship-mounted and cage-mounted pneumatic compensation systems in reducing the cage motion and the tether tension was very similar. However, during extreme sea conditions, snap-loading of the tether occurred with the ship-mounted system but not with the cage-mounted system. This cage-mounted pneumatic compensation system was optimized numerically by Driscoll *et al.* in 2001 [28]. Eide enhanced this 1-D computer simulation of a ROV system by implementing an irregular wave model as well as a ship-mounted active heave compensator in 2003 [29]. This enhanced simulation was used to compare three types of controller: PID, LQG and H_∞; for an active heave compensator. For most of the cases investigated, the performance of the LQG and H_∞ controllers was better than that of the PID controller, for which gain tuning was very time consuming. Furthermore, the performance of the LQG controller proved to be more consistent than the others in minimizing the cage motion, tether tension fluctuations and required compensator power.

1.5 Thesis Organization

The focus of the present work is the investigation of methods for stabilizing the receiver of the LAR multi-tethered aerostat system other than winch control and CPM control.

In Chapter 2, a preliminary study of passive design improvements for the LAR multi-tethered aerostat system is performed. The Penticton experimental one-third-scale facility is first presented [23]. A dynamic simulation of a multi-tethered aerostat system developed by Nahon *et al.* [20][21] is then used to assess the capacity of several passive methods to reduce the receiver motion. These different methods are (a) the modification of the leash properties, (b) the use of a constant force spring, and (c) passive heave compensation. They are applied to the same simulated baseline multi-tethered system in order to compare them with respect to their payload rms motion. Finally, these passive methods are evaluated in terms of their design implications.

In Chapter 3, an analysis similar to the one of Chapter 2 is applied to three active methods: (a) aerostat pitch control using harness shape modification, (b) aerostat pitch control using tailfin deflection, and (c) active heave compensation. They are first simulated in the baseline system to assess their capacity to reduce the receiver motion and then their design implications are evaluated.

In Chapter 4, a detailed design of a bungee leash is performed and implemented in the Penticton facility for testing. The bungee leash arrangement is first designed and then, the Penticton test set-up as well as the launching and retrieving procedures are explained. Finally, the results of the experiments are presented and interpreted, followed by a discussion of the bungee leash approach.

A detailed design of a leash attachment point mechanism is provided in Chapter 5. This mechanism is used to displace the leash attachment point on the harness in order to pitch the aerostat nose up or down. The different components of the mechanism are first selected. Then, the mechanism arrangement is presented and implemented in the simulated baseline system. The simulation results are then interpreted and design improvements are discussed.

Chapter 6 provides the conclusions of this research as well as recommendations for future work.

Chapter 2

Preliminary Study of Passive Methods

2.1. Introduction

In this chapter, a preliminary study of passive methods is performed in order to identify techniques that improve the multi-tethered aerostat system performance. By passive, we mean any device that is not actively controlled. In Section 2.2, we present the Penticton experimental facility and the simulation we use in our study. We also show in that section that more than 90% of the payload perturbations come from the aerostat. Consequently, the three passive approaches studied in this chapter address methods to reduce transmission of these perturbations. These methods are:

- Modification of the leash properties (Section 2.3)
- Use of a constant force spring (Section 2.4)
- Passive heave compensation (Section 2.5)

In Section 2.6, we investigate the design implications of two of the passive methods, and finally, a summary of Chapter 2 is presented in Section 2.7.

2.2. System Configuration and Performance

In this section, the tools used to compare the different passive methods discussed in this chapter are presented. We focus our study on the multi-tethered aerostat system located in Penticton, British Columbia, since it will allow us to perform experimental validation, as

needed. We first present the configuration of this system and then discuss the simulation used to perform the study.

2.2.1 Penticton Facility

A one-third-scale tri-tethered aerostat system is presently being tested in Penticton as a proof of concept for the LAR radio telescope proposal. As mentioned in Section 1.2, the LAR multi-tethered aerostat system is used as a positioning device for the receiver package. The purpose of the Penticton prototype is to validate the dynamics model used in the simulation developed by Nahon *et al.* [20][21], to demonstrate the accuracy of the positioning system and to evaluate the operational issues inherent to multi-tethered aerostat systems. This multi-tethered aerostat prototype is composed of three tethers, three winches, a payload, a leash and a streamlined aerostat (see Figure 2.1).

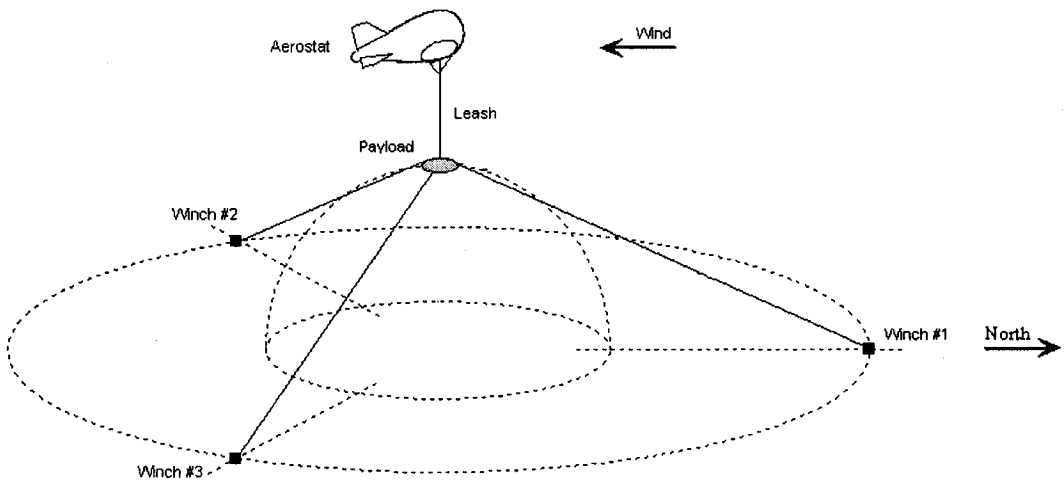

Fig. 2.1. Penticton facility general scheme.

Instruments are mounted at the payload and at the aerostat to measure the system states during flight. Among others, these instruments comprise GPS receivers, load cells, a wind sensor and an inertial measurement unit. These instruments are powered from the ground through the central tether, a fourth tether connected to the payload, as well as through the leash for the aerostat instruments. Data from all sensors are transmitted to a ground computer by two radio modems and via a RS-485 link that pass through the central tether and the leash.

The winches are located at the base of the tethers in order to actively control their lengths. These winches receive their command signals from the ground computer through a fibre optic network. In the multi-tethered aerostat positioning system, the ground winches are used in two different ways: (a) to steer the payload to a new location and (b) to compensate for payload disturbances.

Between experiments, the aerostat is stored in a hangar. When an experiment is to be performed, the aerostat is moved with a trailer to the launch location. The system is launched and retrieved using a main winch located on the trailer, on which are initially spooled the central tether and the leash.

The Penticton facility has a winch radius of 400 metres, a focal length of about 170 metres as well as a leash of 200 metres. The tethers are made of Plasma material while the leash is made of Spectra [30]. All have a diameter of 6 mm. In this chapter, we evaluate the performance of different passive methods by simulating this same system.

2.2.2 Simulation

The dynamics simulation developed by Nahon *et al.* [20][21] uses a mathematical model of the tethered aerostat system that has been widely discussed elsewhere, but we will briefly review its main features.

The aerodynamic forces acting on the streamlined aerostat components (hull and fins) are first calculated separately and then summed to provide the aerostat overall behaviour as well as the magnitude and direction of the force acting at the top of the leash [21]. Each cable is modeled using a lumped-mass model [12], meaning that each continuous tether is discretized into lumps joined by massless segments. The payload joins all the cables together and is modeled as a 0.8-m (the diameter of the instrument platform) sphere whose drag coefficient varies with Reynolds number [21]. The internal forces (stiffness and damping) as well as the external forces (aerodynamics and weight) are used to formulate the equations of motion for each lumped mass. The only input to the system is a wind that varies with altitude as a function of Earth's boundary layer to which is added turbulent gusts following a von Karman spectrum [21]. A fourth-order Runge-Kutta

numerical integration routine is used to solve the resulting system of nonlinear dynamic equations [31].

To be consistent in our analysis, we choose a special case where the system configuration and the wind conditions are fixed. We call this case the baseline system. For the baseline system, the aerostat net lift is chosen to be 2.7 kN, which is the maximum net lift measured in Penticton. Furthermore, the payload is positioned at zero degree in zenith and azimuth, meaning that all three tethers have the same length, which is 435 metres. The mean wind comes from the North and is constant at 5 m/s. Turbulence is included and no winch control is used. For each simulation, values different from the baseline parameters will be specified.

The simulation is divided in two main parts: static and dynamic analysis. The initial state of the system is first calculated by the static analysis and is then used as a starting point by the dynamic analysis to compute the system state at each time step. For the baseline system, the simulation yields the time histories shown in Figure 2.2, where the payload and aerostat errors are calculated with respect to their mean values. The aerostat rotations are calculated with respect to their mean values.

In this chapter, we evaluate the different passive methods by comparing their capacity to stabilize the payload. The Root Mean Square (RMS) of their confluence point position error $\Delta(t)$ is used:

$$\Delta_{RMS} = \sqrt{\frac{1}{T}\int_0^T [\Delta(t)]^2 dt} \tag{2.1}$$

where t is the time and T the total simulated time interval.

The confluence point position rms error of the baseline system is 19 cm. This is the value that we aim to reduce throughout this chapter. Using the simulation, we found that replacing the aerostat by a constant force equal in *magnitude* and *direction* to the baseline system mean leash tension produces a payload rms error of 0.5 cm. We therefore focus our analysis on the perturbations produced by the aerostat and transmitted through the leash.

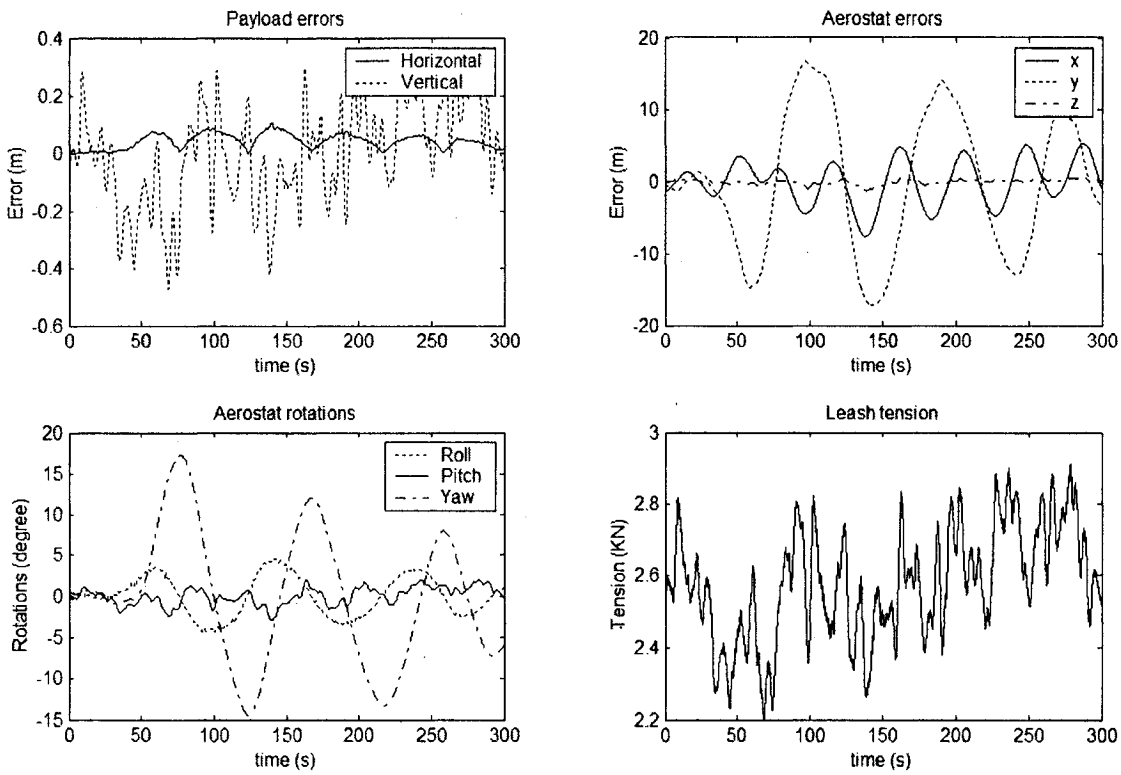

Fig. 2.2. Behaviour of the baseline system.

Since it is unlikely that we could stabilize the aerostat motion sufficiently to get a steady leash orientation, stabilizing the leash tension *magnitude* is our main objective. If the magnitude of the leash tension was constant but its direction fluctuated as in the baseline case, we would get the system behaviour shown in Figure 2.3. In that figure, the top leash tension is equal to the baseline mean leash tension, and the payload rms motion decreases from 19 cm to 5 cm, a reduction of approximately 75% that is still highly desirable. By comparing Figures 2.3 and 2.2 we deduce that variation in the leash tension magnitude leads to fluctuations in vertical payload motion while variation in its direction leads to fluctuations in horizontal payload motion.

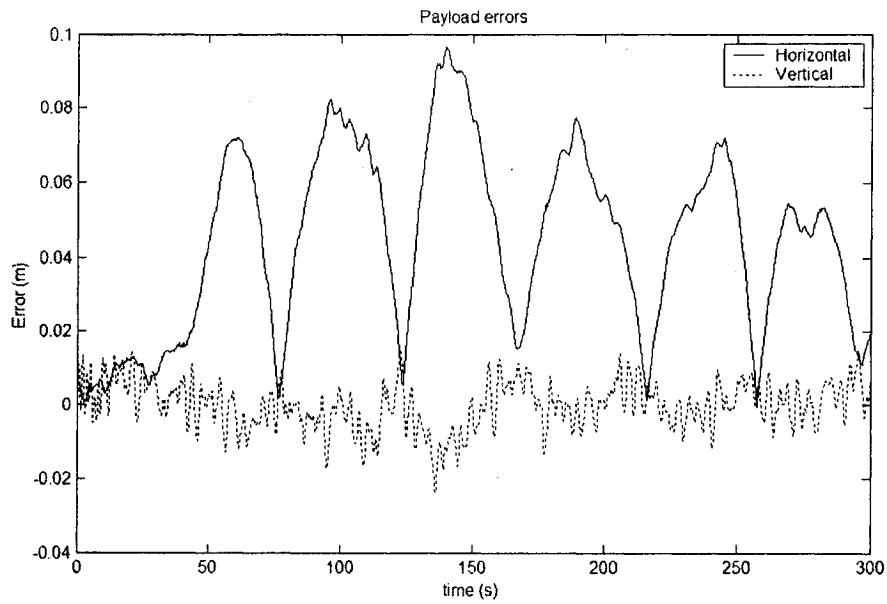

Fig. 2.3. Payload errors of the baseline system with constant leash tension.

2.3. Leash Properties

We saw in the previous section that the disturbances coming from the aerostat through the leash cause more than 90% of the perturbations of the confluence point position. Therefore, one of the simplest ways to improve the performances of the tethered aerostat system would be to choose the leash properties in order to reduce those perturbations. In this section, the effects on the payload motion of the leash length, stiffness and damping are studied.

2.3.1 Leash Length

To study the effect of the leash length on the confluence point motion, we vary the leash length of the baseline system in the simulation. The results are shown in Figure 2.4. From that figure, it seems that a short leash achieves better confluence point stabilization than a longer one. Furthermore, it seems that above 200 metres, the confluence point position error becomes almost constant. However, this is not what is observed in practice. Indeed, a 33-metre leash was initially used in Penticton and the aerostat motion appeared to be very large. To remedy this, the leash was lengthened.

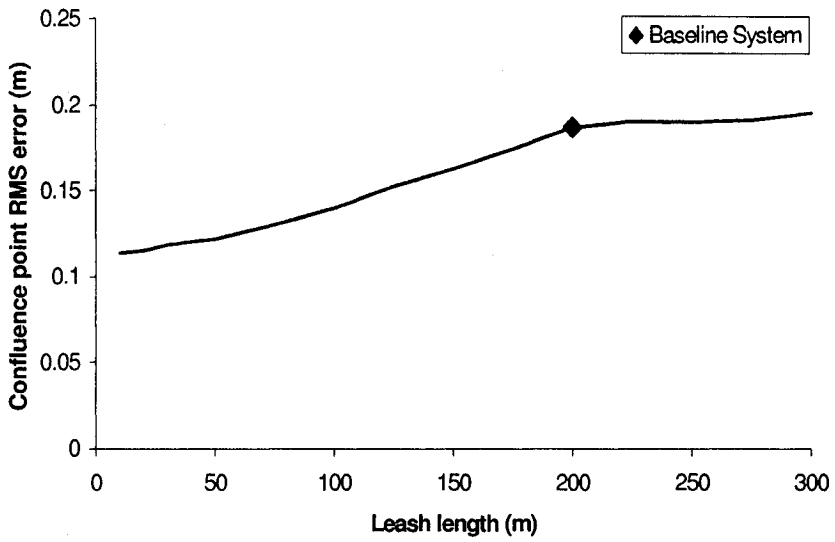

Fig. 2.4. Confluence point position rms error as a function of leash length.

On the other hand, we do not have quantitative results to confirm those observations. It is possible that the perceived behaviour does not truly reflect larger or smaller confluence point motion. For example, an operator tends to observe (and interpret) the frequency and amplitude of oscillation of the aerostat motion. However, confluence point errors are caused primarily by variation in the leash force. It is not clear that the correspondence between these is direct. In order to better understand these issues quantitatively, a small-scale facility is being constructed at McGill to provide more detailed data.

It is clear from the operational standpoint that installing a short leash would not be beneficial. Additionally, the potential performance improvements (Figure 2.4) are not very large. Shortening the leash length is therefore dropped from further consideration in this study.

2.3.2 Leash Stiffness

In this subsection, we study the effect of the leash stiffness on the confluence point motion. The stiffness of the leash is related to three parameters: its section area (A), its unstretched length (l^u) and its Young's modulus (E) according to $k = \frac{EA}{l^u}$. To study the effect of leash stiffness, we vary its Young's modulus from 7.07×10^5 to 7.07×10^{10} Pa in

the simulation, while keeping its unstretched length and its diameter constant. As a result, the leash stiffness varies from 1 to 10000 N/m. The results are shown in Figure 2.5.

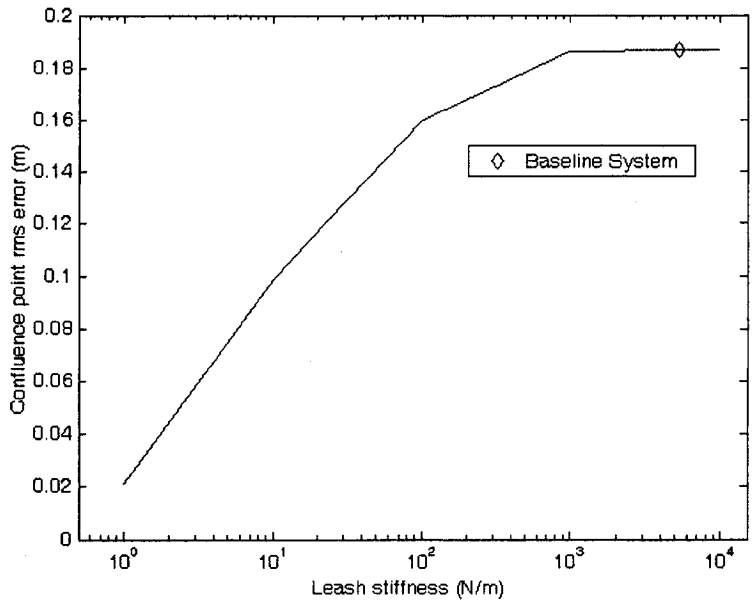

Fig. 2.5. Confluence point position rms error as a function of leash stiffness.

As can be seen in Figure 2.5, a low stiffness leash leads to much lower confluence point motion than a high stiffness one, and this reduction seems much larger than that achievable by changing the leash length. Indeed, it appears that reducing the leash stiffness to 1 N/m from the present 5300 N/m would reduce the confluence point motion tenfold. Note that there is also a leash length effect in Figure 2.5 since the mean leash stretched length is function of the leash stiffness. The mean leash length is 200 metres for a stiffness of 10000 N/m and approximately 2800 metres for a stiffness of 1 N/m.

As we will see in Section 2.6, it is not necessarily possible in practice to reduce the leash stiffness by that much. For example, a 200-metre bungee cable strong enough to support the Penticton aerostat would have a stiffness of approximately 5 N/m, but it is unlikely that a bungee leash of that length could be used in practice.

2.3.3 Leash Damping

In this subsection, we study the effect of the leash damping on the confluence point motion. In order to vary the leash damping in the simulation, its damping ratio (ζ) is

varied from zero to one. The damping ratio is defined as $\zeta = C/C_{cr}$ where C is the actual damping coefficient and C_{cr} is the critical damping coefficient. In our case, the critical damping coefficient of each leash element is calculated at the first time step as $C_{cr} = 2\sqrt{\frac{T_e \cdot k}{g}}$, where T_e is the element tension, k the element stiffness and g the gravitational acceleration. The results are shown in Figure 2.6.

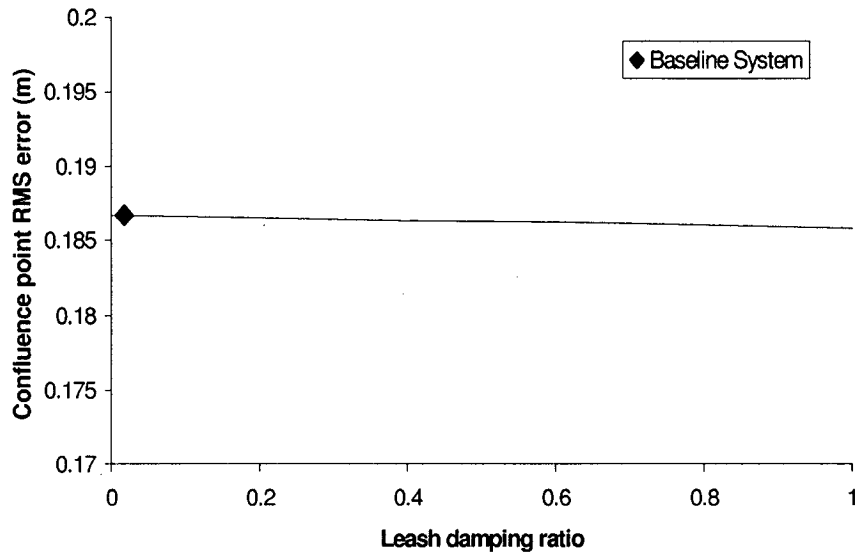

Fig. 2.6. Confluence point rms error as a function of leash damping ratio.

Figure 2.6 shows that the leash damping does not have any effect on the confluence point position error. Indeed, it was found that the damping accounts for less than 0.001% of the total leash tension at each time step. Therefore, the leash damping is dropped from further consideration in this study.

2.4. Constant Force Spring

We are now interested in studying the effects of a constant force spring on the motion of the confluence point. A constant force spring is a roll of prestressed strip that exerts a nearly constant restraining force to resist uncoiling (see Figure 2.7). Since this recoiling force P is produced exclusively by the material in zone X, whose length and curvature are constant, the force P is nearly constant. Such a constant force spring could have a great

influence on the confluence point position error, as it would completely cancel the leash tension disturbances. However, the largest commonly available constant force springs only have a force of 180 N and the longest found is two metres long. Nevertheless, in this section, we investigate the potential benefits of such a device assuming it was available.

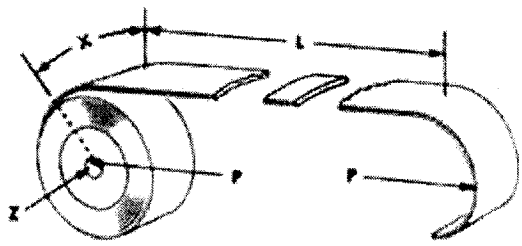

Fig. 2.7. Uncoiling of a constant force spring [32].

The constant force spring is included in the simulation dynamics analysis with a constant force equal to the leash initial tension. Indeed, including the spring in the static analysis with a force different from the leash initial tension produces instability in the simulation. The device is incorporated in the existing finite-element lumped-mass model as a single lumped-parameter element at the bottom of the leash. Furthermore, the constant force spring has a finite length. When one of its limits is reached, the spring becomes ineffective.

The results of two simulations are presented in Figures 2.8 and 2.9 to demonstrate the effects of the constant force spring: the first for a spring with a total travel of 60 metres (±30m) and the second for a spring with a travel of ten metres (±5m). In both cases, the initial leash tension computed in the static analysis is approximately 2.6 kN.

As can be seen in Figure 2.8, the 60-metre spring is long enough for the wind conditions, and its travel limits are never reached. With such a spring, the leash tension is constant for the whole simulation and the rms motion of the confluence point is 5.4 cm instead of 19 cm for the baseline case (≈ 28%).

The results degrade significantly when the constant force spring is too short. Indeed, when the constant force spring hits one of its stops, a discontinuity occurs in the leash tension and the confluence point position error rises sharply. In the case of the 10-metre spring (see Figure 2.9), the rms motion of the confluence point is only reduced to 15 cm.

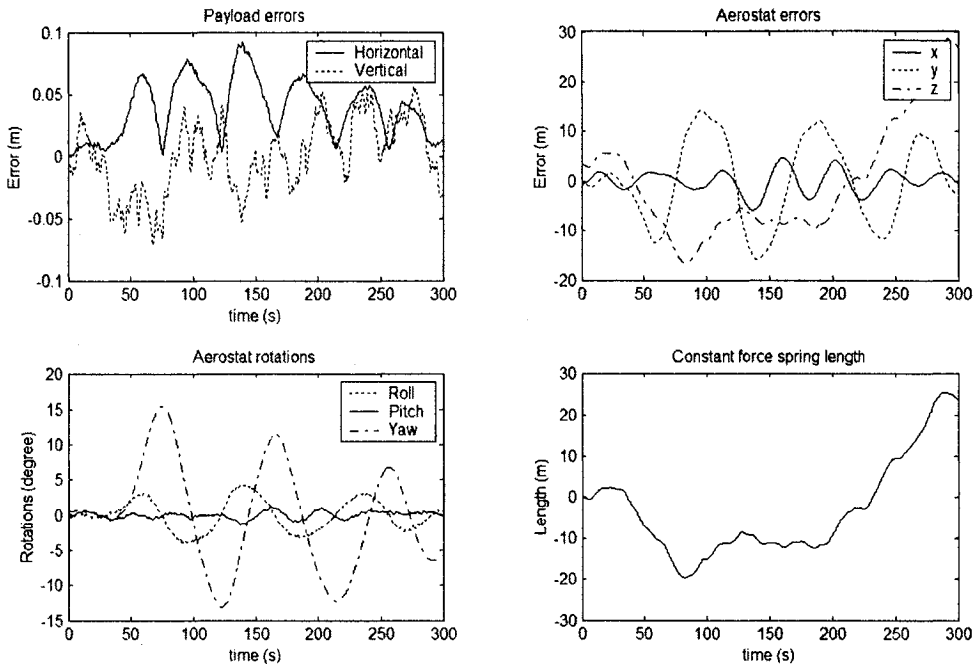

Fig. 2.8. Baseline system with a 60-metre constant force spring.

It was mentioned in Section 2.2 that a system with constant leash tension and direction would have its confluence point motion reduced to 4% of the baseline case. The constant force spring reduces the motion "only" to 30% of the baseline case because it only renders the *magnitude* of the leash tension constant — the direction still fluctuates.

The results of this section emphasize two points: (a) the constant force spring should be long enough not to hit its stops too frequently, and (b) the spring force must be very close to the mean leash tension or the travel required becomes very large. Since that mean tension is a function of the wind conditions, which fluctuate, some other means would have to be used to maintain a constant mean leash tension. Chapter 3 discusses possible approaches for doing this. However, since this would entail too much complexity and it is very unlikely that a suitably sized constant force device could be fabricated, this approach is not considered further.

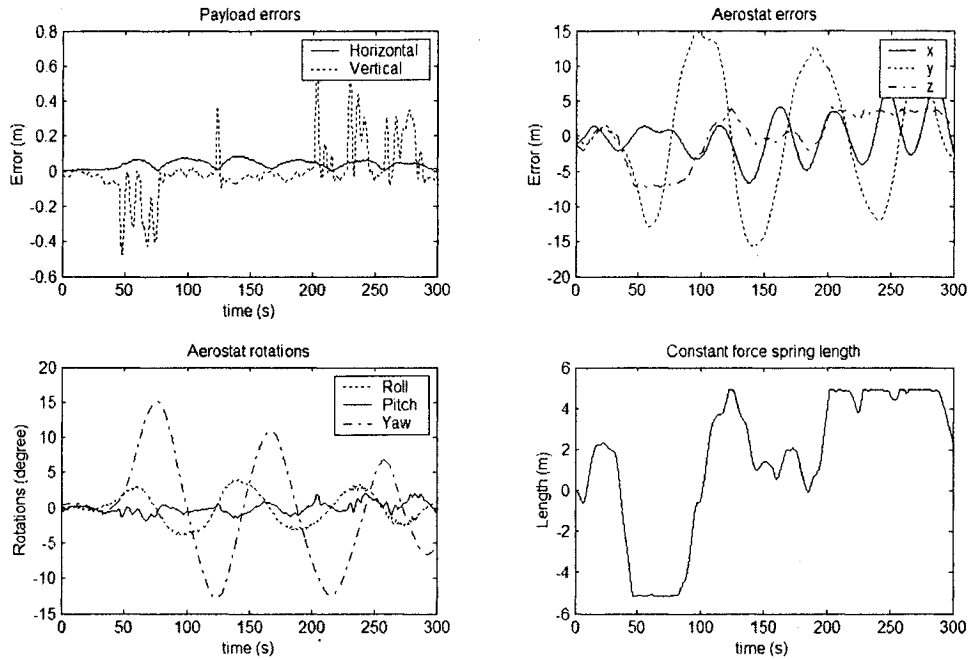

Fig. 2.9. Baseline system with a 10-metre constant force spring.

2.5. Passive Heave Compensation of the Leash

A passive heave compensator is a passive mechanism that includes a spring and a damper that could be installed between the leash and the payload (see Figure 2.10) in order to decouple the payload and aerostat motions. One advantage of such a compensator is that arbitrary properties could be selected without being limited by rope materials.

In the simulation, passive heave compensation is included in the existing finite-element lumped-mass model as a single lumped-parameter element, at the bottom of the leash. The simulation is used to study the effect of the passive compensation stiffness on the motion of the confluence point. Figure 2.11 shows (a) the rms error of the confluence point position as well as (b) the mean value of the compensator length as functions of the compensator stiffness.

As can be seen in Figure 2.11a, it is possible in principle to obtain very small confluence point position error with a passive alleviation stiffness of 1 N/m, which is consistent with the previous results for variations of the leash stiffness (Figure 2.5). Figure 2.11b shows that the mean length of a passive alleviation system with a stiffness of 1 N/m is more than

2.5 km, which is clearly unrealistic. However, the compensator length variation, or its working length, is relatively small compared to its mean length (about 60 metres for the 1-N/m compensator). To reduce the mean compensator length while keeping the same working length, an initial tension must be added to the passive compensation unit.

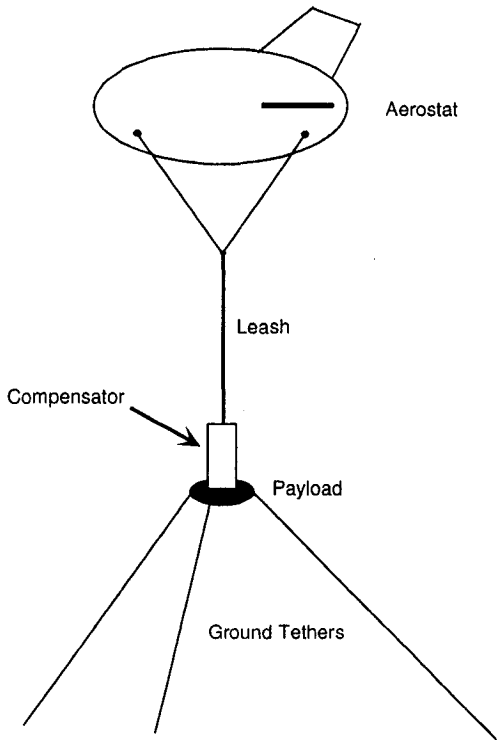

Fig. 2.10. Location of a passive heave compensator in the system.

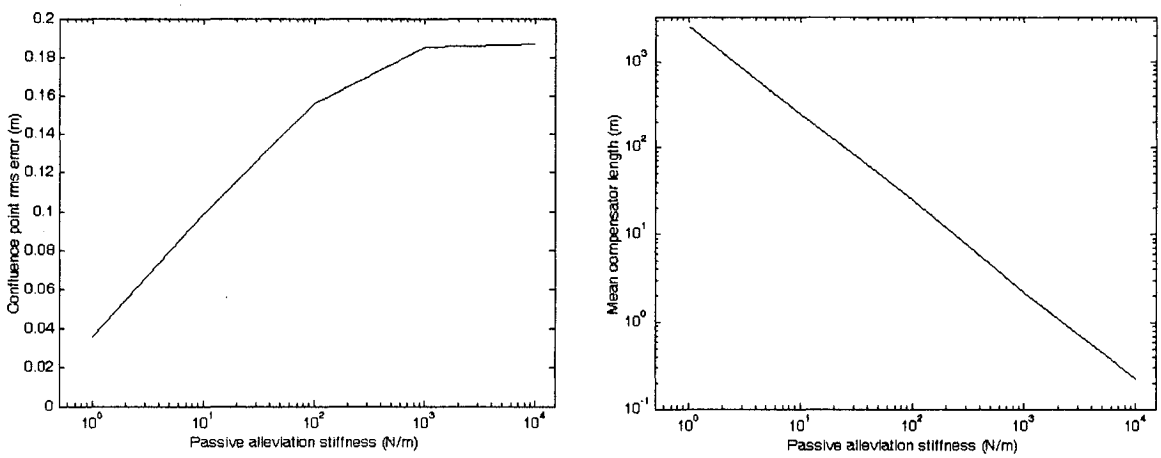

(a) **(b)**

Fig. 2.11. Confluence point rms error (a) and mean compensator length (b) as a function of passive alleviation stiffness.

2.5.1 Pretension

A pretension has to be added to a passive compensator in order to make it usable in practice. Such a pretension would be added to the compensator spring in order to avoid the excessive mean length needed otherwise.

In this subsection, the effects of adding initial tension to the passive alleviation element are studied. In the simulation, the pretension (T_{pre}) is added to the elastic tension ($k\delta$) of the leash bottom element to give the total passive compensator tension (T_p):

$$T_p = k\delta + T_{pre} \tag{2.2}$$

For this study, the passive compensator stiffness is kept at 1 N/m since it is for this stiffness that the best results were previously achieved. In selecting an appropriate value of the pretension, it was found that, as pretension increased, the error of the confluence point tended to increase. Theoretically, this should not have been the case. Indeed, adding pretension to the passive compensator should affect only its mean length. Upon further investigation, it was found that this was due to the effect of the pretension on the aerostat altitude. Indeed, the wind forces, the turbulence and the air density are all functions of altitude. Thus, by modifying the pretension, the altitude of the aerostat and the forces acting on the system vary.

We found that a compensator with pretension and stiffness equal to 2.6 kN and 1 N/m would reduce the confluence point position rms error to 4 cm and would require a working length of about 60 metres (see Figure 2.12).

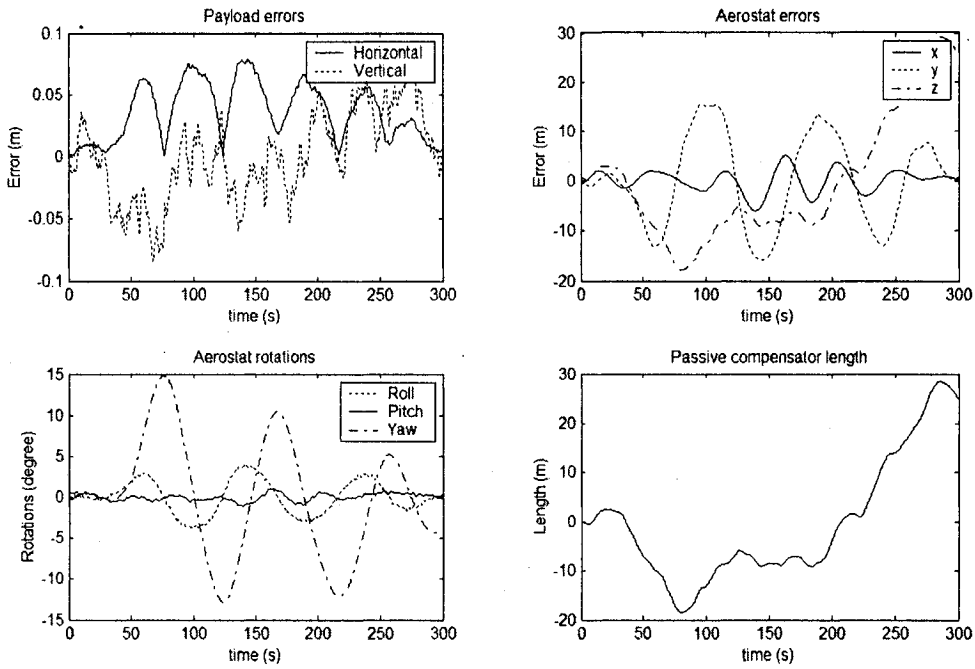

Fig. 2.12. Baseline system with a passive compensator.

By comparing Figures 2.8 and 2.12, we note that the passive heave compensator with a stiffness of 1 N/m has the same effect as the constant force spring. Consequently, the comments related to constant force springs at the end of Section 2.4 are also applicable to passive compensators: (a) the working length of a passive alleviation device should be long enough and (b) the pretension should be kept slightly below the minimum leash tension or the compensator will hit one of its stops; this can be done either by controlling the pretension or the leash tension. Chapter 3 presents some techniques to actively stabilize the leash tension. We will discuss the design implications of building a passive heave compensator with pretension in Subsection 2.6.2.

2.6. Design Implications

Until now, our analysis has mainly concentrated on the reduction of confluence point motion to evaluate the performance of each passive method. However, the feasibility of implementation of each approach is also very important. In this section, we perform a preliminary evaluation of the design implications of two passive methods: reducing the leash elasticity and passive heave compensation. Only those two are considered since the

other approaches did not improve the performance significantly enough or were judged to be impractical.

2.6.1 Reduction of the Leash Elasticity

The results of Section 2.3 indicated that a substantial improvement in system performance could be obtained by reducing the leash stiffness. With this in mind, we first consider the properties of different raw materials used to construct braided ropes. Table 2.1 shows a selection of materials available as fibre:

Table 2.1. Properties of some raw materials available as fibre [33].

Material	Young's Modulus (GPa)	Density (kg/m^3)	Strength (MPa)
Cotton	7.9	1540	225
Hemp	32	1490	300
Bulk Polyester	2.9	1300	50
Bulk Nylon	2.5	1090	63
Carbon Fiber	300	1770	3430
Aramid Fiber	124	1450	3930
Polyester Fiber	13.2	1390	784
Nylon Fiber	3.9	1140	616
Alloy Steel	210	7800	1330

Since their Young's modulus is low, nylon and polyester seem to be the best suited fibres to use for the leash. It should be noted that when these materials are used in a braided rope, the rope's effective modulus is typically lower than the material modulus.

Table 2.2 presents some characteristics of five different ropes available from the *Cortland Companies* [30]. Of these, the Spectra® 12 strand is the one presently used for the leash and the three main tethers in the Penticton installation. It is important to consider not only the rope's elasticity but also its strength. Therefore, the diameter of each rope in Table 2.2 is chosen to have a minimum breaking strength of 24 kN in order to provide a sufficiently large safety factor. The product EA (Young's modulus multiplied by the sectional area of the rope) is calculated for the five ropes. This product is more relevant than the Young's modulus since it represents the stiffness of a one-metre rope.

Table 2.2. Product EA of five *Cortland Cable* ropes [30].

Cable Type	Diameter (mm)	Elongation at Break (%)	Breaking Strength (kN)	Young's Modulus (GPa)	Product EA (kN)
Plasma® 12 strand	5	4	24.5	41.6	817
Spectra® 12 strand	6	6	26.7	18.9	534
Polyester Double Braid	11	15	28.0	1.84	175
Nylon Double Braid	11	30	25.4	0.891	85
N/P Composite	16	30	43.6	0.678	136

The minimum breaking strength available with a N/P Composite rope is 43.6 kN, which is almost double the breaking strength of the Plasma rope. For this reason, even if its Young's modulus is smaller, its product EA is higher than that of the Nylon Double Braid.

Since the Nylon Double Braid has the smallest product EA of the ropes considered, this type of rope should be used to reduce the motion of the confluence point if we want to use a conventional type of rope. However, the Nylon Double Braid only decreases the stiffness of the leash by one order of magnitude. As such, from Figure 2.5, we see that its effects on the confluence point motion are minimal: it reduces the rms position error from 19 cm to 18 cm.

A much lower stiffness could be achieved by using a rubber bungee rope as the leash. This type of bungee cord is commonly used in applications such as "bungee jumping". It is currently possible to design a bungee cord that can hold a load of 3.6 kN with an elongation of 400% (see Chapter 4). Such a bungee cord has a Young's modulus of about 0.85 MPa and a diameter of about 3.8 cm. Its breaking strength is approximately 6 kN and thus four times lower than the breaking strength of the Spectra cable presently used in Penticton. Nevertheless, since a separate Spectra cable would back the bungee leash in case of failure, the safety factor of the bungee can be lower. The product EA of such a bungee leash would be approximately 1 kN, which is about three orders of magnitude less than the EA of a Spectra rope. By using a 200-metre bungee leash, the confluence point rms motion could be decreased from 19 cm to 7 cm according to the simulation.

However, we will see in Chapter 4 that because it can stretch to 400%, there is a practical limit to the length of a bungee leash.

There are some drawbacks associated with a bungee leash. First, it would be much heavier than a conventional rope. Secondly, a tether parallel to the bungee leash would have to be installed for two reasons: (a) as explained in the previous paragraph, a safety cable is needed since the safety factor of a bungee rope would be too low and (b) the electrical wires that connect the aerostat to the ground need the protection of a stiff rope or they will break. Other operational constraints arising from the use of the bungee leash will be discussed in Chapter 4.

2.6.2 Passive Heave Compensation of the Leash

A passive heave compensation system for an underwater remotely operated vehicle system was discussed in [27]. In that application, the mean tension was also very large relative to the tension variations. As can be seen in Figure 2.13, the proposed design uses a pneumatic spring and an accumulator to control respectively the stiffness and the pretension of the compensator. A system of pulleys is included to increase the working length of the compensator.

The passive compensation system presented in [27] appears well suited to our application since (a) the operational problems it addresses are very similar to ours and (b) the pneumatic solution it proposes would be relatively lightweight. In order to determine the complexity that such a passive alleviation would add to the system, we adapt this compensator design to our application.

First, to obtain a reasonably compact system we assume that the pneumatic piston would have a length of 0.5 metre and a stiffness of 1 N/m, the stiffness that resulted in the lowest confluence point rms motion in the previous section. According to the simulations done in Section 2.5, such a passive heave compensator would need a travel of approximately 64 metres. Therefore, a system of seven pulley loops would be needed to get that working length from a 0.5-metre piston ($\frac{64}{2^7} = 0.5$). This system of pulleys would add weight and complexity to the passive compensator.

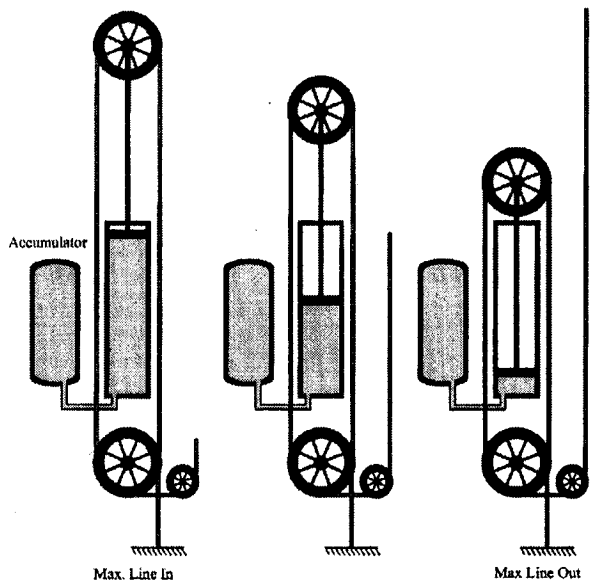

Fig. 2.13. Representation of a passive heave compensation system [27].

According to [27], the volume of the accumulator can be found from:

$$V_R = \frac{A_p \delta_T}{a\left(\frac{1+p}{1-p}\right)^{1/n} - 1} \tag{2.3}$$

where p represents the amplitude of the tension perturbations as a fraction of the mean load, A_p is the piston section, a is the number of pulley loops, δ_T is the working length and n is the ratio of specific heats of the gas which is 1.4 for air. We have already determined that $a = 7$ and $\delta_T = 64$ metres. Once again to obtain a reasonably compact system, we assume a compensator piston diameter of 15 cm, which would have an area of approximately 0.002 m^2. To assess the value of p, we simulate the system with the passive compensator of Subsection 2.5.1 and find that the minimum, the mean and the maximum leash tension values are respectively 2553 N, 2573 N and 2610 N.

Therefore,

$$p = \max\left(\frac{2610-2753}{2753}, \frac{2753-2553}{2753}\right) \cong 0.015$$

and using Equation 2.3 we find an accumulator volume of 0.02 m^3.

This means that the accumulator could be a cylinder of 20 cm diameter with a stroke of 65 cm. The maximum pressure inside the accumulator would be

$$P_{\max} = \frac{aT_{\max}}{A_p} = \frac{7 \cdot 2610}{0.002} = 9.2\,\text{MPa}$$

The values found for the accumulator volume and the maximum pressure appear reasonable and it is likely that a passive heave compensator based on this design would be feasible in practice. However, this mechanism has a few drawbacks, the first of which is weight. A more detailed design would have to be performed to determine the weight of a passive heave compensator but at this point we know that an accumulator, a pneumatic spring, a system of pulleys and the structure needed to maintain everything in place would likely require significant additional aerostat lift. For this reason it would likely be impossible to test such a device in the Penticton facility as the excess lift of that aerostat is limited. On the other hand, since the aerostat of the full-scale LAR will be designed in accordance with the system weight, the passive compensator could likely be accommodated in that design.

Another disadvantage of a passive heave compensator is its complexity. Adding an accumulator, a pneumatic spring and a pulley system with seven loops to the tethered aerostat system would increase the risk of a malfunction. It should also be noted that the compensator would need an additional subsystem to either adjust the pretension or the mean leash tension according to the wind conditions since the mean tension in the leash varies from 2440 N at a wind speed of 1 m/s to 3040 N at a wind speed of 10 m/s (the maximum operating condition). This variation could not be accommodated by the normal travel of a compensator with a stiffness of 1 N/m and working travel of 64 metres, and would therefore have to be dealt with, either by a system to adjust the accumulator pressure or a system to adjust the leash tension according to wind speed. In the next chapter, we discuss some active methods to stabilize the leash tension

2.7. Comparison of the Passive Methods

Table 2.3 compares the several passive methods discussed in the present chapter. This comparison is based on the simulation performance and the design implications of the different approaches.

The analysis done in this chapter showed that only two passive methods for reducing the confluence point motion warrant further investigation: (a) replacing the Spectra leash by a bungee cable or (b) installing a passive heave compensator at the base of the leash. Although the passive compensator has better performance, we chose to implement the bungee leash due to its relative simplicity. Its design is considered in greater detail in Chapter 4.

Table 2.3. Comparison of the passive methods.

Passive Methods	Characteristics	RMS error (cm)	MAX error (cm)	Design Implications	Comments
Baseline system	- Spectra® 12 strand - EA = 817 kN	19	41	- None (Presently implemented)	- Works reliably
Nylon Double Braid leash	- EA = 85 kN	18	42	- Very easy to adopt	- Feasible - Not very effective
Bungee leash	- EA = ~ 1 kN	7.0	16	- Weight issue	- Feasible - See Chap. 4
Constant force spring	- Force = 2.6 kN - Length = 60 m	5.0	10	- Requires a system to adjust mean leash tension	- Not practically feasible
Passive heave compensator	- Stiffness = 1 N/m - Travel = ~ 60 m - Pretension = 2.6 kN	4.0	8.0	- Weight issue - Complexity issue	- Feasible - Not further discussed

Chapter 3

Preliminary Study of Active Alleviation Methods

3.1 Introduction

In this chapter, a preliminary study of two active alleviation methods is performed using the simulation presented in Chapter 2. In order to compare these active methods to the passive methods discussed in the previous chapter, they are applied to the same simulated baseline system. The rms error of the confluence point position is again used to evaluate the performance of each method.

For the reason presented in Chapter 2, that more than 90% of the payload perturbations come from the aerostat through the leash, the two active methods studied in this chapter also address the perturbations coming from the aerostat. These methods are aerostat pitch control and active heave compensation.

3.2 Aerostat Pitch Control

Since the lift and the drag of a streamlined aerostat are functions of its pitch angle, controlling the pitch of such an aerostat may help reducing the variations in the leash tension and therefore reduce the confluence point motion. In this section, the effect of aerostat pitch control on the confluence point stabilization is studied. Since some of the pitch controllers studied use the aerostat harness geometry, we will first describe it in detail. Note that the aerostat pitch control method is functional only if a streamlined aerostat is used.

3.2.1 Aerostat Harness

The harness of the Penticton facility aerostat has 15 loops on each side. As can be seen in Figure 3.1, each side is composed of four levels of loops: the first level has eight loops, the second level has four loops, the third level has two loops and finally the fourth level has a single loop. The ends of the eight loops on the first level are solidly fixed to the aerostat. All the other loop ends are rings that slide on the previous level of loops. The two lowermost loops (one on each side) are fixed together at a point where the leash is solidly attached.

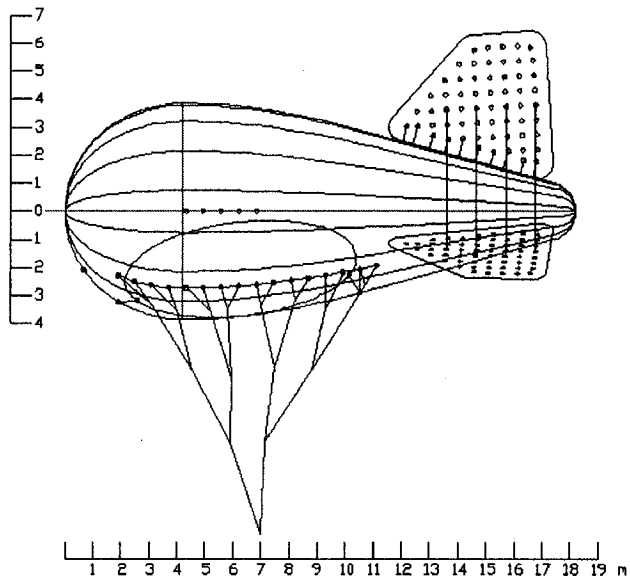

Fig. 3.1. Penticton aerostat and harness.

The dynamics of this harness has been analysed by Teodorescu [34]. She assumed for simplicity that the ends of the loops on the first level lay on a horizontal line and that the loops were always in tension. It was found in this study that for a fixed leash attachment point on the harness, the harness behaves exactly like a rigid body. Furthermore, it was found that when the leash attachment point on the harness is displaced, the harness geometry varies and the leash attachment point follows an elliptical curve with parameters a = 8.56 m and b = 7.94 m, where a and b are the major and minor semiaxes of the ellipse. Consequently, the leash attachment point trajectory would be the same if the harness was a single 17.13-m-long loop with its two fixed ends attached 6.41-m apart on the aerostat.

Using the results of [34], the simulation incorporates two fourth degree polynomials that give us the leash attachment point position with respect to the aerostat center of mass (see Figure 3.2a) as a function of the length of the forward part of the harness lowermost loop (l_{4F}). These two polynomials are [34] :

$$Xl = 1.42 - 3.18l_{4F} - 0.119l_{4F}^2 + 1.37 \cdot 10^{-2} l_{4F}^3 - 3 \cdot 10^{-5} l_{4F}^4 \tag{3.1}$$

$$Zl = 1.55 - 13.0l_{4F} + 5.69l_{4F}^2 - 1.17l_{4F}^3 + 9{,}84 \cdot 10^{-2} l_{4F}^4 \tag{3.2}$$

Since the Penticton harness lowermost loop is 6-m long, we use a value of 3 m for l_{4F} in the simulation to represent the fixed-attachment-point case where the leash is attached at the center of the lowermost loop.

Is it to be noted that the harness amplifies the motion of the leash attachment point. Indeed, we find that for a displacement of 1.4 metres on the harness (±0.7 metre from the centre of the lowermost loop), the leash attachment point motion is approximately 5 metres longitudinally and 0.3 metre vertically (see Figure 3.2b). Thus, a small displacement of the leash attachment point on the harness can have a large effect on the pitch of the aerostat.

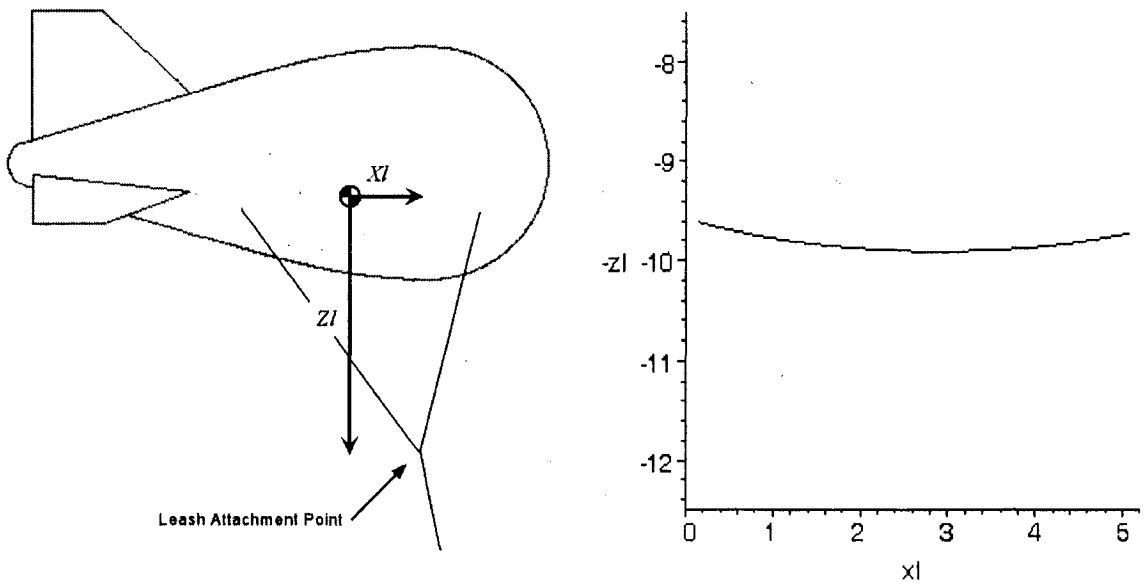

(a) **(b)**

Fig. 3.2. Leash attachment point position with respect to the aerostat centre of mass for a displacement of 1.4 metres on the harness.

3.2.2 Pitch Control

We can change the aerostat pitch by two different actuation methods: (a) by actively controlling the leash attachment point on the harness or (b) by actively controlling the aerostat lateral tailfins. As is illustrated in Figure 3.3, moving the leash attachment point forward pitches the aerostat nose down and moving it rearward pitches the aerostat nose up.

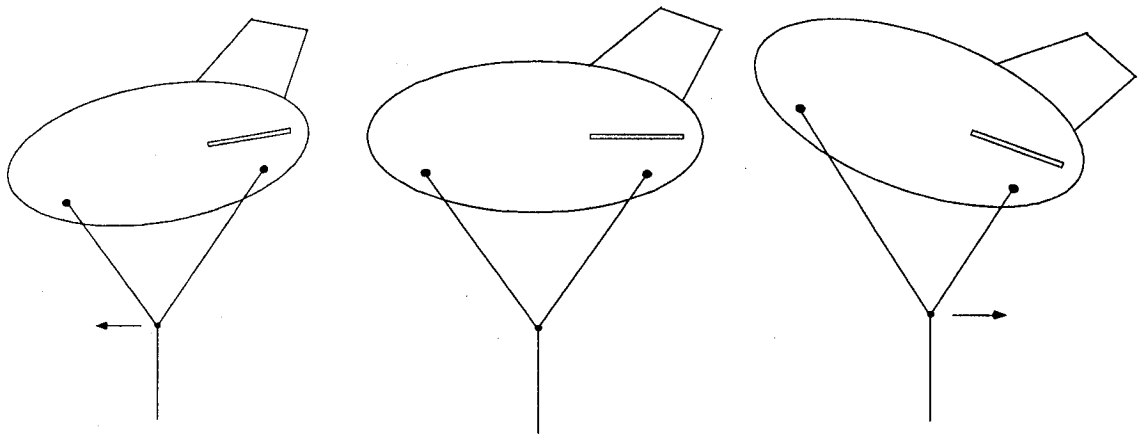

Fig. 3.3. Aerostat pitch controlled using the leash attachment point position.

Figure 3.4 shows how leading-edge-up rotation of the aerostat lateral tailfins pitches the aerostat nose down and a leading-edge-down rotation of the tailfins pitches the aerostat nose up.

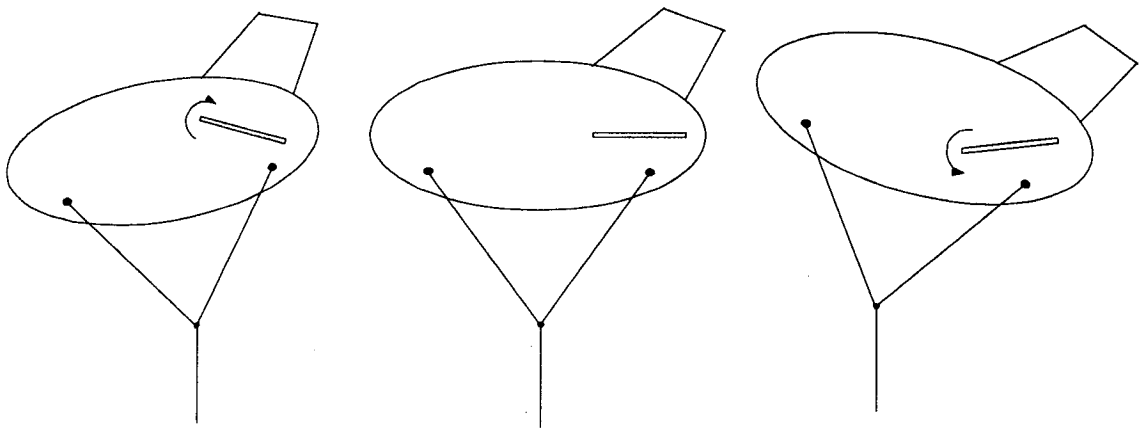

Fig. 3.4. Aerostat pitch controlled using lateral tailfins deflection.

For each of these two actuation techniques, a pitch controller could use one of the following measured states as the feedback variable: the aerostat altitude, the payload

altitude or the leash tension. Indeed, since varying the aerostat pitch affects these states and all are correlated to the confluence point motion, stabilizing them with a pitch controller would have the effect of reducing the payload position error. Therefore, combining the two actuation techniques and the three measured states generates six different pitch control methods that are studied in this section.

For each method, a PID controller is implemented in the simulation. These PID controllers generate a command according to the following formula by using a general error term *e(t)*:

$$\Delta d(t) = k_p e(t) + k_d \dot{e}(t) + k_i \int e(t)dt \tag{3.3}$$

where t is time, k_p, k_i and k_d are the PID gains and $\Delta d(t)$ is the commanded change in leash attachment position or the commanded change in aerostat lateral tailfins angle. The leash attachment position and aerostat lateral fins angle variations are relative to the values used in the uncontrolled baseline system, which are respectively 3 metres and 5.7 degrees. The error *e(t)* is function of the chosen measured state and is calculated according to one of the following three equations:

$$e(t) = \begin{pmatrix} H(t) - H_d & \text{for the Aerostat Altitude} \\ h(t) - h_d & \text{for the Payload Altitude} \\ T(t) - T_d & \text{for the Leash Tension} \end{pmatrix} \tag{3.4}$$

where $H(t)$ and H_d are the measured and desired aerostat altitudes, $h(t)$ and h_d are the measured and desired payload altitudes and $T(t)$ and T_d are the measured and desired leash tensions. The desired values for the aerostat altitude, the payload altitude and the leash tension come from baseline system static equilibrium values and are respectively 383 metres, 172 metres and 2.6 kN. The gains for each controller were optimized manually. Table 3.1 presents the confluence point position rms error produced by the six different pitch controllers.

Table 3.1. Confluence point rms error produced by different pitch controllers.

Pitch controller #	Actuation method	Feedback variable	k_p	k_i	k_d	RMS error (cm)
No controller	-	-	-	-	-	19
1	**Leash attachment point position**	Aerostat altitude	1.5	0.0	0.1	13
2		**Payload altitude**	**3.0**	**1.0**	**0.01**	**7.0**
3		Leash tension	0.7	0.0	0.0	16
4	Aerostat lateral tailfins deflection	Aerostat altitude	2.0	0.0	0.1	14
5		Payload altitude	2.0	0.1	0.3	7.0
6		Leash tension	2.5	0.1	0.1	10

From these results, it is found that a pitch controller could reduce the confluence point rms error of the baseline system from 19 cm to a value as low as 7 cm. The pitch controllers that look most promising are the two payload altitude controllers. Furthermore, it is to be noted that unlike the other controllers, controller #3 quickly becomes unstable as we increase its gains in the simulation. This instability would have to be further analysed to understand its exact cause.

It is emphasized that the PID gains were optimized manually. Therefore, the payload rms error may be further reduced if the gains were optimized more rigorously or if another control method was used. From the results presented in Table 3.1, we cannot conclude whether better payload stabilization would be achieved with an attachment point controller or with control of the lateral fins. In Section 3.4, we discuss the design implications of these two actuation methods.

The time history of the baseline system with pitch controller #2 is presented in Figure 3.5 as an example of the system behaviour with a pitch controller.

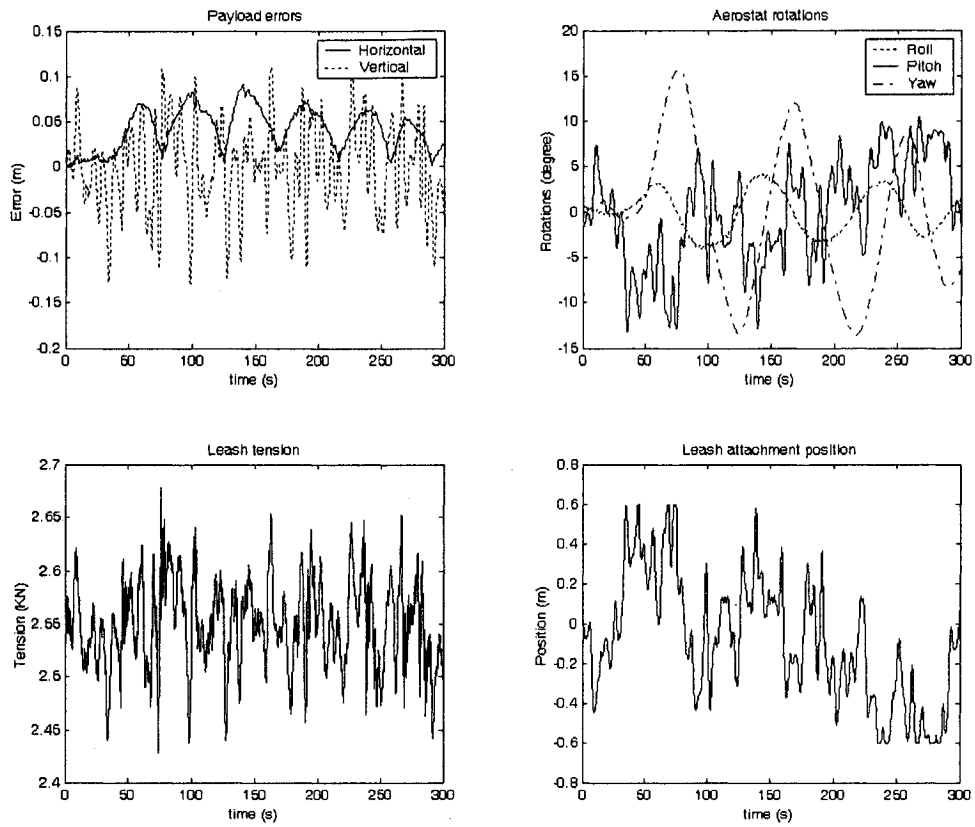

Fig. 3.5. Baseline system with pitch controller #2.

By comparing this figure to the baseline case shown in Figure 2.2, we observe that in addition to reducing the payload error out of the focal plane, an Attachment Point – Payload Altitude controller reduces the leash tension variation and increases the aerostat pitch variation from a few degrees to approximately 20 degrees.

From Figure 3.5, we see that such a pitch controller would need a total displacement on the harness of approximately 1.4 metres, which seems quite reasonable. Furthermore, we find from the simulation that the maximum speed of that controller would need to be around 0.7 m/s. For the tailfin controller #5, the fin deflection and angular speed would need to be around 40 degrees and 20 degrees/s, respectively.

3.3 Active Heave Compensation of the Leash

We saw in Chapter 2 that confluence point motion is closely related to leash tension variation. We saw that if we could stabilize the leash tension magnitude perfectly, the payload perturbations would be reduced by at least 75%. In this section, we implement an

active heave compensator, which would be essentially a motor mounted at the payload used to stabilize the leash tension; and we study its effect on the confluence point motion.

The active heave compensator studied uses leash speed control to maintain the leash tension at a desired equilibrium value. To study this leash speed controller, the following PID controller is implemented in the simulation:

$$\dot{L}_u(t) = k_p e(t) + k_d \dot{e}(t) + k_i \int e(t)dt \tag{3.5}$$

where $L_u(t)$ is the unstretched leash length at time t, and k_p, k_i and k_d are the PID gains. The error term $e(t)$ is given by:

$$e(t) = T(t) - T_d \tag{3.6}$$

where $T(t)$ corresponds to the actual leash tension and T_d to the desired leash tension, which corresponds to the baseline system initial value of 2.6 kN. In the simulation, the leash length change is applied to all the leash elements.

The gains used were optimized by trial and error: k_p = 0.7 s/kg, k_d = 0 s^2/kg and k_i = 0.7 kg^{-1}. With these gains, the leash speed controller reduces the confluence point rms motion from 19 cm for the baseline system to 12 cm. Figure 3.6 presents the baseline system behaviour with leash speed control. As we can see in that figure, the working length needed with such a controller would be approximately 50 metres, while its required speed would be approximately 1 m/s.

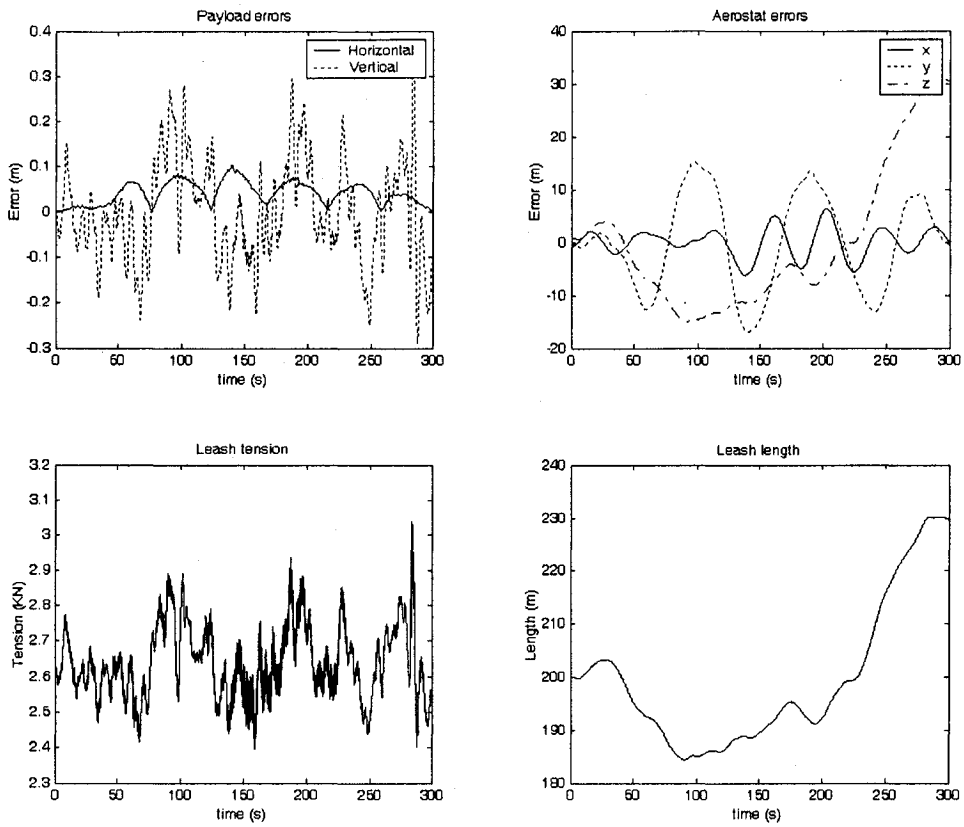

Fig. 3.6. Baseline system with leash speed control.

By comparing this figure to the baseline system case shown in Figure 2.2, we see that such a leash speed controller would decrease the payload error in the vertical direction and increase the leash tension variation frequency.

Furthermore, we find that the leash length variation of such a controller is quite similar to that of a constant force spring (see Figure 2.8). This similarity raises the following possibility: could we transform the active heave compensator with leash speed control into an active constant force spring? Indeed, by supplying a DC servo motor with a constant current, it produces a constant torque [35]. Therefore, rather than controlling the leash speed to stabilize its tension, we could simply use a servo amplifier to ensure that a constant current is supplied to the motor. Using this approach, it would be possible to achieve the performance of the constant force spring described in Section 2.4. The advantage of this active constant force spring approach is that the value of the constant current set point could be adjusted as a function of wind speed. This would then avoid the need for a separate means to compensate for changes in wind speed which we had

concluded was needed in case of the passive constant force approach. In the next section, we consider whether such an active constant force spring is feasible in practice.

3.4 Design Implications

As we did in Section 2.6, we now perform a preliminary evaluation of the design issues inherent in the different controllers discussed in Chapter 3. We focus our study on the complexity, the weight and the power consumption of each approach.

For all the active controllers examined in this chapter, only two types of sensor are required: a load cell and an altitude sensor. The existing multi-tethered system in Penticton already has a load cell at the leash as well as GPS receivers at the payload and at the aerostat. Furthermore, these sensors are planned to be included in the final LAR radio telescope as well. Therefore, the sensors are not considered to be an issue and this section focuses strictly on the design implications of the three actuation methods used in the different controllers discussed in this chapter. These are the actuation of the leash-harness attachment point, the actuation of the aerostat lateral tailfins as well as the actuation of an active heave compensator.

3.4.1 Leash Attachment Point Actuation

In this approach, a device that would control the leash end point displacement on the aerostat harness, shown schematically in Figure 3.7, would be installed between the leash and the harness. It would comprise a motor, a pulley, a geartrain and a structure to maintain everything in place. Such a device would add complexity and weight to the multi-tethered aerostat system. Because of its weight, it may be impossible to test the mechanism in the Penticton facility as the excess lift of the aerostat is limited, but this would not be a problem in the full-scale LAR since that aerostat could be sized in accordance with the system weight.

The advantage of a mechanism like this is that the motor could be relatively small since it would only have to exert the tension *difference* (ΔT) between the two ropes of the harness (see Figure 3.7). Indeed, when the leash attachment point is forced to move, the tension

distribution in the harness changes and the aerostat adapts its pitch to the new equilibrium.

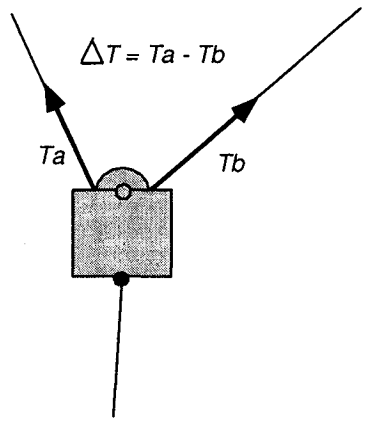

Fig. 3.7. Leash attachment point actuation device.

Because the device discussed here would force the attachment point to move by the use of a pulley, two issues must be considered: (a) the pulley would have to be designed to ensure the rope does not slip when the tension difference in the harness is at its maximum and (b) since the torque at the pulley shaft is only counterbalanced by the leash tension, the moment arm between the shaft and the application of the leash tension must be long enough to minimize rotation of the device. These issues are discussed in greater detail in Chapter 5 where we perform a more comprehensive study and a detailed design of the leash attachment point control device.

The maximum power consumption of a leash attachment point actuation mechanism is estimated to be around 1.5 kW. This power is computed for controller #2 studied in Section 3.2 by multiplying the magnitude of the tension difference in the harness by the magnitude of the leash attachment point speed. Presently in Penticton, 2 kW of electrical power is supplied to each of the three main winches of the multi-tethered aerostat system. Therefore, the 1.5 kW needed by the leash attachment point actuation device seems reasonable.

3.4.2 Lateral Tailfin Actuation

Actuating the tailfins of an aerostat is rarely done, though it occurs commonly in airships. There are two prevalent methods of constructing aerostat fins: rigid and inflatable [36].

The former would be more amenable to be actuated. Presently, the streamlined aerostat used in the Penticton facility has fixed inflatable tailfins (see Figure 3.8) and for this reason, it is very improbable that we could test a fin deflection controller in Penticton.

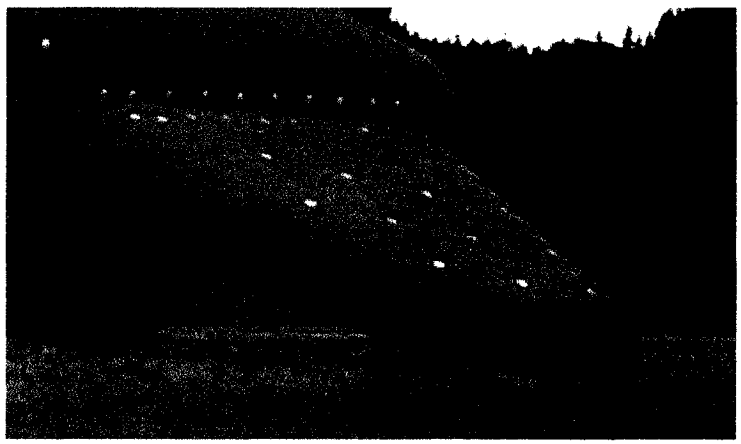

Fig. 3.8. Penticton aerostat lateral fin.

On the other hand, this idea could be implemented in the full-scale LAR if we designed an aerostat with rigid actuated tailfins. The body of such a fin would be solidly fixed to the hull of the aerostat and its rear flap would be actuated in order to modify its shape (see Figure 3.9) and therefore the pitch of the streamlined aerostat. Since the motor would only have to move the flap, rather than the entire fin, we expect that its size would be reasonably small. On the other hand, this method of actuation would also reduce the control authority.

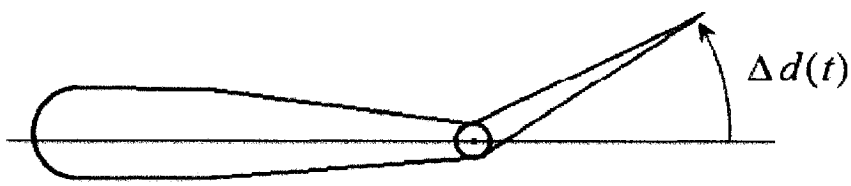

Fig. 3.9. Actuated lateral tailfin.

The primary drawback of this control approach is that the modifications required to implement aerostat tailfin actuation are relatively complicated compared to what would be needed to implement leash attachment point control, and that for similar performance. Therefore, we do not further discuss it and focus our detailed study in Chapter 5 on the leash-harness attachment point actuation method.

3.4.3 Active Heave Compensation Actuation

A device that controls the leash payout speed or better, directly the leash tension, would be installed on the payload platform and would add approximately the same amount of complexity as the leash-harness attachment point control mechanism: it would comprise a motor, an amplifier, a geartrain, a winch spool and the structure to maintain everything in place. However, the relative disadvantage of a leash speed active heave compensation mechanism, and also of an active constant force spring, is that the motor has to sustain the entire leash tension. For that reason, it requires a power of 3 kW, two times that of the attachment point controller. In addition, the fact that it must accommodate approximately 50 metres of cable also increases its weight. As a result, an active heave compensator would add much more weight to the system.

Like the leash attachment point controller, the weight of an active heave compensator could make it impossible to test in the actual Penticton system. However, it could be accommodated in the full-scale LAR since the aerostat will be sized in accordance with the system weight. Nevertheless, it must be noted that increased system weight leads to other problems, such as increased cost and complexity of the aerostat.

3.5 Comparison of Active Methods

Table 3.2 compares the active methods discussed in Chapter 3 and compares them to the existing system and to the bungee leash solution. This comparison is based on the simulated performance and the design implications of the different approaches.

The analysis done in this chapter shows that two active methods for reducing the confluence point motion warrant further investigation: (a) the leash attachment actuation pitch controller and (b) the active constant force spring. The latter achieves the same objective as the passive methods studied in Chapter 2: it reduces the leash stiffness. Since we saw in that chapter that the simplest way of reducing the leash stiffness would be to use a bungee leash, we choose not to study further this active method. Instead, the bungee leash solution is examined in greater detail in Chapter 4.

Aerostat pitch control, on the other hand, uses a completely different approach to reduce the confluence point motion: it directly addresses the aerostat perturbations rather than increasing the leash elasticity. Furthermore, the leash attachment point pitch controller achieves good performance with relatively little added weight and complexity. For these reasons, we focus exclusively on that active method in Chapter 5.

Table 3.2. Comparison of the active methods.

Active Methods	Characteristics	RMS error (cm)	MAX error (cm)	Design Implications	Comments
Baseline system	- Spectra® 12 strand - EA = 817 kN	19	41	- None (Presently implemented)	- Works reliably
Bungee leash	- Passive approach. - EA = 1 kN	7.0	16	- Weight issue	- Feasible - See Chapter 4
Leash attachment point pitch controller	- Power 1.5 kW - Travel = 1.4 metres - Max speed =0.7m/s	7.0	15	- Weight issue - Power issue	- Feasible - See Chapter 5
Fins deflection pitch controller	- Travel = 40 degrees - Max speed = 20 °/s	7.0	15	- Major complexity issue	- Feasible - Not further discussed
Active heave compensation: leash speed control	- Power 3 kW - Travel = 50 m - Max speed = 1 m/s	12	29	- Major weight and power issues	- Feasible - Not further discussed
Active constant force spring	- Power 3 kW - Travel = 50 m - Max speed = 1 m/s	5.0	10	- Major weight and power issues	- Feasible - Not further discussed

Chapter 4

Detailed Study of the Bungee Leash

4.1 Introduction

In Chapter 2, we saw that an effective means of improving the performance of a multi-tethered aerostat system was to decrease the leash stiffness. We also saw that replacing the Spectra leash by a bungee cable would be the simplest way of accomplishing this. In this chapter, we perform a detailed design of this device and implement it at the Penticton facility in order to validate its performance experimentally. The structure of this chapter is as follows: In Section 4.2, we design the bungee cable system for the planned experiment. In Section 4.3, the Penticton test set-up and procedure are explained. The results of the tests are then presented and interpreted in Section 4.4 and finally, general conclusions on the bungee leash approach are discussed in Section 4.5.

4.2 Bungee Leash Design

In this section, we design the bungee leash arrangement that replaces the existing Spectra leash for the experiment. We first study the many different bungee cables available on the market and select one that best suits our requirements. Since the lift of the Penticton aerostat is limited, a crucial issue of this design is the minimization of the weight added to the system. We then design the complete bungee leash arrangement, and finally, the expected performance of this system is presented.

4.2.1 Choice of the Bungee Cable

There are many companies that supply bungee cables, but most of them do not divulge detailed technical data about their products. In order to have a better idea of what elasticity can be achieved in practice, we obtained and tested eight different bungee samples from four different companies: *McMaster-Carr*, *Reef Scuba Accessories*, *Bungee Experience* and *Bungee Consultant International* (*BCI*) [37]. The sample from *BCI* was completely made of rubber and 1.5" thick. The other samples were all sheathed with nylon or polyester and their thickness varied from 5/16" to 1". We analysed different bungee thicknesses to keep open the possibility of using more than one cord in parallel for the Penticton experiment.

To characterize the stiffness of each bungee sample, we measured their elongation under different loads in a laboratory. We first attached the sample cord to a S-type load cell fixed at the ceiling. Using a hydraulic lift, we then attached the bottom end of the cord to a 205-kg load, a garbage container filled with concrete. Finally, we gradually transferred the load from the hydraulic lift to the bungee cord while recording the load cell reading at every tenth of metre. A photograph of the experimental apparatus is shown in Figure 4.1. The bungee cord being tested in this figure is the pure rubber sample provided by *BCI*. Using a tensile testing machine, we also separately performed two tensile tests on *Bungee Experience* 5/8" samples. Both times the cord failed at a load of approximately 360 kg. However, this value should be viewed as a lower breaking load since the cords were weakened by the buckles used to fix the cords in the tensile apparatus.

The first conclusion of this laboratory study is that stiffness and weight could be minimized if we choose a pure rubber bungee cable. This is a result of the fact that the elongation curve of the sheathed bungee cables is non-linear, while the curve for the pure rubber cables is linear. An example of a non-linear elongation curve is given in Figure 4.2 for the *McMaster- Carr* 3/4" sample. The slope of the curve represents the stiffness of the bungee cable.

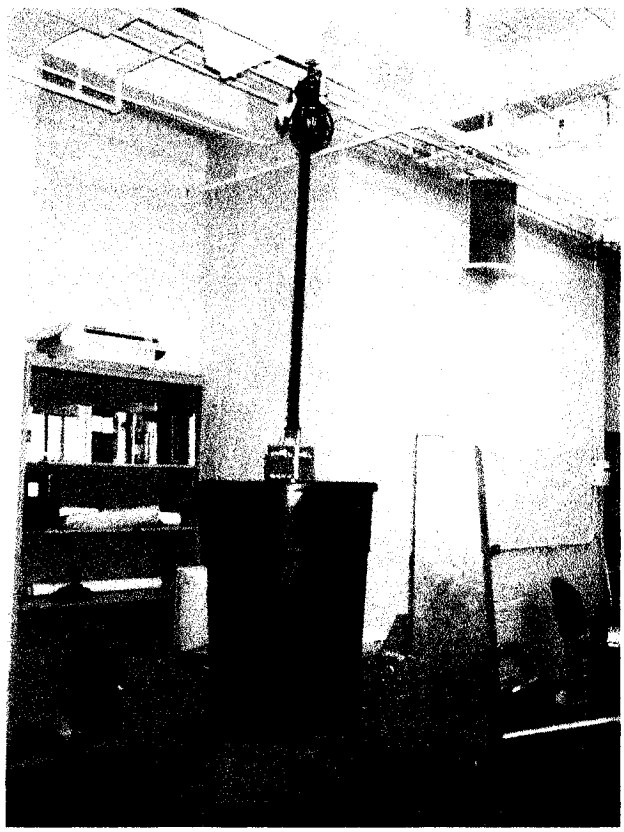

Fig. 4.1. Bungee stiffness characterization experimental setup.

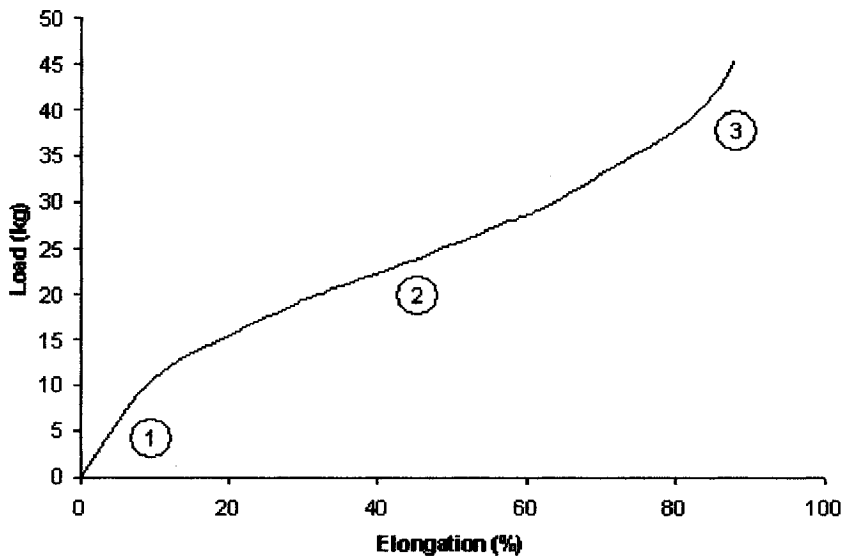

Fig. 4.2. Example of elongation curve for a sheathed bungee cable.

The curve of Figure 4.2 can be partitioned into three distinct sections: The first section of the curve, with high stiffness is due to the fact that during the manufacture of the sheathed

bungee cables, the rubber core is initially stretched and then covered with the sheath, which keeps the rubber in tension. This pretension has to be overcome before the covered bungee enters in its linear section, where the fibres are relaxed and do not interfere with the rubber. In the third section of the elongation curve, the sheath covering the rubber core extends and starts to take the load. This has the effect of gradually increasing the stiffness of the cable and thus the slope of the curve.

Consequently, sheathed bungee cables are less appropriate for our application since the sheath increases the cable stiffness when the load exceeds a certain limit. Furthermore, the elongation curve of a sheathed bungee is more difficult to predict than that of a pure rubber. The latter curve is linear and depends only on its section area, making it simpler to design the bungee leash with a pure rubber cable.

Another conclusion from our study is that the complexity, the stiffness and the weight of the bungee leash would be minimized if we could use a single cord whose maximum elongation matches the maximum expected leash tension. This leads us to custom-made bungee cords. Only two companies were willing to manufacture custom-made cords: *Bungee Experience* based in California and *Bungee Consultant International* based in Ontario. Since *BCI* appeared to be more familiar with the technical aspects of their product, we chose them to supply a pure rubber custom-made bungee cable.

We also used the experimental setup previously presented (see Figure 4.1) to estimate the damping ratio of the *BCI* pure rubber bungee sample. Indeed, by placing the entire 205-kg load on the bungee sample, making it oscillate vertically and recording the tension in the cord, we obtained a load oscillation curve shown in Figure 4.3, from which we extracted the damping ratio. By repeating this experiment ten times and averaging the results, a value of 0.025 was obtained for the damping ratio of the *BCI* bungee sample.

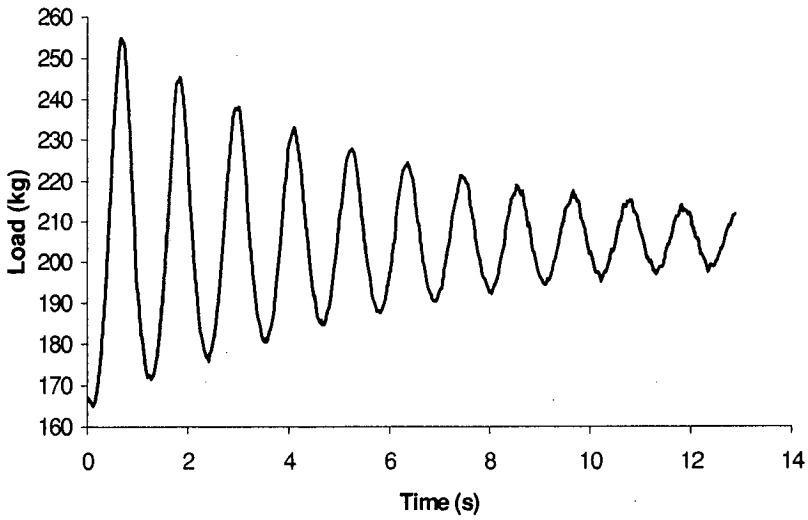

Fig. 4.3. Load curve used to estimate the damping ratio of the *BCI* sample.

4.2.2 Design of the Bungee Leash Arrangement

The design of the pure rubber custom-made bungee leash was iterative and performed over a few months. We started by measuring the properties of the bungee sample provided by *BCI*. These properties are summarised in Table 4.1. Another important piece of information provided by *BCI* is that the pure rubber used in their bungee cables behaves linearly up to an elongation of 400% and that it should be viewed as a maximum limit. We estimated from past experimental data from the Penticton facility that the bungee leash would have to sustain peak and mean loads of 320 kg and 195 kg respectively. Furthermore, we wanted to obtain a mean stretched length of about 150 metres.

Table 4.1. Properties of the *BCI* bungee sample.

Unstretched length	0.46 m
Unstretched diameter	3.56 cm
Unstretched section area	10^{-3} m^2
Weight	0.535 kg
Weight/metre	1.16 kg/m
Stretched length (under 205 kg)	1.47 m
Elasticity	1.07 %/kg
Damping ratio	0.025
Young's modulus	8.5×10^5 Pa

For a maximal bungee cable elongation of 400% under a load of 320 kg, a cable elasticity of 1.25 %/kg was needed, which gave an elongation of 244 % under a load of 195 kg. Therefore, an unstretched bungee length of $150 \cdot 100/344 = 44$ metres was necessary in order to have a mean stretched length of 150 metres. From the bungee sample elasticity, we extrapolated the bungee leash unstretched weight per metre to be $1.16 \cdot 1.07/1.25 = 1.0$ kg/m, which gave a bungee leash weight of 44 kg. For such a design, the leash stiffness would be 18 N/m.

We then performed another test on the bungee sample to study the creep effect. We found that, with time, the stiffness of the bungee sample tended to decrease substantially when loaded. Using the test setup presented in Subsection 4.2.1, we put the bungee sample under a load of 205 kg for a period of five hours. Once per hour, we oscillated it manually for one minute. The final length of the sample bungee cord was 1.70 metres. In order to take into account the fact that the bungee leash might lose some of its stiffness during operation and consequently elongate another 50%, we redesigned a bungee leash that elongated 350% under maximum load, which was revaluated to 367 kg according to new experimental data from the Penticton facility.

Since these two design adjustments had the effect of increasing the bungee leash weight and that the weight of the previous design was already considered to be heavy relative to the Penticton aerostat spare lift, we opted to accept higher leash stiffness and design a part bungee – part Spectra leash. The length of the Spectra part was chosen to be 80 metres, giving a mean stretched length for the bungee part of approximately 70 metres. The elasticity of the leash bungee part was computed to be $350\%/367kg = 0.95$ %/kg, which corresponds to an elongation of 185% under a mean load of 195 kg. An unstretched bungee length of $70 \cdot 100/285 \approx 24$ metres was necessary in order to have a mean leash length of 150 metres. This 24-metre custom-made bungee cord was finally supplied by *BCI* and its weight was measured to be 28 kg (see Figure 4.4). Additionally, the weight of the 80-metre leash Spectra part was measured to be 11 kg. Summarizing, for the final design, the leash stiffness was reduced from 5300 N/m for the original Spectra leash to approximately 40 N/m.

Fig. 4.4. Custom-made bungee cord.

A backup Spectra cable parallel to the bungee part was added to the bungee leash arrangement for multiple reasons: (a) to power the instruments on the aerostat, (b) to help deploy and retrieve the aerostat, and (c) for safety issues. This backup cable was designed to prevent the leash bungee part from elongating beyond 400% and therefore was 120 metres long. Figure 4.5 shows the three components of the bungee leash arrangement.

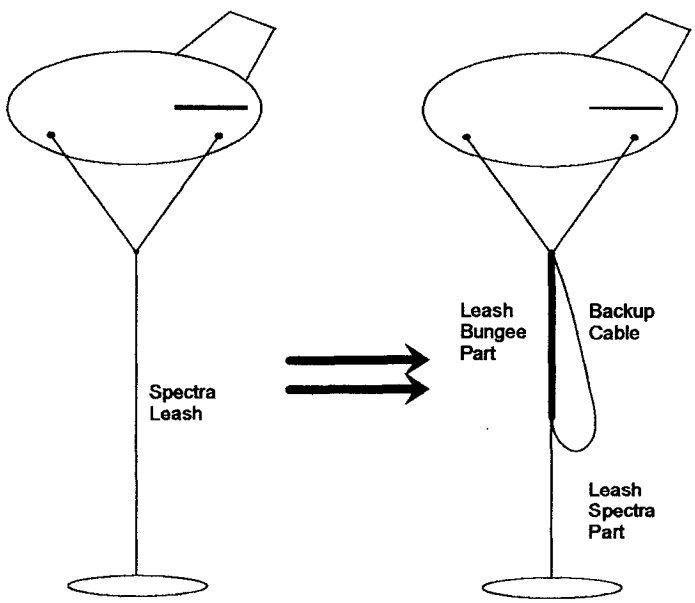

Fig. 4.5. The three components of the bungee leash arrangement.

The total weight of the bungee leash arrangement designed in this subsection is 57 kg. In order to only measure the effect of the leash stiffness on the Penticton aerostat system, we planned to perform both Spectra and bungee leash experiments with the same bungee leash arrangement and then compare their respective payload stabilization. Figures 4.6a and 4.6b show the bungee leash arrangement configurations for both test flights. For the Spectra leash experiment, the leash Spectra part and the backup cable take up the load while in the bungee leash experiment, the leash bungee and Spectra parts take up the load. The aerostat launching and landing procedures with the bungee leash arrangement are discussed in Section 4.3.

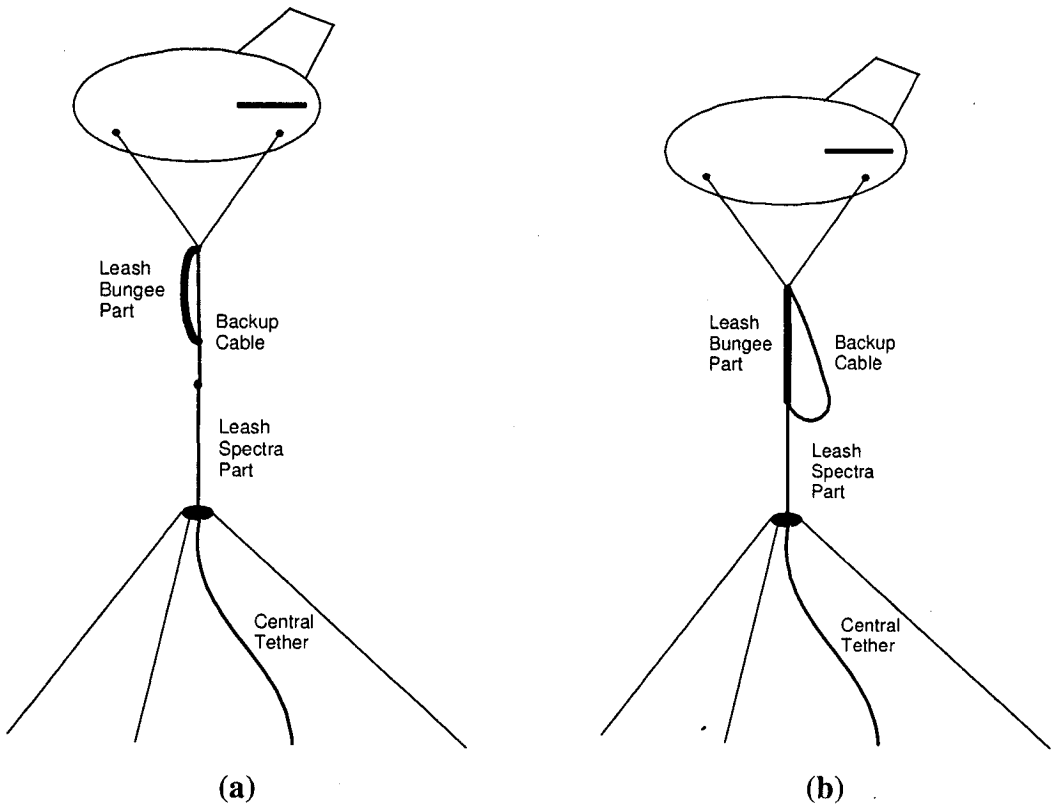

Fig. 4.6. (a) Spectra leash and (b) bungee leash configurations.

4.2.3 Bungee Leash Performance

In order to predict the relative performance of the bungee leash and the Spectra leash, the two configurations shown in Figure 4.6 are implemented in the simulation to replace the leash of the baseline system used in Chapters 2 and 3. The Spectra leash configuration is

implemented by adding the total bungee mass of 28 kg at the baseline leash top node. The bungee leash configuration is implemented by using two types of leash element: the upper two elements have properties consistent with the bungee material and a total unstretched length of 24 metres, while the lower two elements retain the properties of Spectra and their total unstretched length becomes 80 metres. The total mass of the backup cable is added at the leash top node. For both configurations, the net lift of the aerostat is decreased from 2.67 kN used in the baseline system to 2 kN, to reflect the lift expected during the test in Penticton.

Replacing the leash of the baseline system by these two configurations in the simulation, we find that the bungee leash would reduce the confluence point position rms motion from 43 cm for the Spectra configuration to 30 cm (see Figure 4.7).

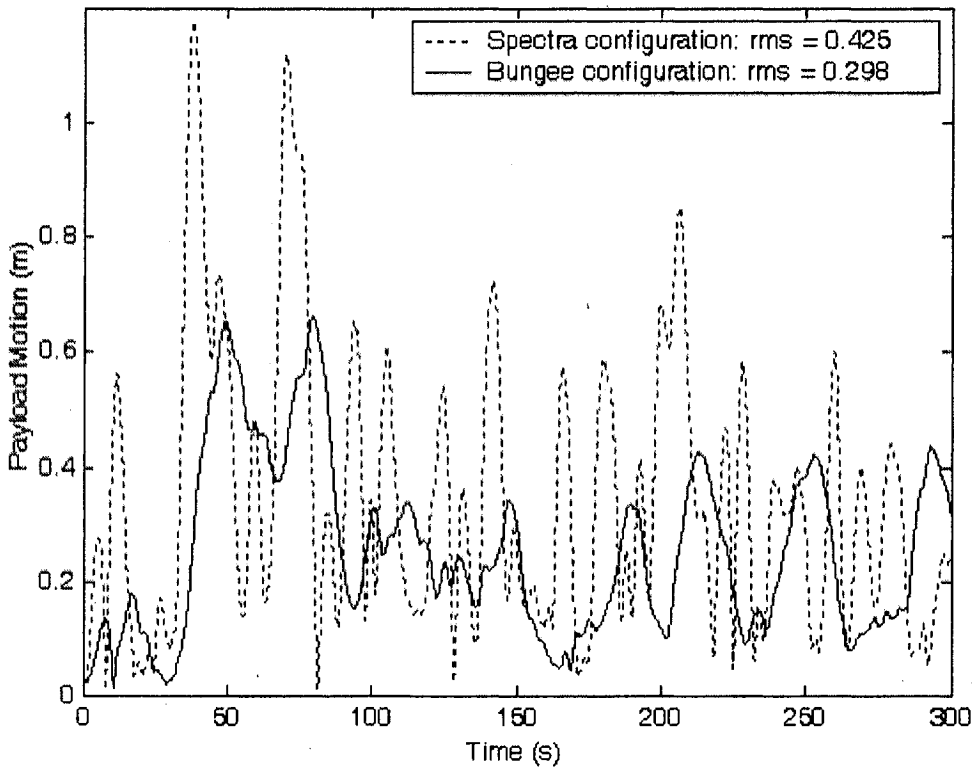

Fig. 4.7. Payload motion for the Spectra and bungee leash configurations.

These results are quite different from what was obtained in Chapter 2: a reduction of the payload rms motion from 19 to 7 cm with the bungee leash. This discrepancy is partly explained by the difference in stiffness of the bungee leash: the stiffness of the 200-m

leash simulated in Subsection 2.6.1 (5 N/m) is eight times less than the stiffness of the 24-m bungee leash studied here (40 N/m). However, the main reasons for this difference are the decreased aerostat net lift and the weight added by the leash bungee part for both configurations. Indeed, the confluence point motion varies inversely with the amount of aerostat net lift, as illustrated in Figure 4.8. A curve for the baseline system leash is also added in this figure to highlight the effect of the bungee weight on the system. Indeed, for an aerostat net lift of approximately 2 kN, the bungee leash leads to worse performance than with the baseline system leash, which has half the weight. With this lift, the detriment due to the increased weight of the bungee leash is greater than the benefit due to its lower stiffness. However, this low-weight baseline leash is not used for the experiment discussed here. As we can see in Figure 4.8, when the Spectra and the bungee leashes weigh the same, the use of a bungee leash always improves the system performance.

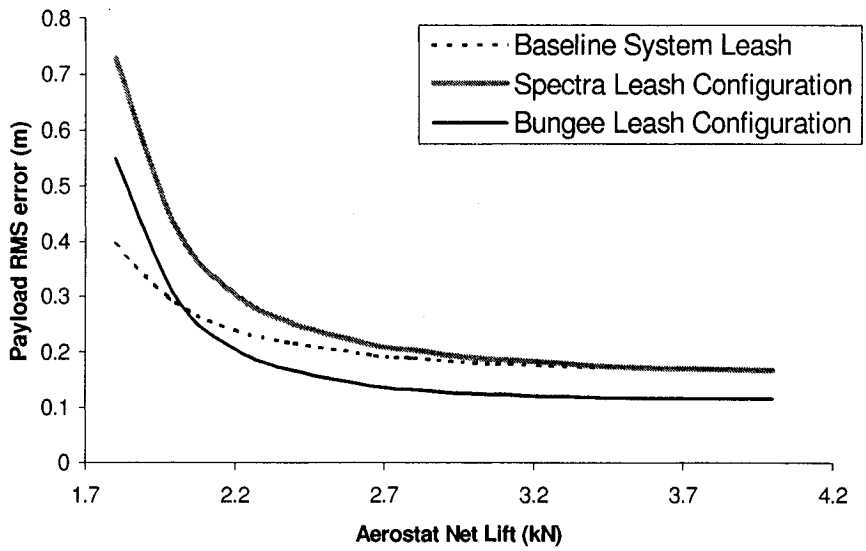

Fig. 4.8. Payload rms error in function of aerostat net lift.

In Table 4.2, we present more details on the comparative performance that would result from the replacement of Spectra leash by the bungee leash of equal weight, for an aerostat net lift of 2 kN and 2.67 kN. This table shows the horizontal and vertical components of the payload and aerostat rms displacement; the ratio of aerostat rms displacement to the

payload rms error ratio in both directions; the leash tension rms variation; and the ratio of that rms variation to the payload rms motion.

As can be seen in Table 4.2, the bungee results in an increase in the vertical motion of the aerostat, which is intuitively reasonable. Furthermore, note that the apparent reduction in aerostat horizontal motion with the bungee leash is due to shorter bungee leash (mean stretched length of 150 m) than Spectra leash (200 m). Also note in Table 4.2 the large increase in vertical ratio aerostat/CP with the bungee leash.

Table 4.2. Simulated Spectra and bungee leashes comparison.

	Lift = 2 kN			Lift = 2.67 kN		
	Spectra	Bungee	Δ (%)	Spectra	Bungee	Δ (%)
CP rms error (m)	0.425	0.299	-29.6	0.211	0.134	-36.8
CP rms horizontal error (m)	0.101	0.110	8.9	0.053	0.051	-3.8
CP rms vertical error (m)	0.413	0.278	-32.7	0.205	0.124	-39.5
Aerostat rms error (m)	11.76	9.70	-17.5	10.47	8.66	-17.3
Aerostat rms horizontal error (m)	11.75	9.29	-20.9	10.47	8.21	-21.6
Aerostat rms vertical error (m)	0.58	2.79	381.0	0.36	2.74	661.1
Leash tension rms variation (N)	171.4	138.6	-19.1	204.7	152.1	-25.7
Ratio aerostat/CP (-)	27.67	32.48	17.4	49.53	64.50	30.4
Horizontal ratio aerostat/CP (-)	116.36	84.22	-27.6	198.93	160.82	-19.1
Vertical ratio aerostat/CP (-)	1.39	10.07	624.5	1.76	22.04	-2.7
Ratio tension/CP (N/m)	403.3	464.3	15.1	968.5	1133.0	17.0

We observe in Table 4.2 that the bungee leash has two beneficial effects on the system other than a payload rms motion reduction: (a) it reduces the leash tension rms variation and (b), it is more effective at reducing the impact of these variations as demonstrated by its larger *Tension/CP* ratio. This larger ratio means that equal leash tension rms variations produce a smaller confluence point rms motion in the case of the bungee leash. Furthermore, in both studied cases, the bungee reduces the vertical payload rms error but not the horizontal error. This is expected since replacing the Spectra leash by a bungee cable decreases its longitudinal stiffness and the leash is vertically oriented.

Figure 4.7 drew our attention to another beneficial effect of the bungee leash: it significantly decreases the frequency of the confluence point motion. This could greatly simplify its stabilisation by other active methods. As an example, if we use a winch controller [21] with gains $k_p = 1$, $k_i = 1\ s^{-1}$ and $k_d = 0.01$ second in the baseline case with a

net lift of 2 kN, the payload rms error is reduced from 30 cm to 3 cm with the bungee leash but only reduced from 43 to 15 cm with the Spectra leash. Figure 4.9 shows the results obtained with such a winch controller.

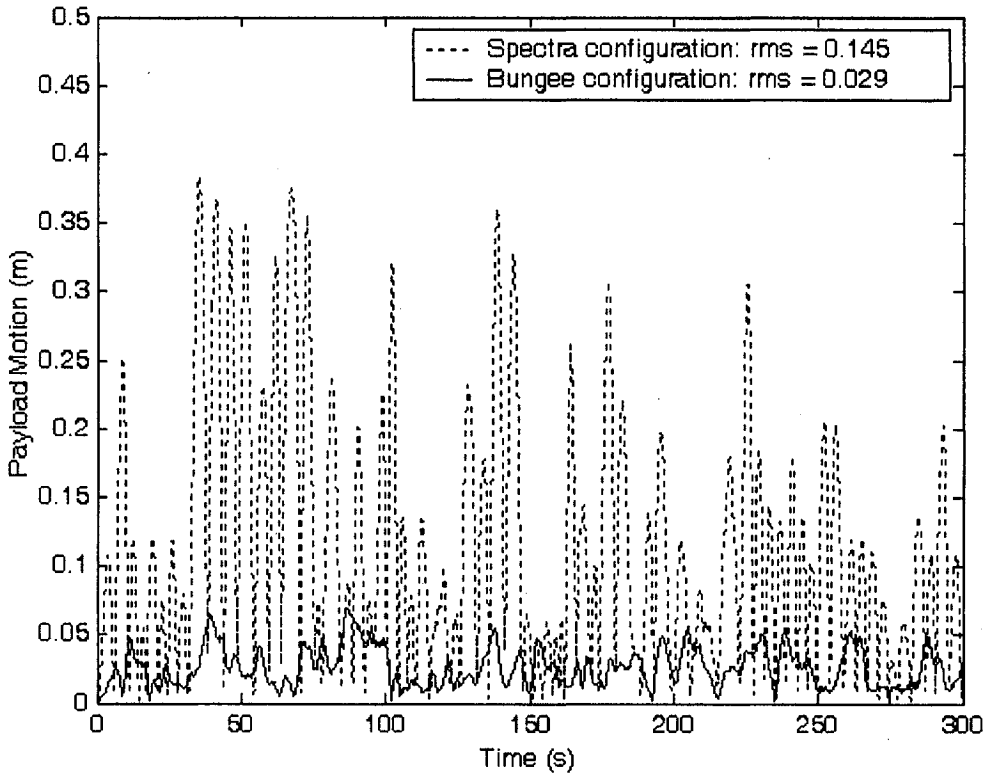

Fig. 4.9. Payload motion for the baseline system with winch control.

4.3 Test Set-Up and Procedure

The Penticton multi-tethered aerostat system (see Figure 2.1) is adapted in order to observe the effects of the bungee leash experimentally. In this section, we present the Penticton facility in greater detail and we describe the procedure used to perform the bungee experiment. This section focuses on the setup and procedure modifications required for the incorporation of the bungee leash in the system.

4.3.1 Test Setup

In Subsection 2.2.1, we illustrated the general features of the Penticton facility. Here, we discuss in more detail the components relevant to the acquisition of test data. In the Penticton facility, all sensors are located on two platforms: the instrument platform (see

Figure 4.10a) and the ballonet platform (see Figure 4.10b). As shown in Figure 4.11, the instrument platform is positioned at the confluence point while the ballonet platform is located on the aerostat.

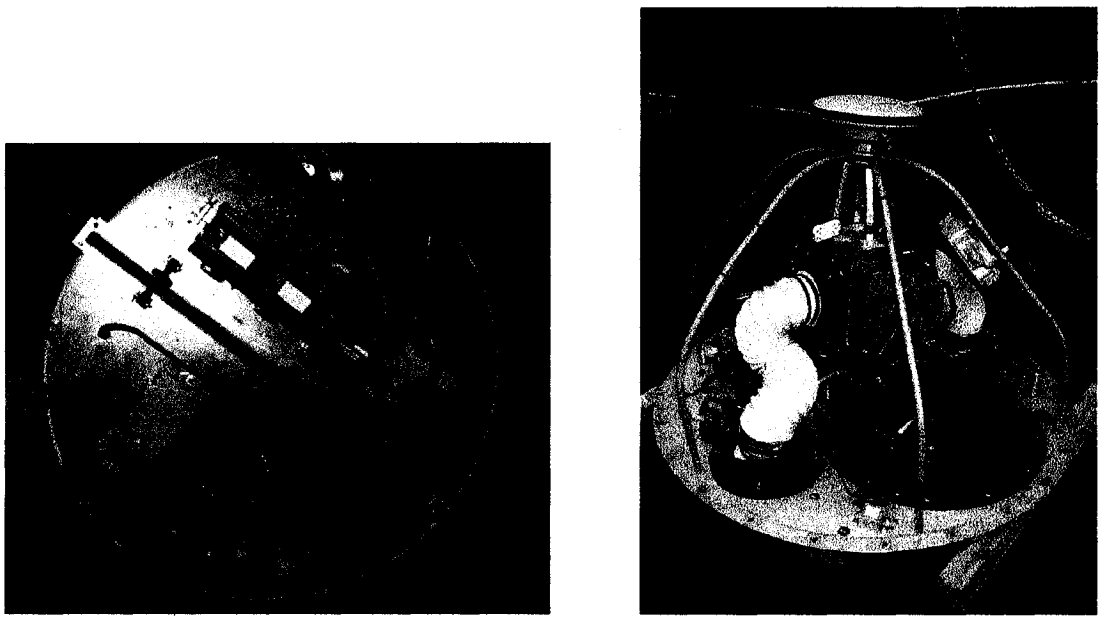

(a) (b)

Fig. 4.10. Instrument platform (a) and ballonet platform (b).

The instrument platform holds a GPS receiver, an inertial measurement unit, a wind sensor, a tilt sensor, a compass as well as a temperature sensor. A load cell is attached to each ground tether at the confluence point and is connected to the instrument platform. The platform is powered through the central tether, which is used to release and retrieve the system. The central tether hangs loose below the instrument platform during flight.

Two blowers located on the ballonet platform are used to keep a constant pressure inside the aerostat's ballonet. This platform also houses a GPS receiver, a tilt sensor, a compass, a pressure sensor as well as a temperature sensor. The load cell that measures the leash tension is located at the top of the leash and is connected to the ballonet platform. This platform is powered from the instrument platform, through the Spectra part of the leash and the backup cable. As a backup to the power supply through this cable, we also installed batteries at the ballonet platform. This system consisted of four battery packs, each of 105 Wh; enough to power the ballonet blowers for up to eight hours.

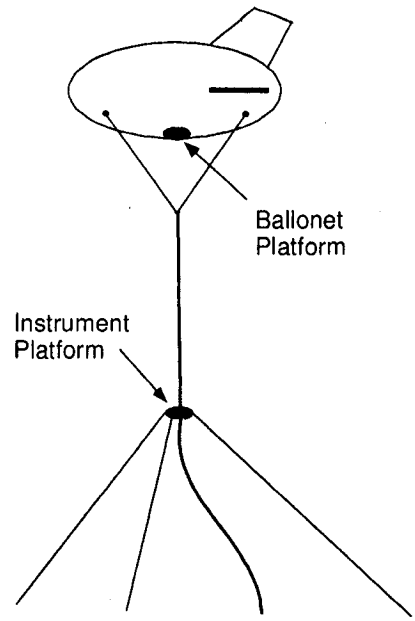

Fig. 4.11. Location of the instrument and ballonet platforms.

Data from all sensors are recorded at the ground at a rate of 10 Hz. The aerostat and confluence point positions measured by the GPS receivers are transmitted by radio modems while the measurements of all other sensors are sent to the ground via a RS-485 link. This data passes through the backup cable, the leash Spectra part as well as the central tether. A backup wireless data transmission system for the ballonet platform sensors was also designed, in case of failure of the safety cable conductors. This system was not functional during the tests, but it was fortunately not needed.

4.3.2 Procedure

To measure the effect of the leash stiffness on the Penticton aerostat system, two test flights are performed: one with a Spectra leash and one with a bungee leash; their respective payload stabilization is then compared. The bungee leash arrangement design ensures that both leash configurations weigh the same. As well, we try to keep the aerostat net lift and the wind conditions as similar as possible between the two experiments by conducting them in quick succession. Due to the presence of the bungee cord in the system, the launch and retrieval procedures must be modified. These procedures are described here.

The first part of the test is in the Spectra leash configuration. The system is launched as follows: the backup cable, the Spectra leash part as well as the central tether are initially spooled on the main winch located on the trailer (see Figure 4.12). The upper ends of the backup cable and the leash bungee part are both attached below the leash load cell. We release the aerostat by spooling out the backup cable from the main winch. After releasing the system for 24 metres, the bungee bottom end is taped loosely on the backup cable, and the launching continues. The backup cable and then the leash Spectra part are completely spooled out. At the junction between the leash and the central tether, the instrument platform is installed and the upper ends of the three tethers are attached. These tethers, which are lying on the ground, are lifted as the central tether is spooled out. When the central tether becomes slack and the three ground tethers hold the entire load, we stop spooling out and the system is ready for data acquisition.

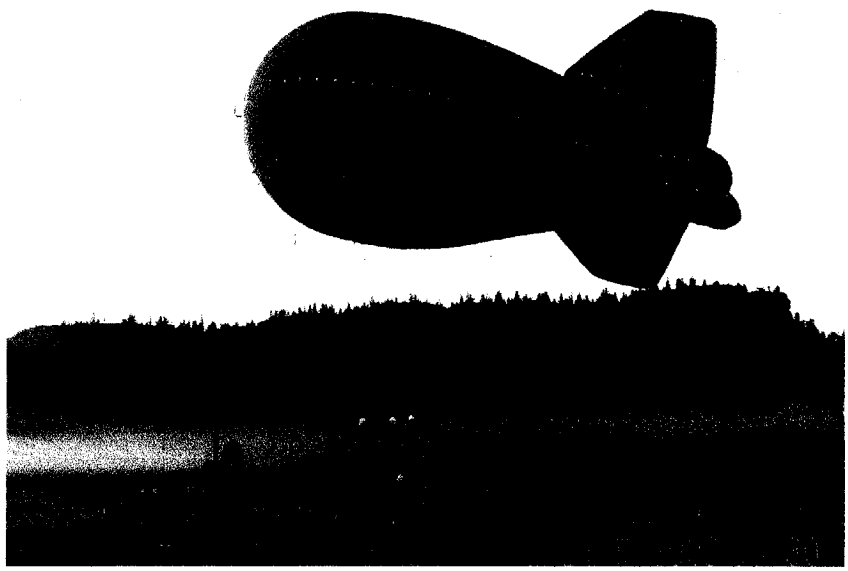

Fig. 4.12. Penticton aerostat and trailer.

After approximately half an hour of data recording with the Spectra leash configuration, the system is recovered to set-up the bungee leash configuration. When the bottom end of the leash bungee part is reached, it is untaped and attached to a tether spooled on a secondary winch also located on the trailer (see Figure 4.13a). Note that this secondary winch is not used for releasing the aerostat but for releasing the tension of the bungee cord during the retrieval phase of the bungee leash flight. After the bungee bottom end

has been attached to the secondary winch, the aerostat is released by spooling out the backup cable from the main winch. While spooling out this cable, the aerostat lift is gradually transferred to the leash bungee part. The backup cable is completely spooled out and the leash Spectra part is attached to the leash bungee part (see Figure 4.13b). The leash bungee part is detached from the secondary winch after the load has been transferred to the main winch. Finally, the leash Spectra part is completely spooled out from the main winch and the launching continues as with the Spectra leash configuration.

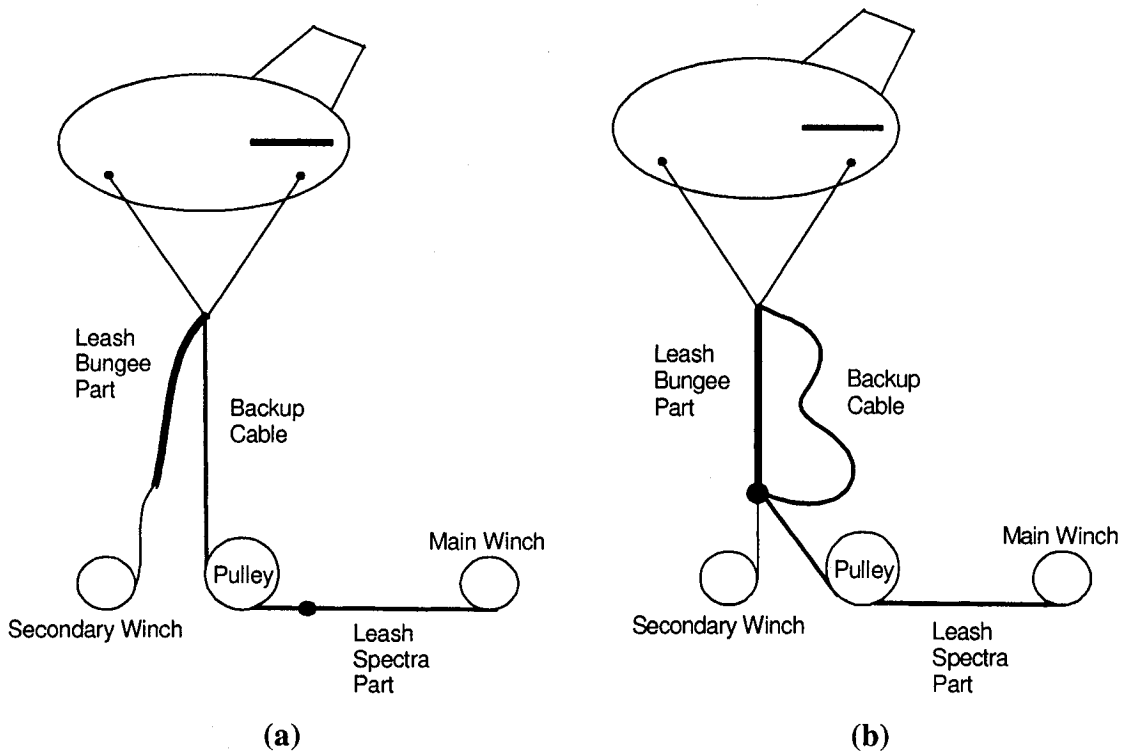

Fig. 4.13. Two steps of the bungee leash releasing procedure.

To recover the system after approximately half an hour of data recording with the bungee leash configuration, the above steps are followed in reverse order until the upper end of the leash Spectra part reaches the pulley. To avoid breaking an electrical connector, we must spool the backup cable under tension on the main winch. Therefore, we need to transfer the aerostat lift from the leash bungee part to the backup cable. This is done by releasing the bungee tension using the secondary winch. When the backup cable holds the entire load, it is spooled on the main winch and the aerostat is recovered.

4.4 Results and Interpretation

In this section, we present and interpret the results of the bungee experiments performed at the Penticton multi-tethered aerostat facility. The Penticton aerostat flew a total of four times with a bungee leash. Of these four flights, which took place on August 6th, August 11th, August 13th and October 13th 2004, only the second produced useful data. During the first bungee experiment, the RS-485 link in the central tether was not functional. The connection was repaired for the subsequent flights. During the August 13th experiment, a major aerostat failure took place between the tether and the bungee parts of the flight. The repair of the aerostat explains why two months separate the third and fourth bungee experiments. Finally, the data from October 13th flight is of little interest since there was almost no wind during that day. For these reasons, this section focuses on the August 11th bungee experiment.

4.4.1 Results

As explained in Subsection 4.3.2, the experiment done on August 11th was separated in two parts: the aerostat was first flown with a Spectra leash for a period of 55 minutes, the leash bungee part was then connected and the aerostat was flown for another 25 minutes. We divide each part of the flight into five-minute samples in order to find two larger samples with comparable wind conditions. The mean wind and turbulence for every five-minute sample is presented in Table 4.3. Note that the wind is measured at the instrument platform, located at the confluence point.

The turbulence intensity is calculated as the ratio of the wind standard deviation to the mean wind speed. It is calculated for both longitudinal (σ_u / W) and lateral (σ_v / W) directions relative to the mean wind direction. We find in Table 4.3 that a good combination would be samples #7 to #10 for the Spectra leash flight and samples #12 to #15 for the bungee leash flight. Since it is impossible to find two large samples with equal turbulences in the August 11th data, these are the two samples studied in this section, even if the bungee sample turbulence is much higher than that of the Spectra sample. Figure 4.14 compares the measured confluence point motion of Spectra and bungee samples.

Table 4.3. Wind conditions sampling of August 11th experiment.

	Sample #	Time	Mean Wind	Turbulence Intensity (σ_u / W)	Turbulence Intensity (σ_v / W)
	-	(min)	(m/s)	-	-
Spectra Leash Flight	1	0-5	2.5	0.123	0.091
	2	5-10	1.8	0.212	0.126
	3	10-15	1.6	0.146	0.132
	4	15-20	2.0	0.106	0.116
	5	20-25	1.6	0.136	0.258
	6	25-30	1.7	0.165	0.210
	7	30-35	3.1	0.169	0.119
	8	35-40	3.9	0.092	0.054
	9	40-45	3.1	0.126	0.083
	10	45-50	3.6	0.088	0.093
	11	50-55	3.4	0.074	0.077
	(7-10)	**30-50**	**3.4**	**0.153**	**0.097**
Bungee Leash Flight	12	0-5	3.7	0.083	0.087
	13	5-10	4.0	0.098	0.146
	14	10-15	4.0	0.279	0.206
	15	15-20	3.0	0.228	0.263
	16	20-25	2.3	0.274	0.295
	(12-15)	**0-20**	**3.5**	**0.253**	**0.219**

We see in Figure 4.14 that the confluence point motion was higher during the bungee leash flight (18 cm) than during the Spectra leash flight (15 cm). This is also what is predicted by the simulation. Indeed, if we simulate the Penticton aerostat system with the same wind conditions as the August 11th experiment, we obtain the confluence point motion presented in Figure 4.15. To simulate the experimental wind conditions, we fit a 10th degree polynomial to the wind speed recorded by the instrument platform sensor for both samples. These polynomials are used in the simulation as the mean wind speed to which is added the experimental total turbulence intensity (σ / W), defined as the ratio of the wind standard deviation to the mean wind speed. The wind direction used in the simulation is constant and equal to the mean experimental wind direction of each sample. An aerostat net lift of 2 kN is used in the simulation, based on the lift measured prior to the experiment.

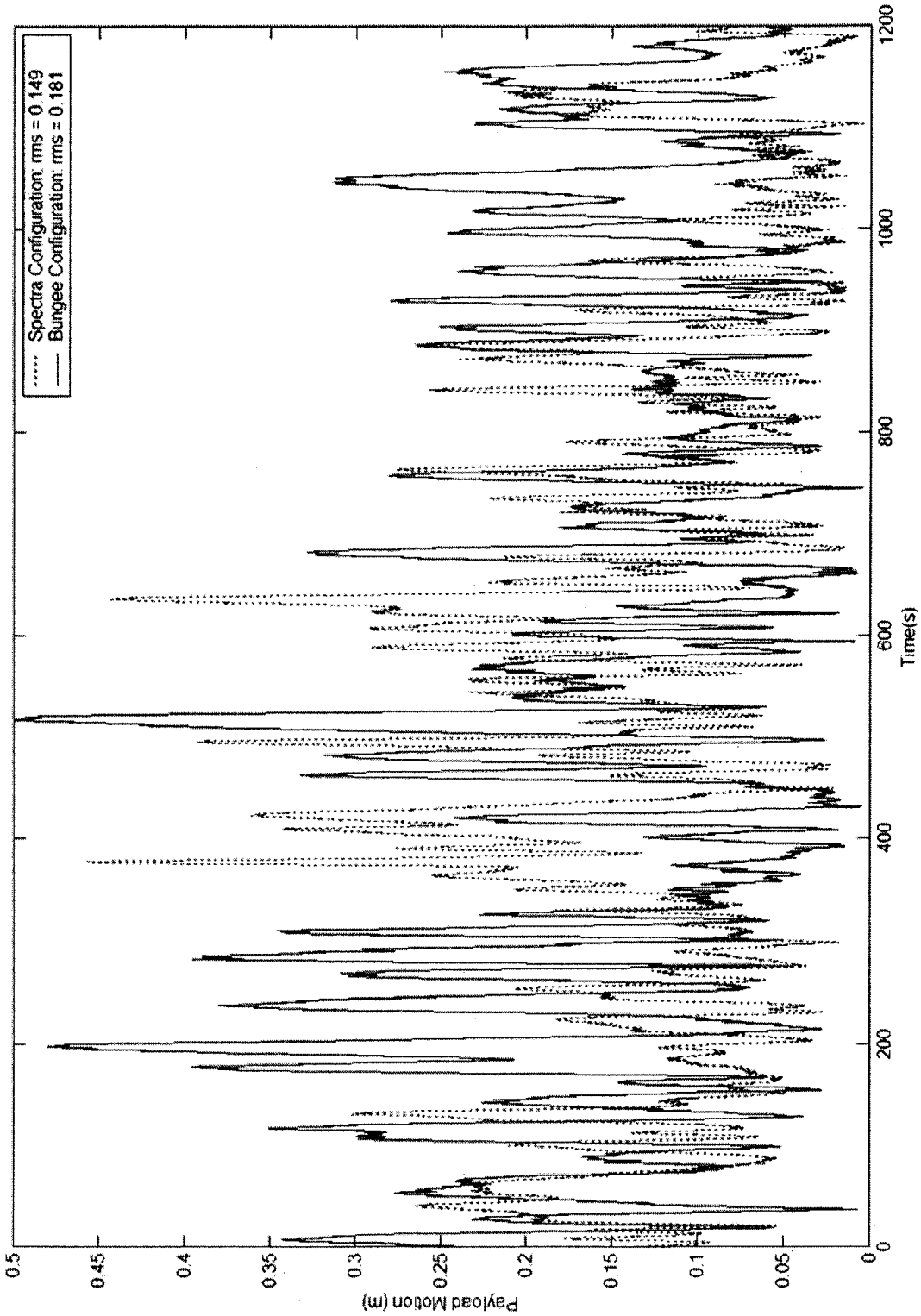

Fig. 4.14. Payload motion for the August 11th experiment.

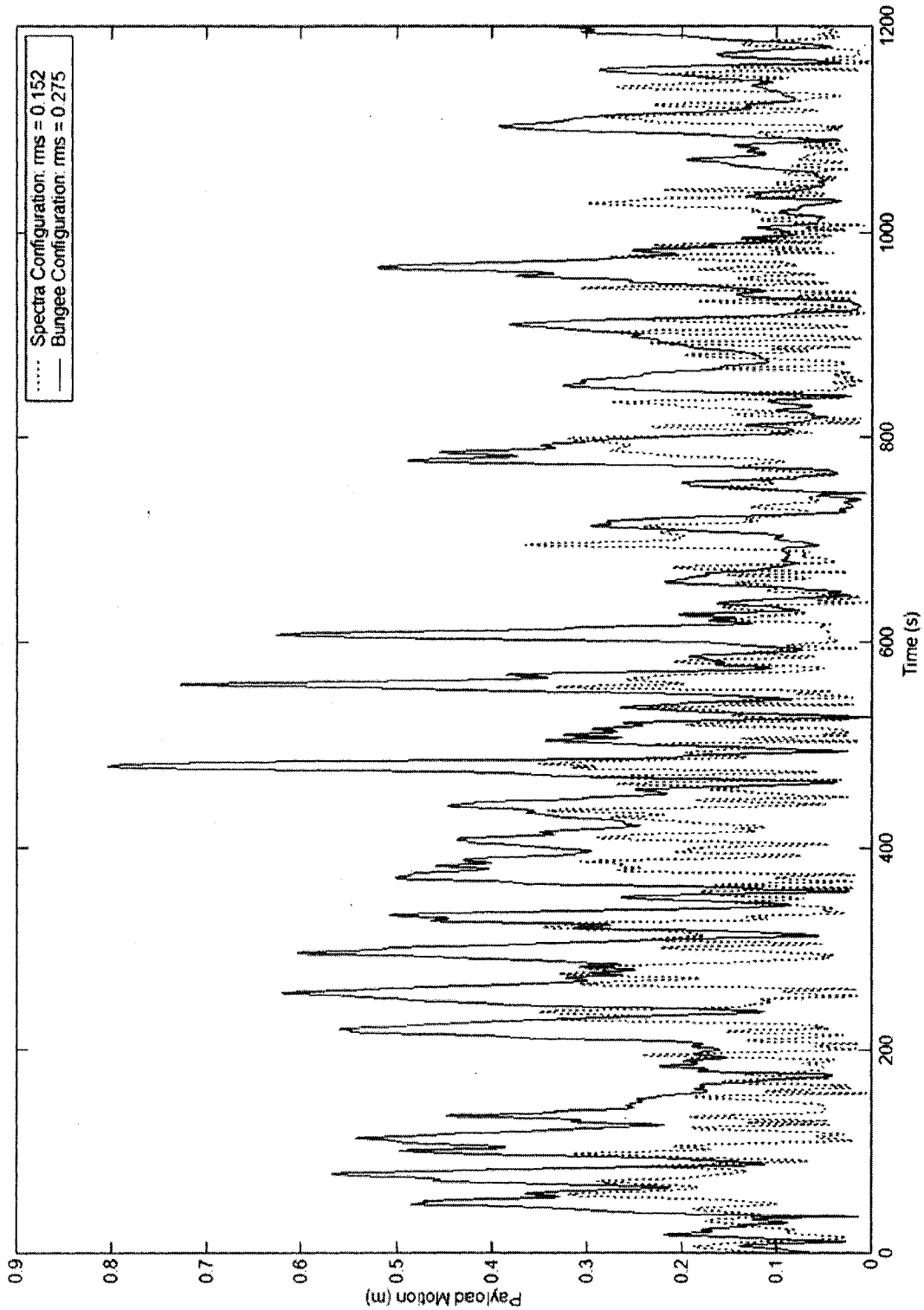

Fig. 4.15. Simulated payload motion with August 11th wind conditions.

It can be seen in Figure 4.15 that according to the simulation, the bungee leash should have produced almost twice the confluence point motion than the Spectra leash. Furthermore, the bungee leash confluence point motion predicted by the simulation is approximately 50% higher than the experimental confluence point motion. In Table 4.4, we present a comparison of the simulated and experimental results for the Spectra and bungee samples. Note the small turbulence intensity mismatch between the experiment and the simulation in the lateral direction (σ_v / W).

Table 4.4. Results in horizontal and vertical directions.

	Simulation			Experiment		
	Spectra	Bungee	Δ (%)	Spectra	Bungee	Δ (%)
Turbulence Intensity (σ / W)	0.150	0.239	59.3	0.150	0.239	59.3
Turbulence Intensity (σ_u / W)	0.149	0.236	58.4	0.153	0.253	65.4
Turbulence Intensity (σ_v / W)	0.046	0.106	130.4	0.097	0.219	125.8
CP rms error (m)	0.153	0.275	79.7	0.149	0.182	22.1
CP rms horizontal error (m)	0.027	0.065	140.7	0.058	0.065	12.1
CP rms vertical error (m)	0.150	0.268	78. 7	0.137	0.169	23.4
Aerostat rms error (m)	3.87	7.03	81.7	5.73	5.83	1.7
Aerostat rms horizontal error (m)	3.87	6.46	66.9	5.72	5.72	0.0
Aerostat rms vertical error (m)	0.17	2.77	1529.4	0.20	1.11	455.0
Leash tension rms variation (N)	68.8	122.0	76.8	42.4	60.8	43.4
Global ratio aerostat/CP (m)	25.31	25.54	0.9	38.42	32.10	-16.4
Horizontal ratio (m)	141.65	100.05	-29.4	98.65	87.63	-11.2
Vertical ratio (m)	1.11	10.34	831.5	1.42	6.57	362.7
Ratio tension/CP (N/m)	450.0	443.2	-1.6	284.3	334.8	17.8

4.4.2 Interpretation

From the simulation results obtained in Section 4.2, we expected that the replacement of the Spectra leash by the bungee leash would reduce the confluence point motion by approximately 30%. This is opposite to what happened in the August 11th experiment. Indeed, the results presented in the previous subsection showed that the confluence point motion was higher in the bungee leash part of the experiment. This discrepancy can be explained by the fact that the turbulence intensity was much higher in the case of the bungee leash. Since the turbulence is an important determinant of the confluence point motion, it is understandable that the confluence point motion is higher in the bungee

sample. Furthermore, this trend is similar for the simulation and experiment and the bungee actually performed better than what the simulation predicted. This makes us believe that for comparable turbulence intensities, the bungee leash would have decreased the confluence point motion.

We are also interested in narrowing down the source of the discrepancy between the simulation and the experiment performed in the previous subsection. We would like to ensure that the discrepancy between the bungee experimental and simulated confluence point motion is not due to the use of an incorrect leash model in the simulation. To do this, we modify the simulation to *remove* the aerostat and wind model, and replace them by applying the *measured* leash tension (magnitude and direction) at the top of the leash in the simulation. This is done for Sample #10 (Spectra leash) and Sample #12 (bungee leash). We then compare the payload error produced by the simulation to the measured payload error. As we can see in Figures 4.16 and 4.17, the good matches obtained suggest that the remaining parts of the simulation (all elements other than the wind and aerostat model) are a good match to reality. This is equally true for the Spectra and bungee leashes.

We therefore conclude that the discrepancy between the simulation and experiment must originate either in the wind or the aerostat model. In fact, we have good reasons to believe that part of the problem lies in the turbulence model. Indeed, we note from Table 4.4 that the simulation appears to over predict the leash tension rms variation. This is something that has been seen in previous Penticton experiments and other projects using the LAR simulation have associated this issue to the turbulence model. It therefore appears that with an improved turbulence model, we will likely get better match between simulation and reality.

Because of the difference in the wind conditions of the Spectra and bungee leash flight parts, it is impossible to use the measurements of August 11^{th} to validate or invalidate the system improvements that could be expected by the replacement of the Spectra leash by a bungee leash. However, two reasons lead us to believe that, for comparable aerostat wind conditions, the bungee leash system would reduce the payload motion: (a) this is predicted by the simulations done in this chapter and Figures 4.16 and 4.17 demonstrates

the validity of the Spectra and bungee models, and (b) the ratio of leash tension rms to payload rms error is higher for the bungee leash, indicating that the bungee leash performs better than the Spectra leash in reducing the transmission of perturbations coming from the aerostat.

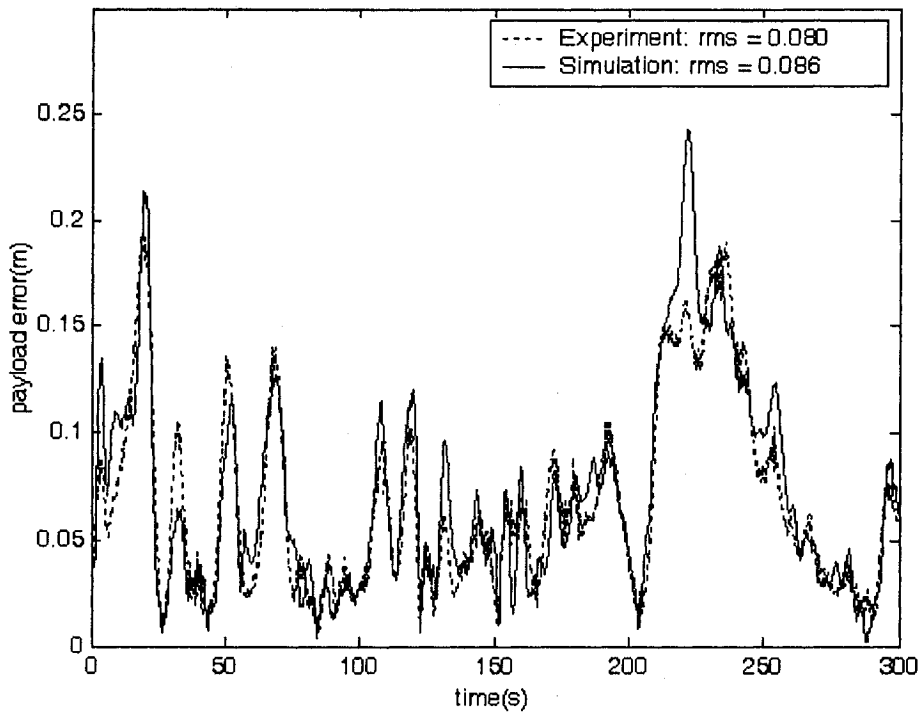

Fig. 4.16. Simulation of Spectra Sample #10 with experimental top leash tension.

In order to make a stronger conclusion regarding the performance of the bungee leash, it would have been best to perform additional bungee experiments until more representative wind conditions could be obtained. This turned out not to be possible since the retrieval procedure with the bungee leash was judged to be too hazardous to allow further flights. Indeed, during the last bungee experiment on October 13th, the aerostat was flown with the bungee leash for almost six hours waiting for good wind conditions. The aerostat flew for so long that upon retrieval, the backup and bungee cables were badly twisted together. In order to untangle them, the backup cable had to be disconnected, leaving the aerostat secured only with the bungee. This was risky since the factor of safety of the bungee cable is only 1.5. A photograph taken during August 11th experiment is shown in. Figure 4.18 and shows what this tangling looks like. Note that in this photograph, the backup cable is much less twisted than during the October 13th experiment.

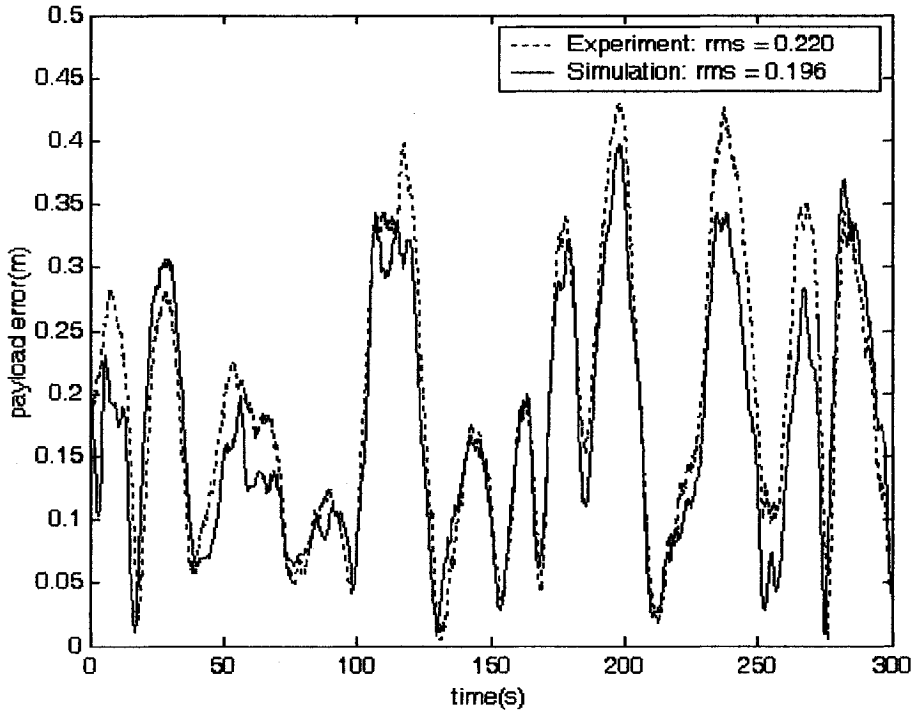

Fig. 4.17. Simulation of bungee Sample #12 with experimental top leash tension.

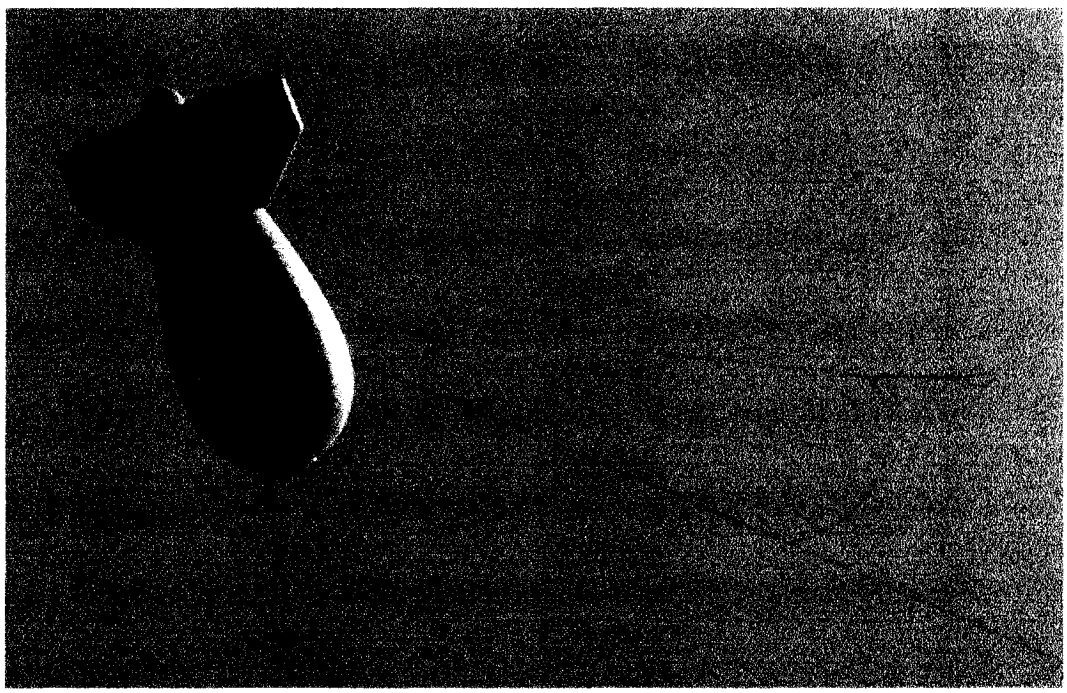

Fig. 4.18. Example of backup cable tangling (August 11th).

4.5 Conclusion

In this section, we summarize the advantages and the disadvantages of using a bungee leash in the LAR multi-tethered aerostat system. The advantages of a bungee leash would be the reduction of the payload motion frequency as well as the reduction of the payload rms error by approximately 30% in a system with sufficient lift (see Figure 4.8). As was discussed in Subsection 4.2.3, reducing the payload motion frequency would improve the effectiveness of other active methods such as the confluence point mechanism or winch control.

The expected reduction in payload motion of 30% with the bungee leash arrangement designed in this chapter is far from the 90% reduction presented in Figure 2.5. The reason for this discrepancy comes from the material limitation. Indeed, there is a practical lower limit to the bungee cable stiffness, which is approximately 40 N/m in our case, since the bungee must be strong enough to transmit the lift of the aerostat. To further decrease the stiffness of the bungee leash, we would have to increase its length and therefore add substantially more weight to the system. Reducing its diameter would not be an option since this would decrease the safety factor of the cord.

As we mentioned earlier, the weight added by a bungee leash is a serious disadvantage of this approach. For the experiment performed in Penticton, the bungee cable added 28 kg to the system and hence doubled the leash weight. A longer bungee leash would easily have tripled or quadrupled the leash weight. In principle, we can size the LAR aerostat to compensate for additional weight, so this is not an unresolvable problem. However, the cost of an aerostat increases with its size. It would be important to further study the performance improvement and weight of the different possible techniques and to choose wisely which ones warrant being implemented in the LAR multi-tethered aerostat system.

The increased complication of the aerostat launching and retrieval procedures is another big drawback of the bungee leash approach. For reasons of safety and power and data transmission, we required a second cable parallel to the bungee cable. To cope with potential conductor breakage, we also had to design a backup power and data collection system. In at least one instance, the bungee and the safety cable became badly entangled.

This tangling made the retrieval procedure so hazardous that we stopped further bungee experiments. In the cables used for bungee jumping, the safety cable is generally a strap wrapped around the rubber core. If we could power the ballonet platform through such a strap and find a way to roll the bungee leash onto a winch, we might have a safer setup that would enable releasing and retrieving of the bungee leash.

Finally, it should be noted that the use of a bungee leash would significantly increase the required maintenance of the LAR multi-tethered aerostat system. Indeed, since the rubber deteriorates with time due to factors such as ambient moisture, sun exposure and mean elongation, the bungee leash would have to be replaced every one or two years. As bungee cables are relatively expensive, this would increase the operational cost of the LAR facility. As an example, *BCI* provided an estimate of the cost of a bungee cord that would sustain the LAR full-scale aerostat lift (estimated at 107 kN). Using multiple off-the-shelf bungee cords attached together with customized attachments, *BCI* could provide us with a 24-metre bungee arrangement 30 times stronger than the custom-made bungee cord used for the Penticton experiments. This full-scale bungee leash would cost approximately 40,000 USD.

Presently, the bungee leash approach seems heavy, complex and expensive for the relatively modest improvement in performance in the multi-tethered aerostat system. For these reasons, we believe that the addition of a bungee leash in the LAR system is of questionable benefit. Other approaches for improving the system performance may prove more worthwhile. Perhaps the bungee leash approach could be revisited if those other approaches turn out to be fruitless.

Chapter 5

Design of a Variable Leash Attachment Point Mechanism

5.1 Introduction

In Chapter 3, we evaluated three approaches to actively reduce the confluence point motion of the multi-tethered aerostat system: leash attachment point pitch control, fin deflection pitch control and active heave compensation of the leash. In that chapter, we concluded that only the leash attachment point controller would be further investigated. This controller displaces the leash attachment point on the lower part of the harness in order to control the aerostat pitch. To perform that in practice, a variable leash attachment mechanism must be devised.

In this chapter, we design this mechanism in greater detail. The purpose of this exercise is not the construction of the mechanism or the implementation of the controller but a more accurate appraisal of its practicalities and the enhancement of the corresponding simulation model. We set out to design a mechanism that would control the location of the leash attachment point in response to errors in the payload altitude, as was done with controller #2 of Table 3.1 in Section 3.2.

The structure of this chapter is as follows: In Section 5.2, we select the different components of the variable leash attachment mechanism. The mechanism arrangement is presented in Section 5.3 and implemented in the simulation in Section 5.4. Finally, some design issues are discussed in Section 5.5.

5.2 Component Selection

The variable leash attachment mechanism is essentially a pulley driven by a motor that rolls along the aerostat harness (see Figure 5.1). The speed of the motor is controlled by a servo amplifier located on the aerostat ballonet platform. Power and control signals to the amplifier are provided from the ground through electrical conductors in the leash and central tether. In this section, we select the main components of the mechanism, which include: a pulley, a motor and gear train as well as an amplifier. To implement this mechanism in the Penticton facility, the aerostat harness would have to be modified. The lower loop on each side of the harness would have to be merged in a single loop on which the mechanism could travel.

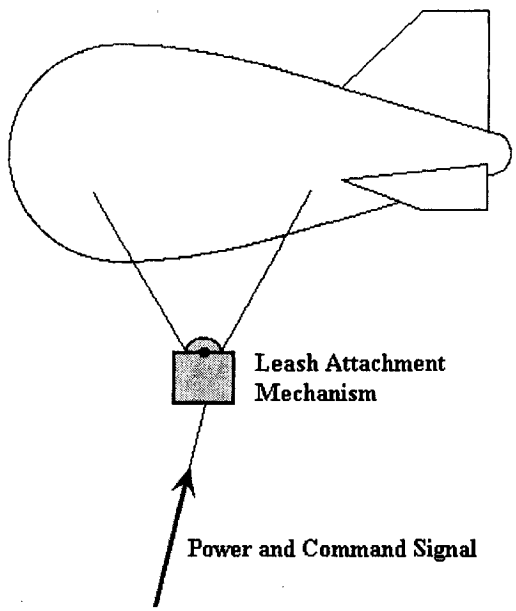

Fig. 5.1. Location of the leash attachment mechanism.

5.2.1 Pulley

From the simulations performed in Section 3.2, we find that when we use the pitch controller #2 on the baseline system, the tension difference ΔT in the harness reaches a maximum value of 2.2 KN. Wrapping the harness on a single pulley would then likely lead to slippage. To avoid this, we design a *double* pulley (see Figure 5.2) that reels in the harness on one side while the other side releases it. It should be noted that due to the

lateral offset of the two cable elements, the mechanism would tend to twist so that the two cables become aligned.

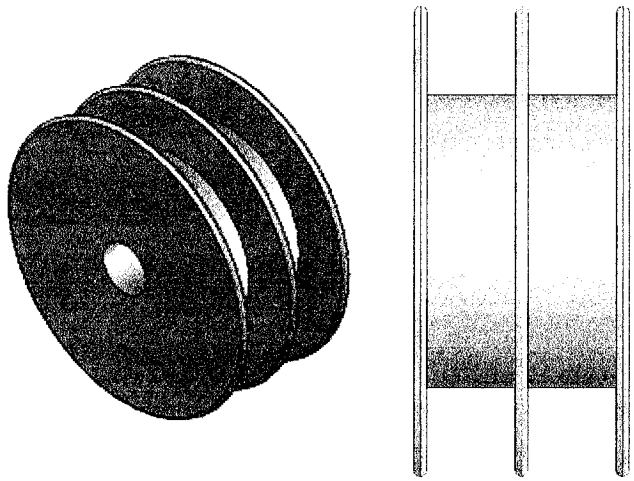

Pulley characteristics	
Hole diameter	15 mm
Pulley diameter	68 mm
Flange diameter	110 mm
Space between flanges	20.5 mm
Flanges width	3 mm
Total pulley width	50 mm
Weight estimate	0.75 Kg

Fig. 5.2. Pulley schemas and characteristics.

The outside diameter of the pulley is set at 68 mm. We saw in Section 3.2 that the pitch controller #2 needs a total displacement of 1.4 metres on the harness. Therefore, the other dimensions of the pulley are chosen to fit 1.4 metres of 6-mm spectra cable on each side on two layers. Because of this second layer, we use a value of 80 mm for the outside diameter when we verify the motor torque requirements in the next subsection.

5.2.2 Servo Motor

Based on the preliminary evaluation of controller #2, the selected motor would have to hold a maximum tension of 2.2 kN at a maximum speed of 0.68 m/s and therefore produce a maximum power of 1.5 kW. In order to minimize the size of the motor, we inspect the harness tension difference and speed curves presented in Figure 5.3 to see if we could trade off some system performance for significant weight reduction.

Based on Figure 5.3, the size of the motor is minimized by two different ways. The first way does not trade off performance and consists of selecting a motor that could exert a *continuous* tension of 1.75 kN and a *peak* tension of 2.2 kN. Indeed, we find that the peaks at 1.75 kN are approximately five seconds long and therefore it is reasonable to use this value as the requirement for the motor continuous range. The second way to decrease

the motor size is to reduce its maximum speed from 0.68 m/s to 0.28 m/s. This speed reduction reduces the motor weight at very little penalty since the mechanism speed only exceeds 0.28 m/s two percent of the time. In fact, by implementing a speed limit of 0.28 m/s into controller #2, the simulation shows that we would reduce the payload rms motion from 19 cm in the baseline system to 8 cm (compared to 7 cm for the controller without the speed limit).

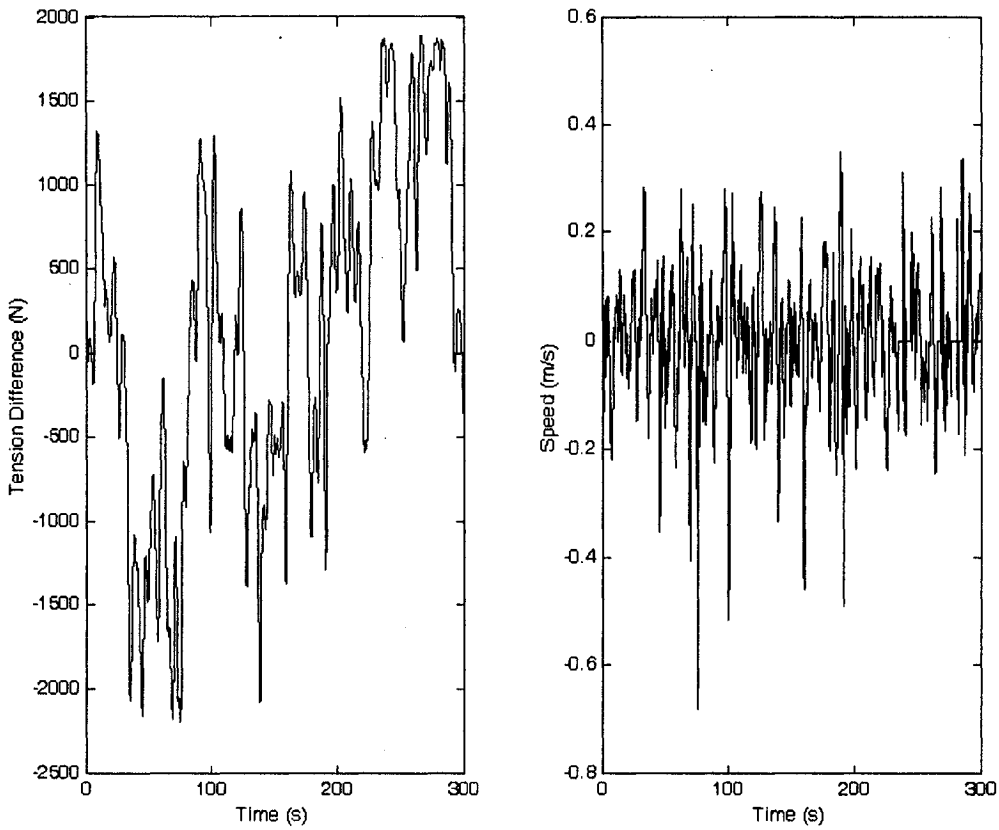

Fig. 5.3. Harness tension difference and speed for controller #2.

To satisfy these tension and speed requirements, we select the BSM80N-150AA AC Brushless Servo Motor from *Baldor Electric Company* [38] as it produces a torque of 1.65 Nm at a rotational speed of 3500 rpm. Since the pulley has two layers, we use its *minimal* outside diameter of 68 mm to verify the speed requirement and its *maximal* outside diameter of 80 mm to verify the tension requirements. With a gear ratio of 44.4:1 and a pulley diameter of 68 mm, a speed of 0.28 m/s is achieved with this motor. For a pulley diameter of 80 mm, it produces a maximum continuous tension of 1.83 kN, which fits our requirement. Finally, the required peak tension of 2.2 kN corresponds to a motor

torque of 2 Nm which is also perfectly achievable by the BSM80N-150AA. Figure 5.4 shows some characteristics of this motor:

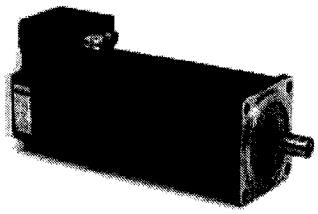

BSM80N-150AA Servo Motor Characteristics	
Continuous stall torque	1.65 Nm
Continuous stall current	3.05 Amps
Peak torque	6.60 Nm
Rotational speed	3500 rpm
Current for a torque of 2 Nm	3.6 Amps
Weight	3.63 Kg

Fig. 5.4. BSM80N-150 motor and characteristics [38].

5.2.3 Servo Amplifier

In order to control the speed of the motor, we use *Baldor's* FlexDrive^{II} FDH2A05TR-EN23 AC servo amplifier [38]. Figure 5.5 shows some characteristics of this device:

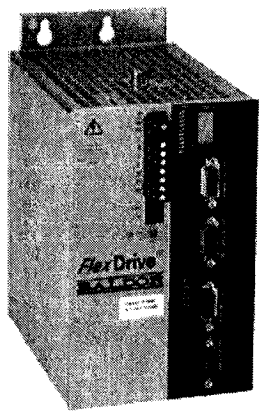

FDH2A05TR-EN23 Characteristics	
Input Voltage	230 VAC single Φ
Command Signal	±10 VDC
Maximum current	5 Amps
Dimensions	15.3 x 9.3 x 20.5 cm^3
Weight	3 kg

Fig. 5.5. FDH2A05TR-EN23 amplifier and characteristics [38].

This amplifier controls the speed of the motor according to a command signal that would be generated by the PID controller. Note that the FlexDrive^{II} servo amplifier accepts either a ±10 VDC command signal or a pulse and direction input. As mentioned previously, the power and command signal would be provided through the central tether and the leash (a total length of 370 metres). Therefore, in addition to the component weight, the variable leash attachment point system also adds weight due to electrical power wires.

In order to estimate this weight, we start with the assumption that three 370-m wires are required to provide a ground and supply the servo amplifier with 230 VAC single phase at 3.6 Amps (the maximum motor current). If three AWG 12 copper wires were used, with properties taken from [39], these conductors would weigh:

$$W = 3LA\rho = 3 \cdot 370 \cdot \frac{\pi \cdot 0.002052^2}{4} \cdot 8920 \approx 33\,\text{kg}$$

Since the resistance of the AWG 12 wire is 5.32 ohms per km, the voltage drop at peak current in the conductors would be:

$$\Delta V = RI = 5.32 \cdot 0.37 \cdot 3.6 \approx 7.1\,\text{Volts}$$

which corresponds to a drop of 3.1% relative to the 230 VAC supply voltage. For performance issues, the National Electric Code recommends a maximum voltage drop of 3% [40]. Therefore, the maximum voltage drop obtained with AWG 12 wires is acceptable.

5.2.4 Gearing

In Subsection 5.2.2, we saw that the gear ratio required to reduce the motor speed is 44.4:1. Since the motor rotational speed of 3500 rpm is relatively high, we first use a 10:1 precision gearhead, the Mijno MRP 090 [41]. To achieve the remaining 4.4:1 gear ratio and transmit the rotation from the motor axis to the pulley axis, we use one set of bevel gears followed by one set of spur gears, both supplied by Quality Transmission Components [42]. Figure 5.6 shows the characteristics of these different gear components.

Note that the gear efficiencies have not been taken into account when the motor was selected. The final design of the leash attachment point mechanism should account for losses in the geartrain. In the next section, we present how the different selected components are arranged.

Mijno MRP 090 Precision Gearhead Characteristics	
Input Speed	3500 rpm
Input Torque	3.5 Nm
Gear Ratio	10 :1
Weight	3 kg

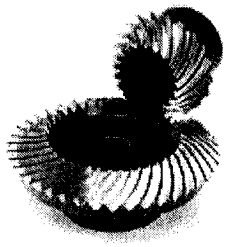

QTC MBSG2 Bevel Gears Characteristics	
Input Torque	24 Nm
Gear Ratio	2 :1
Weight	0.72 kg

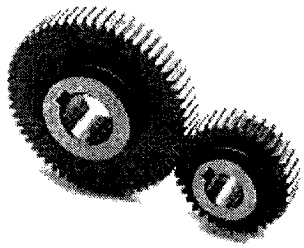

QTC MSGA1-45 and MSGA1-100 Spur Gears Characteristics	
Input Torque	44 Nm
Gear Ratio	2.22:1
Weight	0.86 kg

Fig. 5.6. Gear components and characteristics. [41][42]

5.3 Mechanism Arrangement

In this section, a preliminary design for the leash attachment point mechanism is proposed. We first present drawings of the mechanism and then we discuss its main parts.

The proposed mechanism arrangement transmits the rotation of a vertical motor to the pulley via two sets of gears. Figure 5.7 shows isometric and front views of the mechanism. Its dimensions are 52x17x10 cm^3 and its weight is estimated to be 15 kg (this excludes the weight of the amplifier and of the conductors). Therefore, the overall system would add approximately 50 kg to the Penticton multi-tethered aerostat facility.

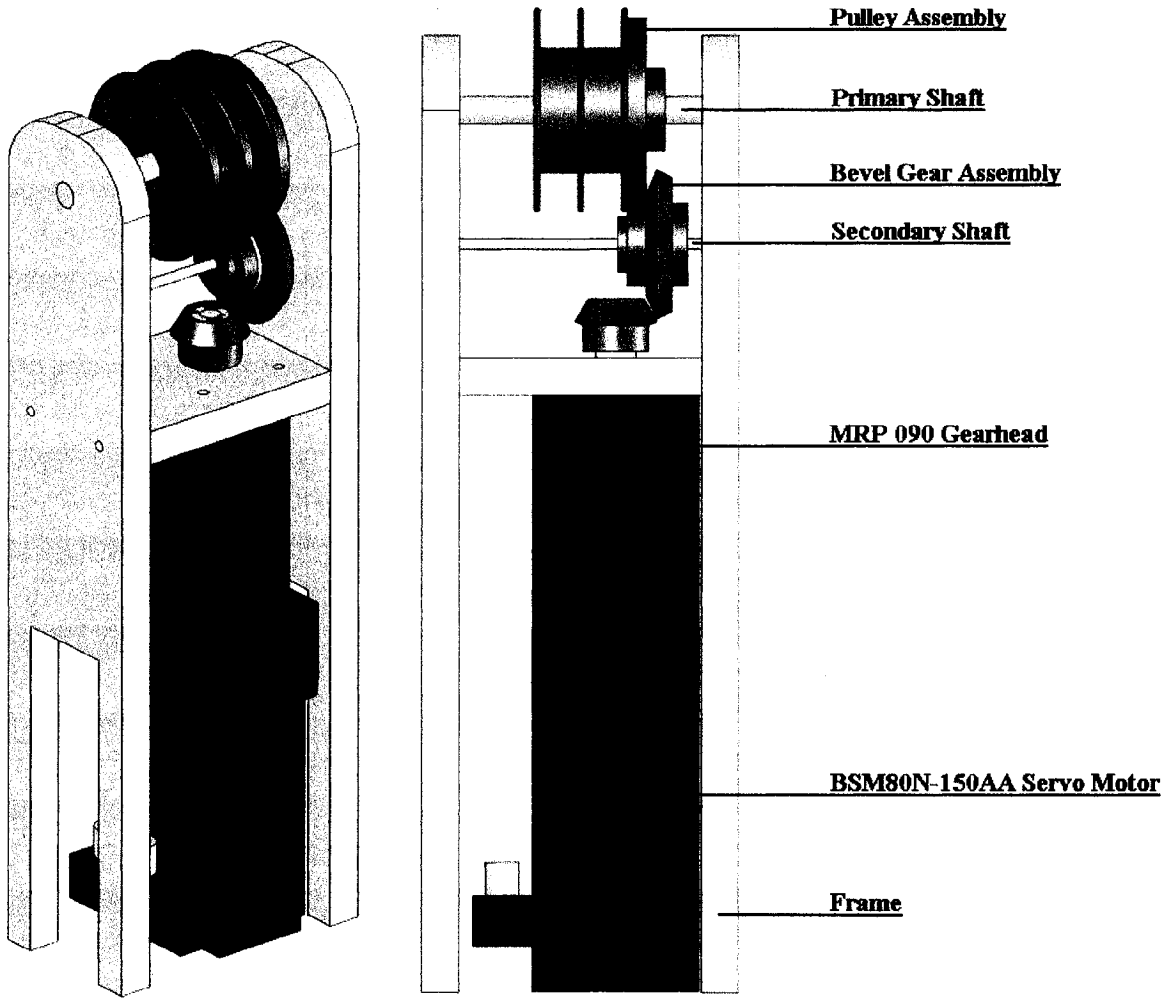

Fig. 5.7. Leash Attachment Point Mechanism.

No stress analysis was performed on the mechanism structure. Therefore, to make sure that they can support the different forces, the frame and shafts should be more precisely dimensioned in a future detailed design. Both shafts are fixed: the primary shaft is bolted while the secondary shaft is embedded. Furthermore, the secondary shaft can be smaller than the primary shaft since it does not support the aerostat lift. In the present design, the diameters of the primary and secondary shafts are respectively 15 and 6 millimetres.

The pulley and the large spur gear are machined and bolted together to create the pulley assembly shown in Figure 5.7. Needle bearings are installed inside the pulley assembly to permit rotation on the primary shaft. The *SKF NA 6902* needle bearing [43], with an outside diameter of 3 cm, would fit perfectly inside the pulley assembly and support the

full lift of the aerostat. In order to centre the pulley on the primary shaft, a *SKF 51103* thrust bearing [43] positioned with a collar (not shown in Figure 5.7) would be used on each side of the pulley assembly.

The large bevel gear and the small spur gear combine to make the bevel gear assembly (see Figure 5.7). To allow this to spin on the secondary shaft, a *SKF NAO 6x17x10 TN* needle bearing [43] would be fit in the assembly. Furthermore, the assembly would be accurately positioned using a *SKF BA 7* thrust bearing [43] on the bevel gear side (not shown in Figure 5.7).

5.4 Performance

In this section, we evaluate the performance of a variable leash attachment point controller that uses the mechanism designed in Sections 5.2 and 5.3 and we compare it to the performance of controller #2 presented in Section 3.2. To accomplish this, we implement a pitch controller with the variable leash attachment mechanism characteristics and limitations in the simulation of the baseline system.

The mechanism characteristics and limitations are implemented in the simulation as follows: (a) the servo amplifier weight of 3 kg is added at the ballonet platform, (b) the mechanism weight of 15 kg is added at the leash top node, (c) the leash density as well as the payload weight are increased to account for the added conductor weight of 33 kg, and finally (d) position and speed limits of respectively ±0.7 m and ±0.28 m/s are implemented in the controller to limit the motion of the leash attachment point on the aerostat harness.

We implement a PID controller very similar to controller #2 of Section 3.2 in the baseline system. This controller stabilizes the payload altitude by varying the leash attachment point position on the aerostat harness. The only differences between this controller and controller #2 are the gains of the PID. Indeed, the speed limit imposed here forces us to reduce the PID gains for the system to remain stable. By optimizing these gains by trial and error we obtain: $k_p = 2$, $k_i = 0.8\ s^{-1}$ and $k_d = 0.01$ second. Figure 5.8 shows the system

behaviour with a pitch controller that uses the variable leash attachment mechanism designed in this chapter.

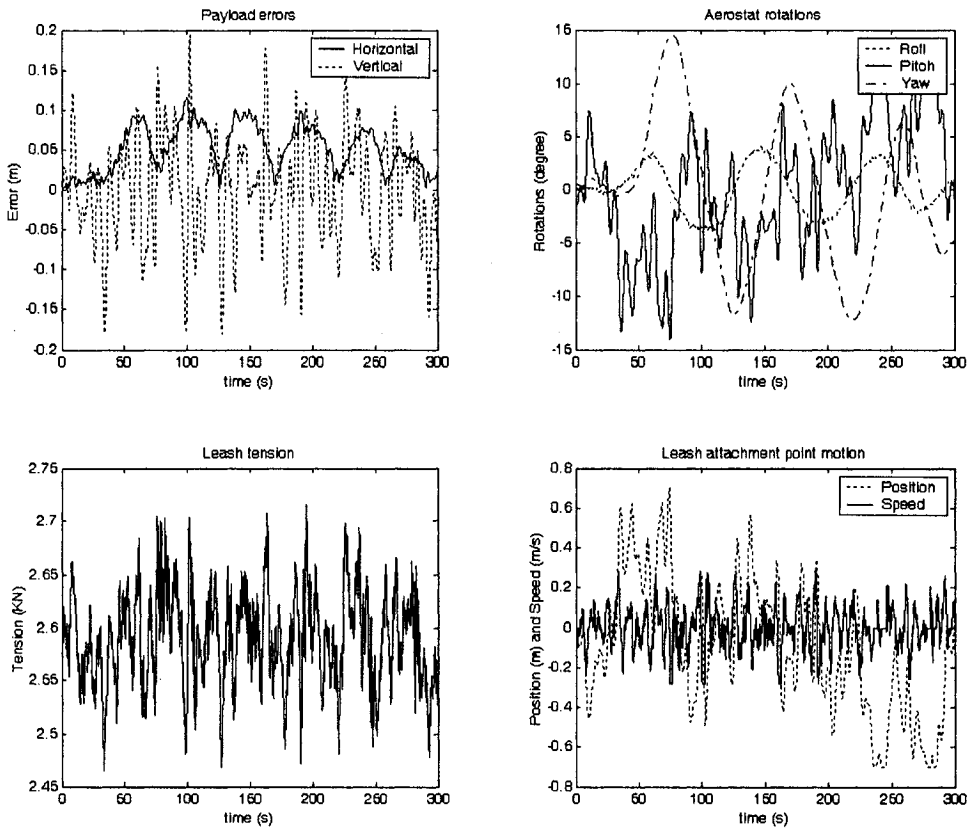

Fig. 5.8. Baseline system behaviour with the leash attachment mechanism.

By comparing Figures 5.8 and 3.5, we find that such a pitch controller behaves similarly to controller #2 of Section 3.2: it increases the aerostat pitch oscillation amplitude from a few degrees (see Figure 2.2) to approximately 20 degrees. However, its payload rms motion reduction is slightly less: from 19 cm in the baseline system to 9 cm for the pitch controller with the variable leash attachment mechanism compared to a payload rms motion of 7 cm for controller #2 in Section 3.2. Two reasons explain this difference: (a) the added weight of the mechanism and (b) the speed limit that forces a reduction of the PID gains. Nevertheless, the proposed mechanism should achieve a better payload rms motion reduction than what can be achieved with the bungee leash: a reduction of roughly 50% compared to 30% for the bungee leash.

5.5 Design Issues

During this first design iteration of the leash attachment mechanism, two issues were noted that would have to be addressed in future designs. The first considers the possibility for unwanted oscillations of the mechanism. The second considers the option of using batteries to power the mechanism.

5.5.1 Mechanism Oscillation

As can be seen in Figure 5.9, the tension difference in the harness and thus the motor torque is only counterbalanced by the leash tension acting at an angle θ to the mechanism. If we neglect the dynamics of the mechanism and take moments about its mass centre, we find:

$$M = r(T_2 - T_1) = TL\sin\theta \tag{5.1}$$

$$\theta = \sin^{-1}\left[\frac{r(T_2 - T_1)}{TL}\right] \tag{5.2}$$

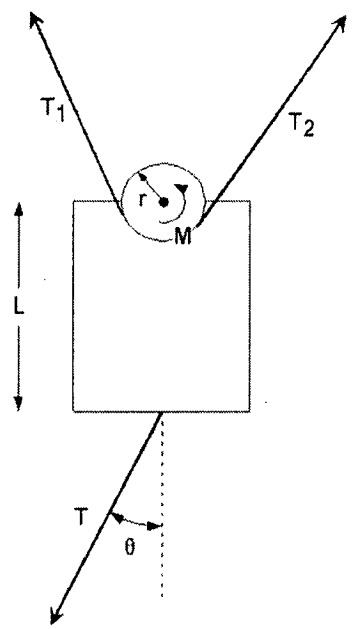

Fig. 5.9. Static equilibrium of the leash attachment mechanism.

As the tension difference in the harness varies from one extreme to another, the mechanism oscillates to counterbalance it. This oscillation was not modeled in the

simulation performed in the previous section and therefore its effect on the controller performance should be further evaluated in the future. Using Equation 5.2, the mechanism angle θ was computed for the manoeuvre of Figure 5.8. The mechanism oscillation is presented in Figure 5.10. From this figure, we note that the amplitude of oscillation would be approximately $\pm 8^{\circ}$. If it proves to be problematic, there are two ways to reduce the mechanism oscillation: (a) reducing the pulley diameter and (b) increasing the moment arm L of the leash tension. The values of r and L used in this exercise were 8 cm and 52 cm, respectively.

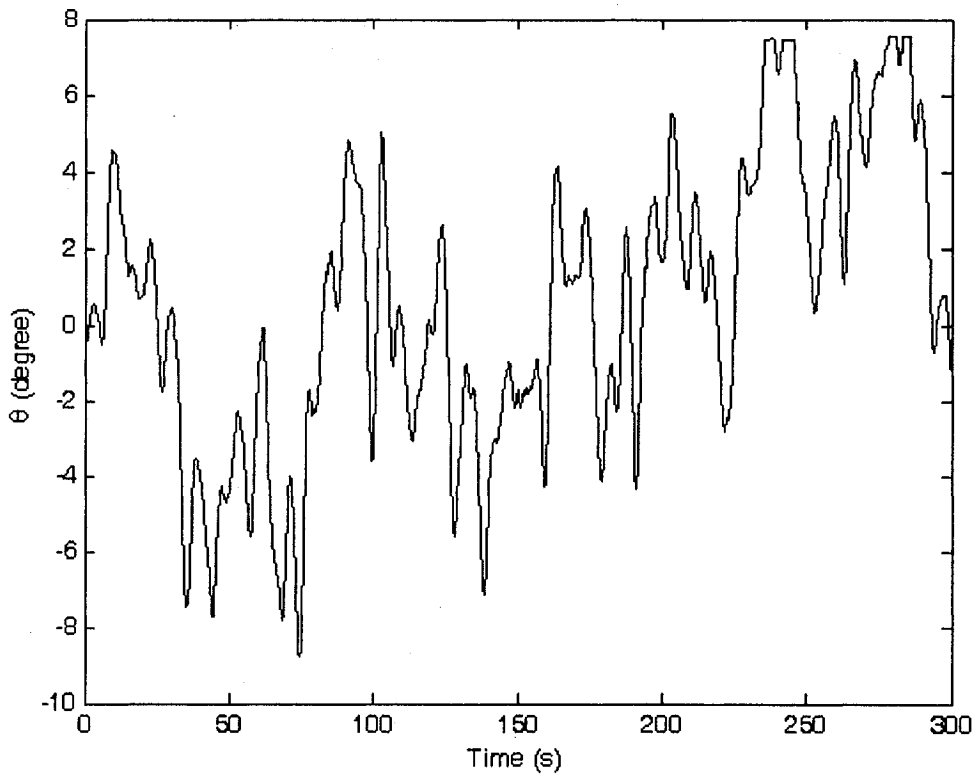

Fig. 5.10. Mechanism oscillation for the simulation of Section 5.4.

5.5.2 Battery Power

In Subsection 5.2.3, we estimated the weight of the electrical conductors required to supply the leash mechanism motor to be approximately 33 kg. Here we investigate the possibility of instead using batteries to supply power to the motor. In order to estimate the weight of the batteries required, we assume that Sanyo Twicell HR-DU [44] nickel-metal hydride batteries would be used. Each of these batteries weighs 178 grams, has a nominal

voltage of 1.2 volts and a capacity of 9 amps-hour. Consequently, the energy provided by a HR-DU cell is 10.8 watts-hour.

For the five-minute manoeuvre of Figure 5.8, the mechanism requires approximately 6 watts-hour. We obtained this energy value by integrating the absolute value of the instantaneous power, obtained by multiplying the mechanism speed by the tension difference in the harness. The absolute value of the power is used since it is conservatively assumed that there is no energy recovery in the system and that generating *negative* power consumes as much energy as generating *positive* power. Therefore, we estimate that seven HR-DU cells would be needed to power the leash attachment point mechanism for an hour. Since these cells would only add 1.3 kg to the system, which is 25 times less than added by electrical conductors, and because the experimental flights are usually no longer than one hour, powering the mechanism with batteries seems to be an attractive option for testing. The motor and amplifier selected in Section 5.2 would have to be changed if we chose this option, as they work on AC power.

In the case of the full scale LAR system, we would have to power the mechanism from the ground through the central tether and the leash. Indeed, since the LAR aerostat system will be flying for much longer (and indefinite) periods of time, the battery approach would be infeasible.

5.6 Conclusion

In this chapter, we designed a mechanism that displaces the leash attachment point on the harness in order to control the pitch of the aerostat. This design was preliminary in nature. After the implementation of the proposed mechanism into the simulation, we found that the use of leash attachment pitch control could reduce the payload rms motion by 50%. This active method looks therefore more promising than the bungee leash approach, for which we found a payload rms motion reduction of 30% in Chapter 4. However, as we learned from the bungee leash experiment, pitch control may prove to perform less well when implemented in practice. It is thus important to further develop leash attachment pitch control in order to test it on a tethered aerostat system.

Chapter 6

Conclusion

In this thesis, we considered different ways of reducing the payload motion of the LAR multi-tethered aerostat system. By simulating this system, it was first discovered that most of the payload perturbations were produced by the aerostat and transmitted to the payload through the leash. Indeed, by replacing the simulated aerostat of the baseline case by a constant force equal in *magnitude* and *direction* to the mean top leash tension of this same case, we found that the payload rms motion was reduced by nearly 95 percent. A similar test in which the aerostat was replaced by a constant leash tension magnitude while allowing its direction to vary as in the baseline case showed that the variations in the leash tension magnitude were responsible for approximately 75 percent of the payload rms motion. For this reason, this thesis focused on reducing variations in the leash tension magnitude as a way of reducing the payload motion.

By varying the leash properties of the baseline system in the simulation, it was discovered that among its length, its stiffness and its damping, the leash property that has the largest effect on the payload motion is its stiffness. Indeed, by sufficiently reducing the leash stiffness in the simulation, the magnitude of the leash tension as seen by the payload became nearly constant and the payload rms motion was reduced by 75 percent. In order to reduce the leash stiffness in the physical system, three passive methods were considered: (a) a constant force spring, (b) a passive heave compensator and (c), a bungee leash.

A constant force spring is a roll of prestressed strip that exerts a nearly constant restraining force to resist uncoiling. As expected, it was found by simulating the system

that the payload motion could be reduced by 75 percent if we placed such a spring at the base of the leash. However, it was also noted that a constant force spring would require a travel length of approximately 60 metres and be able to oppose a force of 2.6 kN. Since such large constant force springs are unavailable, the constant force spring was rejected as a solution for the LAR multi-tethered system.

A passive heave compensator at the base of the leash would include a pneumatic spring, an accumulator and a pulley system to increase the mechanism travel length. By simulating the baseline system with a passive heave compensator with a stiffness of 1 N/m, it was found that the required pretension and travel length would be respectively 2.6 kN and 64 metres, and the rms motion of the payload would be reduced by 78 percent. To avoid hitting its stops, the passive heave compensator would have to be used jointly with a system that would actively control either its pretension or the mean leash tension with changes in wind speed. The added weight and complexity of the passive heave compensator were seen as excessive, and this solution was not pursued further.

The last passive method considered to reduce the leash stiffness was the replacement of the present Spectra leash whose stiffness is 5300 N/m by a bungee leash with a stiffness of 5 N/m. With the bungee leash, simulations showed that the payload rms motion would be reduced by 63 percent. Since this method seemed very promising and simple, we chose to implement it on the one-third-scale test platform in Penticton, British Columbia. Due to the limited lift of the Penticton system, we were forced to use a half Spectra – haft bungee leash with a stiffness of 40 N/m. An additional safety cable was used in parallel with the bungee part to (a) back the bungee part in case of failure, (b) power the ballonet platform, and (c) ease the launching and retrieval procedures. By simulating this arrangement, we expected to observe two things in the experiment: a reduction of the payload rms motion of 30 percent and a significant reduction of the payload oscillation frequency. The reduction in payload frequency would greatly simplify its stabilisation by other active methods.

The experimental results obtained did not demonstrate any reduction in payload rms motion or frequency with the bungee leash. This was attributed to much higher turbulence conditions existing during the part of the flight with the bungee leash. However, the

bungee leash performed better than what was predicted by the simulation. We concluded that the available data was not sufficient to validate or invalidate the system improvements expected with the bungee leash. Nevertheless, the data collected allowed us to validate the bungee and Spectra leash models, which increased our confidence in the simulation results. The implementation of a bungee leash on the test platform in Penticton highlighted some drawbacks of the bungee approach, including its weight and operational complexity. We concluded that the addition of a bungee leash in the LAR system was of questionable benefit since it seemed heavy and expensive for a relatively small improvement in performance.

Two active methods were considered in order to improve the payload stability of the LAR multi-tethered aerostat system: (a) active constant force spring and (b) aerostat pitch control.

The active constant force spring approach was derived from an evaluation of an active heave compensator controlling the leash speed. This consisted of a motor mounted on the payload used to control the leash speed in order to stabilize the leash tension. Since it is possible to produce a constant torque by supplying a DC servo motor with a constant current, we proposed simply using a servo amplifier to ensure that a constant current was supplied to the motor. With this approach, the performance obtained with a constant force spring, a reduction of 75 percent of the payload RMS motion (note that this performance does not take into account the weight of the device), could be achieved with the added advantage that changes in wind conditions could be compensated for by simply changing the value of the current set point. However, such a device would add complexity and weight to the LAR aerostat system, and would require substantial power at the confluence point, thus leading us to reject this approach.

We investigated two ways of controlling the pitch of a streamlined aerostat: aerostat tailfin deflection control and leash attachment point control. We found that a tailfin-based pitch controller might reduce the payload RMS motion by as much as 63 percent. However, we did not further investigate this approach since it was impossible to test it in Penticton, as the streamlined aerostat used has fixed inflatable fins.

A leash attachment point pitch controller would displace the leash attachment point on the lower loop of the harness in order to control the aerostat pitch. This mechanism, which comprises a pulley, a servo motor, a servo amplifier and a geartrain, would be powered from the ground through the central tether and the leash. We estimated that the overall weight added by a leash attachment mechanism would be 50 kg, and would lead to a reduction of 50 percent in the payload rms motion. Finally, we also found that this device would require substantially less power at the confluence point than the active constant force spring. The relative simplicity of this active system led us to recommend it for future detailed investigation.

6.1 Recommendations for Future Work

A number of recommendations for future work are now suggested as worthwhile continuations of the research performed here.

1. Develop a systematic technique to determine if two data samples provided by the Penticton facility have comparable aerostat wind conditions.

2. Improve the launching and landing procedures of the bungee experiment. Safety should be the main concern.

3. Perform additional bungee leash experiments jointly with Spectra leash experiments at the Penticton facility in order to get two samples with comparable aerostat lift and wind conditions. Confirm or disprove the simulation results, which predict a 30% reduction in payload motion with the bungee leash.

4. Use the McGill small-scale facility to obtain reliable and quantitative data on the effect of the leash length on tether tension and angle variations. These could then be used in the LAR simulation to predict the resulting payload motion (the McGill facility is single-tethered; has no payload).

5. Perform a detailed design of a passive heave compensator in order to get a better idea of its weight and complexity.

6. Refine the design of a leash attachment point mechanism. Implement it at the Penticton facility or at the McGill small-scale facility and test the leash attachment point pitch controllers.

References

[1] R. van de Weygaert, T.S. van Albada., "New Challenges for Cosmology," *The Westerbork Observatory, Continuing Adventure in Radio Astronomy, Astrophysics and Space Science Library*, Vol. 207, pp. 225-259, 1996.

[2] Legg T.H., "A Proposed New Design for a Large Radio Telescope," *Astronomy and Astrophysics Supplement Series*, Vol. 130, pp. 369-379, 1998.

[3] Schilizzi R.T., "The Square Kilometre Array," International SKA Project Office, (http://www.skatelescope.org/).

[4] Hall P.J., "The Square Kilometre Array: An International Engineering Perspective," International SKA Project Office, (http://www.skatelescope.org/).

[5] Carlson B. *et al.*, "The Large Adaptive Reflector: a 200-m Diameter, Wideband, cm-m Wave Radio Telescope," *Proceedings of the SPIE International Symposium on Astronomical Telescopes and Instrumentation*, pp. 33-44, 2000.

[6] Dewdney P.E., Nahon M., and Veidt B., "The Large Adaptive Reflector: A Giant Radio Telescope with an Aero Twist", *Canadian Aeronautics and Space Journal*, Vol. 48, No. 4, pp. 239-250, 2002.

[7] DeLaurier J.D., "A Stability Analysis for Tethered Aerodynamically Shaped Balloons," *AIAA Journal of Aircraft*, Vol. 9, No. 9, pp. 646-651, 1972.

[8] DeLaurier J.D., "Prediction of Tethered-Aerostat Response to Atmospheric Turbulence," *AIAA Journal of Aircraft*, Vol. 14, No. 4, pp. 407-409, 1977.

[9] Jones S.P., and Krausman J.A., "Nonlinear Dynamic Simulation of a Tethered Aerostat," *AIAA Journal of Aircraft*, Vol. 19, No. 8, pp. 679-686, 1982.

[10] Jones S.P., and DeLaurier J.D., "Aerodynamic Estimation Techniques for Aerostat and Airships," *AIAA Journal of Aircraft*, Vol. 20, No. 2, pp. 120-126, 1983.

[11] Badesha S., and Jones S.P., "Aerodynamics of the TCOM 71M Aerostat," *AIAA Paper* 93-4036, pp. 36-42, 1993.

[12] Lambert C., and Nahon M., "Stability Analysis of a Tethered Aerostat," *Journal of Aircraft*, Vol. 40, No. 4, pp. 705-715, 2003.

[13] Redd T., Bland R., and Bennet R.M., "Stability Analysis and Trend Study of a Balloon Tethered in a Wind, With Experimental Comparisons," NASA TN D-7272, Langley Research Center, 1973.

[14] Humphreys D.E., "Validation of the Dynamic Characteristics of a Towed, Scaled Aerostat," *Proceedings from the 12th AIAA Lighter-Than-Air Systems Technology Conference*, pp. 227-236, 1997.

[15] Jones S.P., and Shroeder L.D., "Nonlinear Dynamics Simulation of a Tethered Aerostat: A Fidelity Study," *Journal of Aircraft*, Vol. 38, No. 1, pp. 64-68, 2001.

[16] Leclaire R.C., and Rice C.B., "The Local Motions of a Payload Supported by a Tri-Tethered Natural Shape Balloon," *US Air Force Report* AFCRL-TR-73-0748, 1973.

[17] Leclaire R.C., and Schumacher H.L., "Local Motions of a Payload Supported by a Nolaro Tri-Tethered Balloon," *Proceedings of the 8th AFCRL Scientific Balloon Symposium*, Air Force Cambridge Research Lab., Bedford, MA, pp. 233-255, 1974.

[18] Le Coroller H., Dejonghe J., Arpesella C., Vernet D., and Labeyrie A., "Tests with a Carlina-Type Hypertelescope Prototype," *Astronomy and Astrophysics*, Vol. 426, pp. 721-728, 2004.

[19] Fitzsimmons J.T., Veidt B., and Dewdney P.E., "Steady-State Analysis of the Multi-Tethered Aerostat Platform of the Large Adaptive Reflector Telescope," *Proceedings of the SPIE International Symposium on Astronomical Telescopes and Instrumentation*, 2000.

[20] Nahon M., "Dynamics and Control of a Novel Radio Telescope Antenna," A Collection of the *AIAA Modeling and Simulation Technologies Conference Technical Papers*, pp. 214-222, 1999.

[21] Nahon M., Gilardi G., and Lambert C., "Dynamics and Control of a Radio Telescope Receiver Supported by a Tethered Aerostat," *AIAA Journal of Guidance, Dynamics and Control*, Vol. 25, No. 6, pp. 1107-1115, 2002.

[22] Lambert C., "Dynamics Modeling and Conceptual Design of a Multi-Tethered Aerostat System," M.Sc. Thesis, Dept. of Mechanical Engineering, University of Victoria, Victoria, BC, Canada, Jan. 2002.

[23] Lambert C., Saunders A., Crawford C. and Nahon M., "Design of a One-Third Scale Multi-Tethered Aerostat System for Precise Positioning of a Radio Telescope Receiver," *CASI Flight Mechanics and Operations Symposium*, Montreal, Canada, 2003.

[24] Nahon M., Lambert C., Chalmers D., and Bo W., "Model Validation and Performance Evaluation for the Multi-Tethered Aerostat Subsystem of the Large Adaptive Reflector," *Experimental Astronomy*, 2005.

[25] Niedzwecki J.M., and Thampi S.K., "Heave Compensated Response of Long Multi-Segment Drill Strings," *Appl. Ocean Res.*, Vol. 10, pp. 181-190, 1988.

[26] Hover F.S., Grosenbaugh M.A., and Triantafyllou M.S., "Calculation of Dynamic Motions and Tension in Towed Underwater Cables," *IEEE Journal of Oceanic Engineering*, Vol. 19, pp. 449-457, 1994.

[27] Driscoll F.R., Nahon M., and Lueck R.G., "A comparison of Ship-Mounted and Cage-Mounted Passive Heave Compensation System," *Journal of Offshore Mechanics and Artic Engineering*, Vol.122, pp. 214-221, 2000.

[28] Driscoll F.R., Buckham B., and Nahon M., "Numerical Optimization of a Cage-Mounted Passive Heave Compensation System," *Proceedings of Oceans'2000*, 2000.

[29] Eide L., "Modeling and Control of a Vertically Tethered Marine Platform Using an Active Heave Compensation System," M.Sc. Thesis, Dept. of Ocean Engineering, Florida Atlantic University, Boca Raton, Florida, USA, Dec. 2003.

[30] The Cortland Companies, http://www.thecortlandcompanies.com.

[31] Press W.H., Teukolsky S.A., Vetterling W.T., and Flannery B.P., *Numerical Recipes in C*, Cambridge University Press, Cambridge, England, U.K., pp. 710-714, 1992

[32] Stock Drive Products – Sterling Instruments, http://www.sdp-si.com.

[33] Materials group, Department of Engineering, University of Cambridge, http://www-materials.eng.cam.ac.uk/mpsite/short/OCR/ropes/default.html

[34] Teorodescu A., "Analysis of an Aerostat Harness," B.Eng. Thesis, Department of Mechanical Engineering, McGill University, 2005.

[35] Nasar S. A., *Electric Machines and Power Systems - Volume 1*, McGraw-Hill, New-York NY, 1995.

[36] Aerostar International Inc., http://www.aerostar.com/.

[37] Bungee Consultants International, http://www.bungeeconsultants.com/.

[38] Baldor Electric Company, http://www.baldor.com.

[39] Floyd T. L., *Electric Circuit Fundamentals, Sixth Edition*, Prentice Hall, 2003.

[40] National Fire Protection Association, *National Electric Code 2002*, Thomson Delmar Learning, 2001.

[41] Mijno Precision Gearing, http://www.mijno.com.

[42] Quality Transmission Components, http://www.qtcgears.com.

[43] SKF Group, http://www.skf.com.

[44] Sanyo, http://sanyo.com.